Bioremediation of Arsenic Contaminated Groundwater in Northwest Florida: Mineralogy, Geochemistry, and Microbiology Changes

by

Eric John Levitt

A thesis submitted to the Graduate Faculty of
Auburn University
In partial fulfillment of the
Requirements for the Degree of
Master of Science

Auburn, Alabama
May 7, 2017

Keywords: arsenic, bioremediation, Florida, geochemistry, microbiology, groundwater

Journal Style: Geology

Approved by

Dr. Ming-Kuo Lee, Chair, Robert B. Cook Professor of Geology
Dr. James Saunders, Professor of Geology
Dr. Ashraf Uddin, Professor of Geology

Abstract

This research demonstrates that the stimulation of natural sulfate-reducing bacteria (SRB) in groundwater can precipitate biogenic pyrite nanoparticles that play an active role in sequestering dissolved arsenic from contaminated groundwater. This process is executed through the sorption and co-precipitation of arsenic onto biogenic pyrites. This pilot experiment is one of the first applications of this bioremediation technology at the field scale. At an industrial site where the groundwater within a shallow unconfined aquifer is contaminated by arsenic, a nutrient solution was injected to stimulate the activity and metabolism of SRB. The injection of biodegradable organic carbon, ferrous iron, sulfate, and fertilizers successfully stimulated SRB metabolism one week after the initial injection. The microscopic, X-ray, and electron microprobe analyses have confirmed the bio-mineralization of pyrite. Over time, these pyrite nanoparticles grew to form 1 to 10 μm in diameter, and formed euhedral crystals and spherical aggregates that contain 0.05 to 0.4 wt. % arsenic. The data suggest that the biogenic pyrite formed at the site has an excellent capacity to sequester arsenic to their iron sulfide solids. Arsenic sequestration in pyrite through adsorption and co-precipitation led to dissolved arsenic concentrations decreasing from initial concentrations of 0.3-0.5 mg/L to below the regulatory clean-up standard for the site of 0.05 mg/L just weeks after the injection. This study also demonstrated that the iron sulfide biominerals remain stable in the aquifer even after organic carbon from the injection is exhausted during fluctuations of redox conditions. The ongoing stability of the biominerals allowed for sequestration of arsenic to continue for months after their main growth stage. The results of this

experiment have implications for the future remediation of both natural and industrial sites where high arsenic levels contaminate local water supplies. In addition to the potential of this remediation tool, it is also possible that the application of this technique can be down-sized and optimized to inexpensively treat contaminated aquifers in which groundwater is withdrawn from individual wells for drinking, cooking, and irrigation uses, , which remains a concerning human health problem throughout the world today.

Acknowledgments

Without grants from the National Science Foundation and Auburn University this research would not have been possible. Many thanks are given to the following people who generously gave their time, advice, criticisms, and guidance: Dr. Ming-Kuo Lee, Dr. James Saunders, Dr. Ashraf Uddin, and the entire faculty at the Auburn Department of Geosciences. Dr. Lee has been a monumental figure in my continuing education, and his willingness to give me the opportunity to study at this University has given me everything I hoped for in a graduate education. I thank him again for his patience, mentorship, leadership, and integrity. Special thanks to Dr. Jim Redwine, Justin Marks, and Rick Hagendorfer, who helped to facilitate the injection process and field sampling, as well as data collection. I would also like to extend my gratitude to Brett Surles, and fellow students Ted Wilson and Brian Miller. They provided critical assistance in both sample collection and laboratory work. I want to thank Dr. Mehmet Billor for his support in ICP-MS and XRD laboratory work, as his contribution was invaluable to the success of this research. Thanks also to Dr. Luxin Wang and Dong Han, who were immensely helpful in the microbiology assessments. I want to also extend heartfelt gratitude to all graduate students that I had the pleasure of meeting and cultivating friendships with over this period of our lives. A special thanks must also be given to my parents and brother, who have stood as unwavering supporters of all of my goals and ambitions, and I cannot thank them enough for their work to provide these blessings in my life. The author finally must thank Emily Bennett, a person who sacrificed countless hours and days to push me forward and help realize

all of my potential. Her moral and emotional support is something that I cannot begin to describe in its importance.

Table of Contents

List of Tables

List of Figures

List of Abbreviations

As	Arsenic
Ca	Calcium
CASIC	Hubbard Center for Advanced Science, Innovation, and Commerce
AU	Auburn University
DOC	Dissolved Organic Carbon
EPA	Environmental Protection Agency
Fe	Iron
H_2S	Hydrogen Sulfide
IC	Ion Chromatogrpah
ICP-MS	Inductively Coupled Plasma Mass Spectroscopy
Mg	Magnesium
Na	Sodium
ORP	Oxidation-Reduction Potential
Ppb	Parts per billion
SEM	Scanning Electron Microscope
SO_4	Sulfate
SRB	Sulfate Reducing Bacteria
XRD	X-Ray Diffraction
XRF	X-Ray Fluorescence

Introduction

Arsenic is a common metalloid contaminant found in soils and groundwaters derived from both natural and anthropogenic sources (Welch et al., 2000; Smedley and Kinniburgh, 2002; Harvey et al., 2002; van Geen et al., 2003). The worldwide problem of arsenic contamination of potable drinking water supplies (Figure 1) has contributed to new interest and research into arsenic geochemistry (Nordstrom, 2002; McArthur et al., 2004; O'Day 2006). Research has shown that the metabolic effects of Fe-reducing bacteria and Mn-reducing bacteria are responsible for releasing arsenic and other metal contaminants into alluvial aquifers worldwide (Nickson et al., 2000; Mukherjee et al., 2001; Dowling et al., 2002; Saunders, 2005). It has been proposed that arsenic is mobile under Fe-reducing conditions and immobile under sulfate-reducing conditions (Saunders et al., 2005; Dhakal, 2010). Arsenic sequestration in sulfide minerals is an emerging technology for remediating arsenic contaminated groundwaters. Research has shown that pyrite can be effective in sorbing and removing arsenic from water, and has been proposed as a water-treatment technique (Jingtai and Fyfe, 2000; Zouboulis et al., 2003; Bulut et al., 2014). Saunders et al. (2008) proposed that arsenic-bearing pyrite is the principal arsenic phase formed under sulfate-reducing conditions in the cirum-neutral pH range. Dissolved arsenic occurs in two oxidation states in most natural waters: As(V) (arsenate) under oxidizing conditions, and As(III) (arsenite) under moderately reducing conditions. Orpiment (As_2S_3), realgar (AsS), and arsenopyrite (FeAsS) are the most commonly occurring arsenic minerals under reducing hydrothermal conditions in nature, although metal-arsenide minerals do

occur rarely. Scorodite ($FeAsO_4 \cdot 2H_2O$) may form in some low-temperature, oxidizing environments as in mine tailings or acid mine drainage. Under highly reducing conditions, As-bearing pyrite appears to control arsenic solubility in reducing environments containing reactive iron and sulfur (Lowers et al., 2007). Studies performed previously by Starnes (2015) and Saffari et al. (2016) have demonstrated that iron sulfides form naturally in a shallow unconfined aquifer at an industrial site that is contaminated with arsenic. These studies also concluded that iron sulfides have played a role in sequestering arsenic in the groundwater through co-precipitation and adsorption on the newly formed biomineral FeS.

By using technology that aims to stimulate sulfate-reducing bacteria growth, the precipitation of sulfide biominerals can be induced, and this study hypothesizes and explores the removal of arsenic and other metal contaminants from the groundwater through the co-precipitation and adsorption processes. As the iron sulfide minerals form, arsenic is incorporated into their crystal structure and adsorbed to their surfaces. Data suggest that this technology can offer a cost-effective remediation alternative for contaminated groundwater (Lee, 2015). The main hypothesis of this study is that high surface areas of sulfide biominerals have the capacity to adsorb arsenic metal/metalloid contaminants over time from groundwater after bacterial activity has ceased or slowed. To test this hypothesis, an injection experiment, with amendments of $FeSO_4 \cdot 7H_2O$ and carbon source molasses, has been conducted at a Florida industrial site to monitor the long term (one year) changes of water chemistry, mineralogy, and microbial community. This research represents the first long-term, field-scale studies that investigates and characterizes sorption and attenuation of arsenic on sulfide biominerals. It is necessary to

conduct field and laboratory investigations to evaluate if SRB could indeed prove useful in remediating arsenic-contaminated groundwater. This experiment is also one of the first field studies that examines how biogeochemical reactions occur along groundwater flow paths, including changing redox conditions and stimulated biomineralization that alters the solution composition as well as concentrations and speciation of arsenic in a contaminated aquifer. From the results of this research, a better understanding of the physical, chemical, and biological processes as they relate to arsenic contaminant behavior. This research characterizes groundwater geochemistry and As-sorbed Fe-S solids during the different stages of pre- and post-SRB metabolism, while also monitoring the changes in SRB activities in the treated groundwater. It also documents a year-long assessment of the efficacy of SRB metabolism to remove arsenic contaminants from groundwater. This study also investigates the iron sulfide biominerals' capacity to remain stable for arsenic sequestration under changing redox conditions.

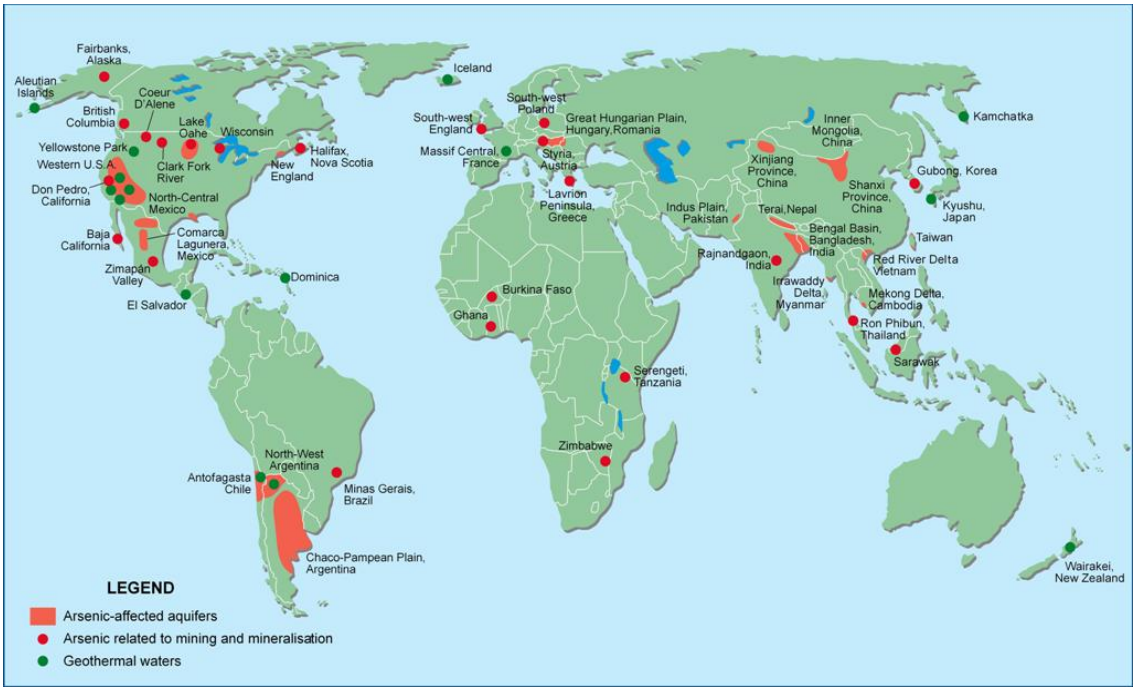

Figure 1. Map of arsenic-contaminated groundwater in major aquifers worldwide. Areas in blue are lakes (Smedley and Kinniburgh, 2002).

Background

Geologic Setting and Hydrogeology

The 0.3-acre industrial substation is located in northwest Florida, approximately 5 miles north of Panama City in Bay County (Figure 2). The site became contaminated with high levels of arsenic after heavy herbicide and pesticide use during its years of operation. Pump-and-treat methods were originally used to clean up the site after its closing, but these efforts have ceased and arsenic contamination has re-emerged at the level of hundreds of parts per billion (ppb). The industrial site lies within the coastal plain of the Florida panhandle, where thick sequences of marine sediments are deposited underneath the area within the Apalachicola Embayment (Figure 3). The Apalachicola Embayment is a regional basin whose axis plunges to the southwest, producing increased sediment thickness in the direction toward the coastline (Schmidt and Clarke, 1980). These sediments deposited as marine terraces represent ancient sea floors receiving sedimentation. The other regional structures of note are the Chattahoochee Anticline and the Ocala Arch (Veach and Stephenson, 1911). Underneath the Bay County itself there are four different physiographic subdivisions: Sand Hills, Sinks and Lakes, Flat-Woods Forest, and Beach Dunes and Wave-cut Bluffs. The Flat-Woods Forest subdivision takes up the largest portion of Bay County.

Figure 2. Map of the Florida panhandle with the general location of the industrial site outlined with a red box (adapted from Starnes 2015).

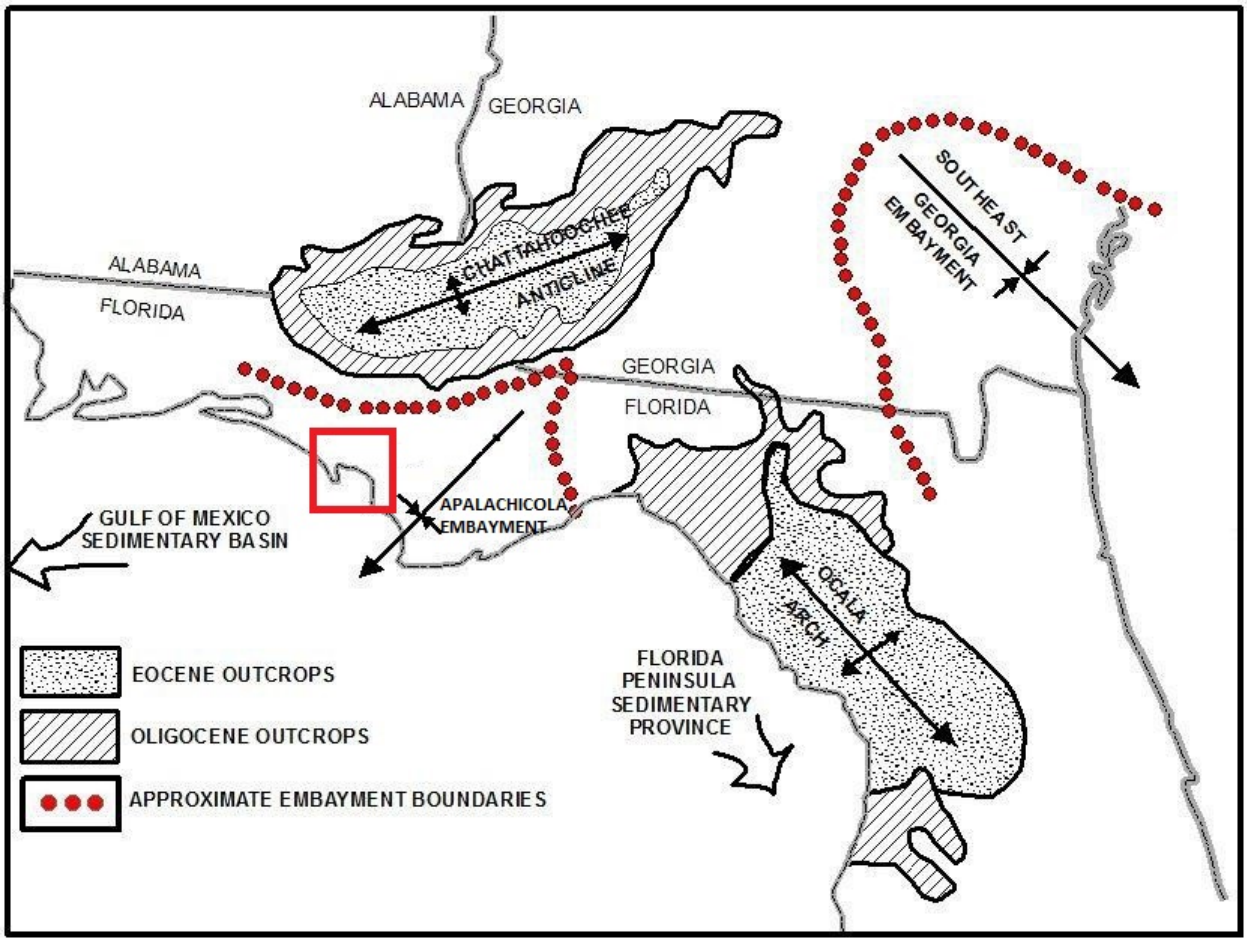

Figure 3. Map showing the regional geologic structures of the Gulf Coastal Plain. This map highlights the main features controlling regional deposition in the area. The red box outlines location of the industrial site relative to these features (Modified from Schmidt and Clark, 1980).

The oldest rocks found in outcrops exposed in the county are Early Miocene limestone units (Schmidt and Clark, 1980). The youngest sediments found in the county are Pleistocene to Holocene aged undifferentiated quartz sands, clayey sands, and gravels. These sands overlie the limestone units which can extend to depths of about 915 meters, and below these limestone units, sandstones and shales extend to granitic basement rocks (Schmidt and Clark, 1980).

There are four major hydrogeologic units that are generally recognized in the state of Florida: the surficial aquifer system, the intermediate confining unit, the Floridian aquifer system, and the sub-Floridian confining unit (Figure 4). Three of these hydrogeological units occur in the shallow subsurface beneath the site, from top to bottom as follows: surficial aquifer, the Jackson Bluff confining bed, and the Intracoastal Formation aquifer (Schmidt and Clarke, 1980). The surficial unconfined aquifer extends from the surface to a depth of approximately 6-7.6 meters. Groundwater from the surficial aquifer discharges into local streams or springs, or it potentially could migrate into the deeper Floridian aquifer system in places where the two aquifer systems are hydraulically interconnected. This aquifer consists predominately of fine to medium-grained quartz sand, with less than 10% made up of silt, clay, and coarse sands. In the surficial aquifer, the water table typically occurs at approximately 1.5 m below the surface. The average measured horizontal conductivity is approximately 7.1×10^{-4} cm/sec (Mintz and Miller, 1993). Due to the shallow groundwater table and flat topography, modeling results show that groundwater flow direction can change with precipitation events (Starnes, 2015). Historically at the site, groundwater flow direction has been to the northwest and west from the site and it migrates at a rate of a few meters per year (Figure 5). Organic material that manifests as dark

brown zones is present in the surficial aquifer (Schmidt and Clarke, 1980). There is a 0.9-1.5 m thick, laterally continuous layer of organic material in the quartz sand at a depth of about 1.5-3 m. This layer has been observed to thicken to the north (Schmidt and Clarke, 1980). The surficial aquifer at the site is injectable, as approximately 1 gallon per minute of treated groundwater was re-injected into wells during previous pump-and-treat remediation.

The Jackson Bluff confining bed consists of a dark olive green, silty clay. The clay is mostly made of kaolinite and illite, with minor quartz sand and shell fragments. The confining bed occurs from approximate depths of 6.09-9.15 m, and ranges from thicknesses of 15-2 m. The vertical hydraulic conductivity for the Jackson Bluff is approximately 1.6×10^{-7} cm/sec (Mintz and Miller, 1993). The Jackson Bluff exhibits low permeability and high adsorption capacity, so this unit can locally prevent the migration of arsenic from the surficial aquifer to the Intracoastal Formation aquifer below (Schmidt and Clark, 1980). Because of irregular deposition and erosion, the Jackson Bluff Formation occurs intermittently in the southern portion of Bay County and is more common in the northern parts of the county.

The Intracoastal Formation aquifer occurs immediately below the Jackson Bluff confining bed. The formation consists of grayish green calcareous sands, microfossils, black minerals, and some silt and clay (Schmidt and Clarke, 2015). The material is generally classified as silty or clayey sand.

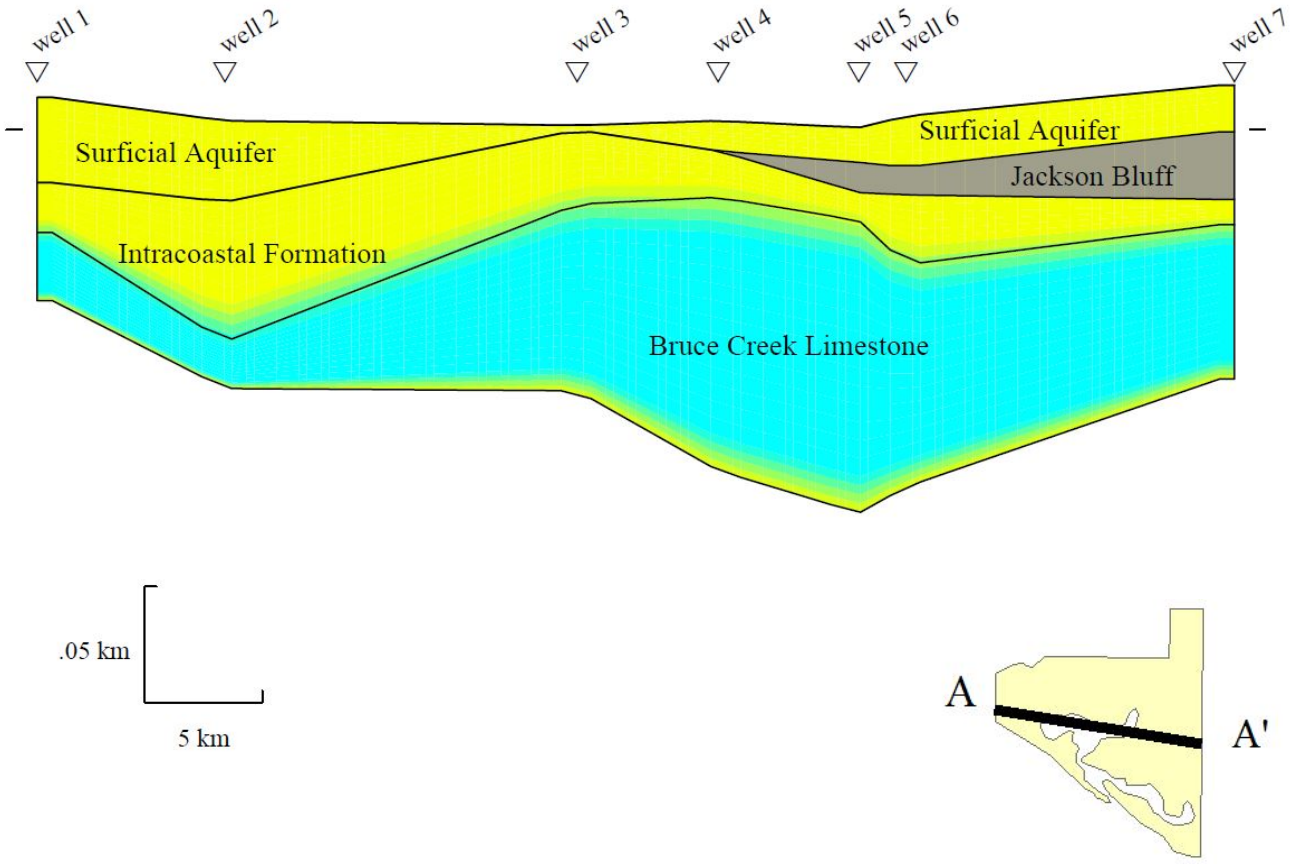

Figure 4. Hydrogeologic cross section of the Floridian aquifer system at the study area (from Starnes 2015).

Figure 5. Map of the industrial site with monitoring well locations.

Previous Research

Arsenic sequestration in sulfide minerals has been considered as an emerging remediation technology for contaminated groundwater for many years (Saunders et al. 1998, 2005, 2008; DeFlaun et al. 2009). Studies conducted from 2004 to 2005 demonstrated that iron sulfides forming naturally in aquifers were sequestering up to 1 weight percentage of arsenic (10,000 milligrams per kilogram or more) (Saunders, 2005). If site conditions are optimized to enhance naturally occurring sulfate reducing bacteria (SRB), then iron sulfide minerals can be allowed to form. Saunders et al. (1997) has shown that arsenic can be incorporated into the crystal structure of iron sulfides, and these studies have shown that up to 5% weight of arsenic is stable in iron pyrite (FeS_2), a common sulfide mineral. Arsenic sulfides also include realgar (AsS), orpiment (As_2S_3), and arsenopyrite (FeAsS) formed under hydrochemical environments that are much different than regular shallow groundwater aquifers (Smedley and Kinniburgh, 2002). All of these minerals can potentially remove arsenic and other trace elements from groundwater whether they occur naturally or are stimulated to precipitate (Saunders, 2005). These minerals also have low solubility, which allows for groundwater contaminant sequestration to be sustained over time (Lee and Saunders, 2003; Saunders et al. 2008). Saunders (1998) has previously described the in-situ sequestration of arsenic in sulfides. Soluble sources of organic carbon, ferrous iron, and sulfate can be injected into the subsurface to stimulate the conditions for sulfate-reducing bacteria growth. This growth eventually leads to the formation of the sulfides that sequester arsenic through adsorption and co-precipitation.

At the Avon Park Air Force Range, a Florida site similar to the study area, DeFlaun et al. (2009) and Onstott et al. (2011) performed groundwater remediation and arsenic sequestration tests on a sandy, naturally anaerobic aquifer. In the column studies on aquifer media, indigenous SRB were stimulated using sodium lactate, ethanol, ferrous iron, and sulfate under anaerobic conditions. Laboratory analysis of dissolved arsenic indicated that only 2 percent of the arsenic sequestered was re-mobilized after aerobic water was passed through. These results indicated that there is permanence to the treatment by SRB. Studies were then scaled up to model arsenic retention in solids over a long period of time, and the model indicated that 98 percent of the arsenic would be retained in solid phases after 16 years (months?) of fully oxygenated conditions. For other sites that were under more anaerobic conditions, the dissolution of the arsenic would be even less (DeFlaun et al. 2009).

The laboratory results led to the implementation of a small field-scale pilot in a 3x3 meter zone in the area of highest arsenic concentrations. In the field pilot, arsenic concentrations decreased by up to two orders of magnitude from greater than 160 μg/L to about 1.4 μg/L in 6 months. Reductions of arsenic concentrations in the field were actually greater than those observed in the laboratory column experiments (DeFlaun et al. 2009). By the end of the pilot project, total arsenic concentration in the aquifer solids in the treated area was up to three times greater than in the untreated aquifer solids (DeFlaun et al. 2009; Onstott et al. 2011), indicating the removal of arsenic from the dissolved phase to the solid phase (Figure 6).

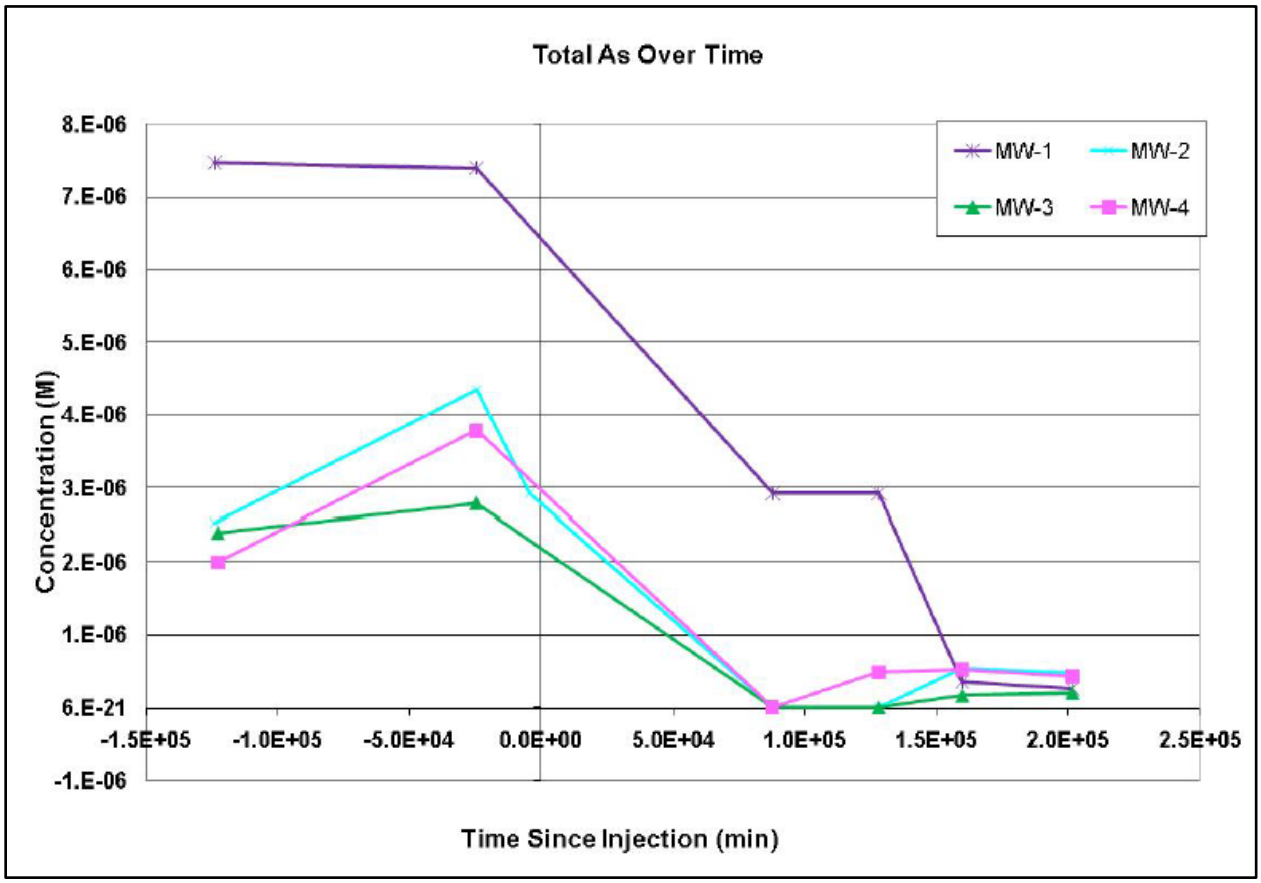

Figure 6. The decrease in arsenic concentration over time from the DeFlaun et al. (2009) pilot study.

From 2004 to 2005, Dr. James Saunders of Auburn University performed a successful proof-of-concept laboratory study for biogenic sequestration in sulfides on soil and groundwater samples from the study site. This work included chemical and mineralogical characterization of precipitates recovered from monitoring wells as well as sulfur-isotope geochemistry to demonstrate the biogenic origin of the sulfides. Geochemical modeling was also conducted for modeling the co-precipitation and adsorption of arsenic on oxides and sulfide solids (Lee et al., 2005; Saunders et al., 2008). Saunders (2005) discovered that seawater is the likely source of sulfate in the shallow groundwater at the site. This finding is probably typical for coastal regions. Saunders (2005) also found that the sulfur isotope values at the site are very similar to those seen in marine sediments, where sulfate-reducing bacteria forms iron sulfide minerals such as pyrite.

Starnes (2015) modeled the groundwater Fe speciation at the Florida industrial site (Figure 7). The Eh and pH data provided evidence that the surficial aquifer is a moderately reducing environment with near neutral pH. The modeling results also show that the dominant iron species is ferrous iron (Starnes 2015). This set forth the hypothesis that stimulation of sulfate-reducing bacteria with the injection of organic carbon and $FeSO_4$ can create a drop in redox potential that would result in a reducing environment where sequestration of arsenic is possible, and arsenic-sequestering solid pyrite phases are stable. These results and the results from Saunders et al. (2005) strongly support the concept that biogenic sulfate reduction is occurring at the industrial site and precipitation of sulfide minerals can remove arsenic from the

groundwater. The 2005 study provides evidence for pyrite formation in XRD analysis and enrichment of lighter sulfur isotopes in groundwater, which indicates a biogenic origin.

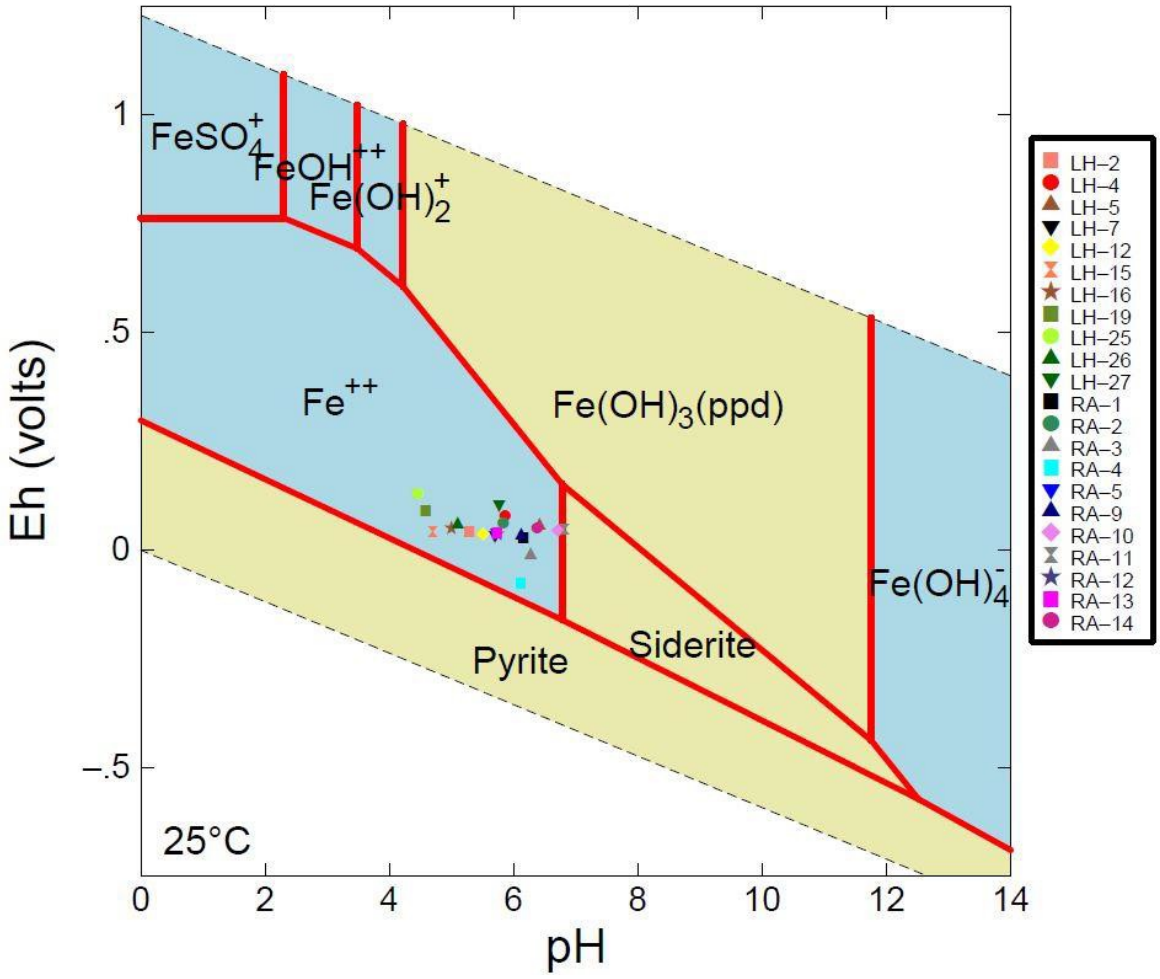

Figure 7. An Eh-pH diagram showing stable Fe species under various redox conditions (blue fields are aqueous phase and tan fields are solid phases). Plotted on the diagram are the redox conditions for each water sample collected. (From Starnes 2015).

Starnes' (2015) results support the notion that the site contains hydrogeochemical conditions that may be amenable for immobilizing or sequestering arsenic in groundwater through the precipitation of biogenic pyrite. XRD and XRF analyses of sediment slurry show the formation of arsenic-rich iron sulfides, suggesting that sulfate reducing bacteria are removing some arsenic naturally at the site by precipitating pyrite (Starnes 2015), even under sulfate-limited environments. Included within the study at the Florida site, Starnes (2015) also developed hydrological models that simulated the reactive transport and adsorption of arsenic in the contaminated aquifer (Figure 8). What was discovered was that with the increased sorption by the solid iron-sulfides, the overall distribution of arsenic through the aquifer was substantially decreased (Figure 9). This result shows that the overall distribution of the dissolved arsenic would decrease due to the increased sorption of arsenic by the sediments, however the model did not consider the effects of iron-sulfide precipitation or co-precipitation of arsenic under highly reducing conditions.

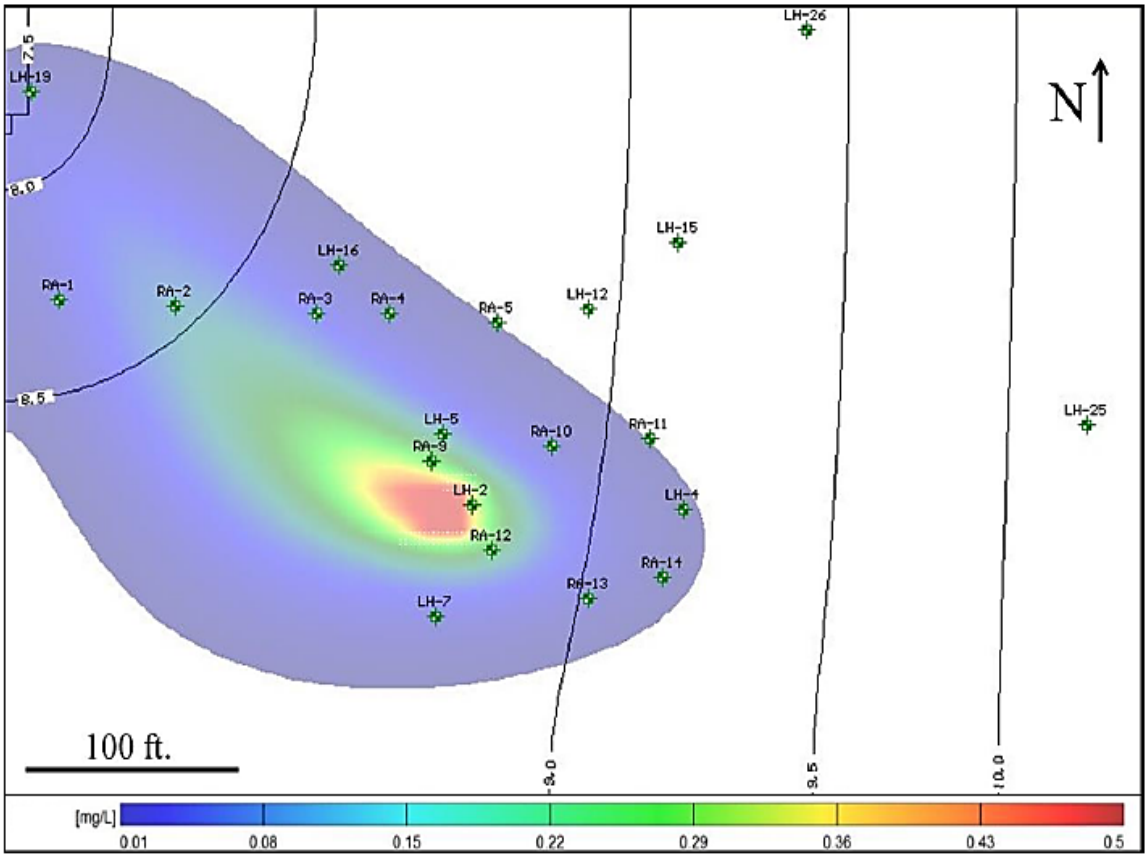

Figure 8. Map showing the simulated distribution of arsenic at the industrial site after 10 years and no adsorption; Kd=0 (From Starnes 2015).

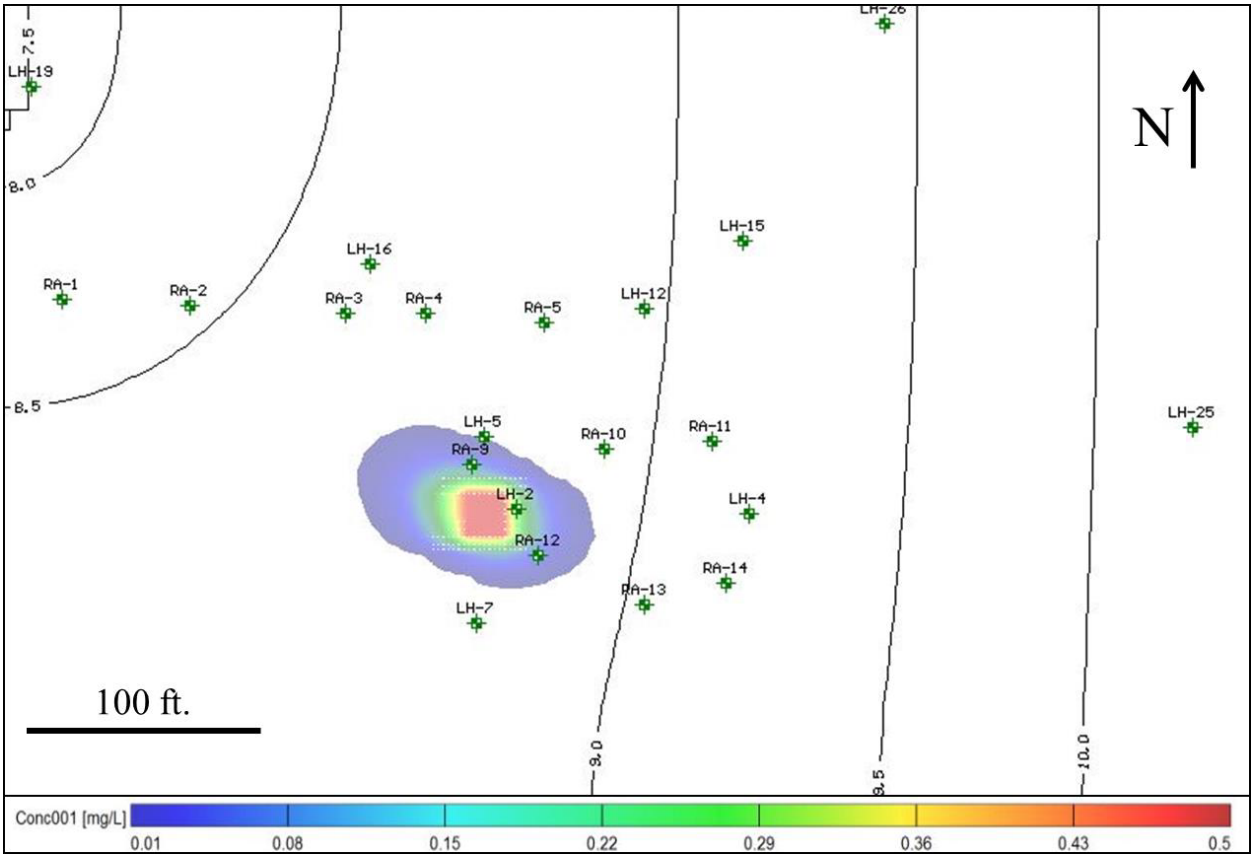

Figure 9. Map showing the simulated distribution of arsenic at the industrial site after 10 years with Kd=10 (from Starnes, 2015).

Methodology

Well Drilling and Injection Process

On January 12th, 2016, wells I-1, I-2, M-1, and M-2 were drilled at the industrial site where the surficial aquifer was contaminated by arsenic-bearing herbicides. A number of existing monitoring wells were present at the site, and the four new wells were drilled for this study. The drilling procedure was carried out in the area of high dissolved arsenic concentration (Figure 5) using a hollow-stem auger and mud rotary drill rig. The wells were drilled into the surficial aquifer to a depth of 20-25 feet, and solid sediment samples were collected for mineralogical and geochemical study. I-1 and I-2 were designated as 10-cm injection wells where the injection solution would be delivered. The 5-cm monitoring wells M-1 and M-2 were installed approximately 1.5 meters downgradient from the injection wells I-1 and I-2 for long-term monitoring. Simple volume balance calculations show that the total injection volume of 3000 gallons will displace all pore water residing in the aquifer within 1.5 meters away from the injection points. The injection wells were screened over the entire thickness of the surficial aquifer to facilitate the injection.

On February 15th, 2016, Eric Levitt, Shahrzad Saffari, Brian Miller, Dr. Ming-Kuo Lee, and Dr. James Saunders participated in pre-injection sampling of the groundwater aquifer. Beginning on February 16-18, I-1 was injected with 2,000 gallons of a “weak” injection solution. On February 19-20, I-2 was injected with 1,000 gallons of a “strong” injection solution (Table 1). The solution injected into well I-1 had the following mixture ratio per 1000 gallons of water:

2.5 kilograms of Ferrous Sulfate, 2 pounds (0.9 kg) of 10/10/10 All Purpose Fertilizer, and 60 pounds (27.2 kg) of molasses. The mixture ratio for the I-2 injection solution per 1000 gallons had 5 kilograms of ferrous sulfate, 2 pounds (0.9 kg) of 10/10/10 All Purpose Fertilizer, and 60 pounds (27.2 kg) of molasses. In the strong solution, the amount of $FeSO_4$ is doubled relative to the weak solution per 1000 gallons of water. A chemical breakdown of both solutions was conducted by the Test America Laboratory and is outlined in Tables 2 and 3. These solutions were injected in an attempt to provide a bounty of organic carbon (as electron donors), electron acceptors (sulfate), and nutrients to stimulate the activity and growth of SRB. The cultivation of SRB growth is meant to in turn facilitate the removal of arsenic in the groundwater by the previously discussed co-precipitation and adsorption to pyrite.

Mixture Ratios of Injection Solutions

	Solution 1 - Well I-1		Solution 2 - Well I-2	
	Per 1,000 gallons	**Total**	**Per 1,000 gallons**	**Total**
Ferrous Sulfate	2.5 kg	5 kg	5 kg	5 kg
10/10/10 All-Purpose Fertilizer	2 lb	4 lb	2 lb	2 lb
Molasses	60 lb	120 lb	60 lb	60 lb
Water Volume	2,000 gallons		1,000 gallons	

Table 1. Mixture ratios of the injection solutions injected into wells I-1 and I-2.

Aluminum	**0.24**	**mg/L**
Ammonia	**7**	**mg/L**
Arsenic	**0.0028**	**mg/L**
Bicarbonate Alkalinity as CaCO3	**0.98**	**mg/L**
Calcium	**53**	**mg/L**
Carbonate Alkalinity as CaCO3	**0.98**	**mg/L**
Chloride	**210**	**mg/L**
Dissolved Organic Carbon	**1900**	**mg/L**
Fluoride	**0.22**	**mg/L**
Hardness as calcium carbonate	**250**	**mg/L**
Hydroxide Alkalinity as CaCO3	**0.98**	**mg/L**
Iron	**300**	**mg/L**
Magnesium	**28**	**mg/L**
Nitrate as N	**0.062**	**mg/L**
Nitrate Nitrite as N	**0.062**	**mg/L**
Nitrite as N	**0.021**	**mg/L**
Orthophosphate as P	**0.1**	**mg/L**
Potassium	**320**	**mg/L**
Sodium	**16**	**mg/L**
Specific conductivity	**1800**	**umhos/cm**
Sulfate	**610**	**mg/L**
Total Alkalinity as CaCO3	**0.98**	**mg/L**
Total Dissolved Solids	**4600**	**mg/L**

Table 2: Chemical breakdown of weak solution injected into well I-1

Aluminum	**0.48**	**mg/L**
Ammonia	**12**	**mg/L**
Arsenic	**0.0055**	**mg/L**
Bicarbonate Alkalinity as CaCO3	**0.98**	**mg/L**
Calcium	**56**	**mg/L**
Carbonate Alkalinity as CaCO3	**0.98**	**mg/L**
Chloride	**200**	**mg/L**
Dissolved Organic Carbon	**1800**	**mg/L**
Fluoride	**0.20**	**mg/L**
Hardness as calcium carbonate	**270**	**mg/L**
Hydroxide Alkalinity as CaCO3	**0.98**	**mg/L**
Iron	**680**	**mg/L**
Magnesium	**31**	**mg/L**
Nitrate as N	**0.038**	**mg/L**
Nitrate Nitrite as N	**0.038**	**mg/L**
Nitrite as N	**0.021**	**mg/L**
Orthophosphate as P	**0.1**	**mg/L**
Potassium	**350**	**mg/L**
Sodium	**17**	**mg/L**
Specific conductivity	**2400**	**umhos/cm**
Sulfate	**1100**	**mg/L**
Total Alkalinity as CaCO3	**0.98**	**mg/L**
Total Dissolved Solids	**5400**	**mg/L**

Table 3: Chemical breakdown of the strong solution injected into well I-2.

Field Sampling

Groundwater and aquifer slurry from ten wells (Figure 5), including the two injection wells and two monitoring wells, were sampled prior to injection to obtain baseline information. After the injection, the same ten wells were sampled weekly for the month following the injection, and then monthly thereafter. Monthly sampling trips took place around the midway point of each month, with the conclusion of the sampling trips taking place on February 15th, 2017, one year to the day from the initial sampling of the pre-injection groundwater. Field sampling practices measured a broad spectrum of parameters. An YSI multi-parameter 556 hand-held instrument was used in the field to measure the water quality parameters in each well, including temperature, pH, dissolved oxygen, oxidation-reduction potential (ORP), and electrical conductivity. Prior to groundwater sampling, the water level depth was measured, and then the wells were purged using a peristaltic pump until all the water quality readings became stable. Once stable, water samples were filtered, acidified, and preserved using U.S. EPA standard procedures (filter pore diameter of 0.45 µm adopted from U.S. Geological Survey protocol). The line filter used was a medium capacity disposable filter manufactured by Geotech Environmental Equipment, Inc.

Since regulatory standards apply to unfiltered (total recoverable) samples, a set of unfiltered groundwater samples were collected from the ten wells for comparison. With these unfiltered samples, colorimetric techniques were conducted in the field to measure redox-sensitive parameters. Dissolved sulfide concentration was measured in the field immediately after collection using the Methylene Blue Method in a HACH DR2700 spectrophotometer

(USEPA Method 8131) in micrograms/liter (µg/L). It must be disclosed that in the month of August a malfunctioning part in the spectrophotometer made it necessary to take sulfide measurements using a HACH DR900 colorimeter as a replacement. The DR900 was then used from the month of August until the conclusion of the sampling in February 2017. It must also be stated that the colorimeter measured sulfide using the same method that was previously described. However, the colorimeter displayed readings in milligrams/liter (mg/L) instead of µg/L. Ferrous iron concentration was measured in the field in mg/L using a HACH DR820 colorimeter following the 1, 10-Phenanthroline Method (USEPA Method 8146). Alkalinity was measured using the HACH digital titrator test kit (USEPA Method 8203).

The filtered groundwater that was collected in the field was then separated into labeled vials marking the parameters to be tested in the laboratory. Using a disposable 50 ml syringe, the filtered water was taken from the collection beaker, and placed into one of three 30 ml vials for storage. One vial was labeled Anion IC/DOC and the water placed in this vial was measured by the lab at Test America for anion and dissolved organic carbon concentrations. There was a second vial for cation concentration measures, and a third for arsenic speciation. The Anion/DOC bottle was not acidified for preservation, it was simply filled with the filtered water and placed in dry ice storage. The vial for cations was filled with the filtered groundwater, then subsequently acidified using 5% nitric acid (HNO_3) drops for preservation purposes. For the measurement of arsenic speciation, a disposable arsenic speciation cartridges (Meng and Wang, 1998) was used to facilitate the separation of arsenate As(V) and arsenite As(III) species in the filtered water samples by passing the water through a highly selective aluminosilicate adsorbent.

This is done because As(III) predominately exists in the form of the uncharged complex H_3AsO_3, while As(V) is predominately in the form of the anionic complex $H_2AsO_4^-$ (Saunders, 2008; Lee et al, 2005). Thus, the neutral As(III) complex passes through the cartridge while the anionic As(V) complex is retained. The As(III) is measured in the cartridge effluent and As(V) is calculated from the difference between total As and As(III). After the water was filtered through the 45 micron filter, the arsenic speciation cartridges were attached to the syringe, and the first 5 mL of filtrate was discarded prior to the placement of the filtered water into the vial. The arsenic speciation sample was also acidified using HNO_3 for preservation. Once the three 30 ml vials were filled and sealed, they were placed in a cooler with dry ice for field storage until they were transported back to Auburn University. Upon transport back to Auburn University, the sampled groundwater vials were placed in refrigeration in the Hubbard Center for Advanced Science, Innovation, and Commerce Building (CASIC) until they could be analyzed.

Solid samples that precipitated from the groundwater were collected every other month using a peristaltic pump from the bottom of the wells where they accumulated through gravity settling. The solid samples were collected in the field in 50 ml centrifuge vials, then subsequently frozen using dry ice in a separate cooler to preserve the redox state. This same procedure was also used for the collection and preservation of microbiology samples that were taken from the field every other month. When transported back to Auburn University they were stored in a designated freezer (-18°C) in CASIC.

Recordkeeping was vital for the accurate and precise collection of measurements in the field. Once a procedure was carried out and a reading was obtained from the instruments, the

value was immediately recorded on a standardized data sheet. The configuration of this data sheet was consistent for every sampling trip, and the data that was collected for each parameter was consistent in its recording of the same unit measures for respective parameters. This log also made sure that the date of the sample collection was recorded and what samples were collected from each well for future laboratory analysis.

Geochemical Analysis of Groundwater and Biominerals

Laboratory analysis of the groundwater samples were conducted using an Agilent 7900 quadrupole inductively coupled plasma mass spectrometry (ICP-MS) at Auburn University. The Agilent ICP-MS was used to measure major cation and trace element concentrations in the groundwater samples that were collected in the field. In preparation for ICP-MS analysis, the sample vials were taken out of refrigerated storage and then transferred to individually labeled test tubes to ensure proper recording of data collected by the ICP-MS. The ICP-MS was also used for measuring the concentration of arsenate and arsenite relative to one another. Analysis by the ICP-MS was typically conducted within 10 days after the initial sample collection in the field. Measuring for anion concentration was completed by Test America using a Dionex 2000 ion chromatograph (IC). To track changes in our groundwater redox conditions and arsenic speciation after injection, measured Eh-pH values were projected onto activity-activity diagrams using Geochemist's Workbench (Bethke, 2008). It was necessary to add to the program thermodynamic data for thioarsenite species as well as arsenian pyrite (Saunders et al., 2008). This was done to study the arsenic speciation through the diagrams and to help us understand

what redox conditions are necessary for biomineralization of arsenian-pyrite as a result of SRB biogenic activity.

The precipitated solids that were collected were investigated through multiple means to study their crystalline structure, chemistry, and more importantly, the arsenic contents. A main technique used to analyze these traits was the use of X-ray diffraction (XRD) at the Department of Geosciences at Auburn University. To prepare solid samples for XRD analysis, the frozen solid sample bottles were removed from storage and thawed. The solids were then collected in vials labeled for each well, and the vials underwent centrifugation. We transferred the solids from the vials into marked crucibles, where they were placed on a hotplate and dried out completely under a fume hood over a period of several days. With the solids dried and powdered, they were then analyzed using a Bruker D2 Phaser X-ray Diffractometer. The D2 Phaser uses a scintillation counter and Lynxeye detector using Cu-Kα radiation. To determine the mineral composition of the samples, a peak search and match procedure was carried out using the DIFFRAC.EVA software. At the conclusion of XRD analyses, the bulk powder samples were analyzed by the portable Bruker Elemental Tracer IV-ED XRF in the Auburn Geoscience Department. The Bruker XRF has the capability to qualitatively and quantitatively measure elements with an atomic number of 11 (Na) or higher. Following the XRF analyses, the solids were imbedded in epoxy, ground, and polished with 1 to 6 μm diamond paste for the purposes of optical microscopy. The samples were investigated in reflected light using a Nikon Labophot research petrographic polarizing microscope. Further imaging of the solids was done through the use of a Zeiss EVO 50VP scanning electron microscope (SEM) at Auburn University. For the

SEM the powder samples needed to be mounted and sputter-coated for investigation in three dimensions. As it pertains to the arsenic contents in the pyrite solids, these were characterized more precisely by the JEOL 8600 electron microprobe located at the University of Georgia. This microprobe used a 15kV accelerating voltage, a 10 nA beam current, and 10-30 second counting times. The quantitative analyses were performed with wavelength dispersive spectrometers (WDS) automated with the Probe for EPMA software (Advanced Microbeam), and standards for Fe, S, and As.

Microbiology Analysis

Microbial changes at the aquifer site were studied using genomic assay facilities at Dr. Luxin Wang's laboratory in the Auburn Animal Sciences Department. The purpose of these assays were to better characterize the microbial community structure, particularly the sulfate reducing bacteria that occupy the aquifer. The total DNA of each aqueous slurry sample collected from the wells was extracted using Powersoil® DNA isolation kit (MO BIO, Carlsbad, CA) following the manufacturer's instruction. The concentrations of the total sulfate reducing bacteria were determined through real-time PCR targeting the *dsr*A gene (Ben-Dov et al. 2007). DNA samples extracted from known concentrations of an ATCC reference strain, *Desulfovibrio vulgaris subsp. Vulgaris* (ATCC 29579), were used to establish the standard curve for calculation. Real-time PCR was carried out using PerfeCTa SYBR® Green SuperMix (Quanta, Gaithersburg, MD) and on an ABI 7500 machine (Applied Biosystems, Foster City, CA).

Results

On-Site Groundwater Monitoring

As stated previously, there are a set of parameters that were tested directly on site at time of collection each sampling event. The parameters for which values were measured are: ORP, pH, electrical conductivity, dissolved oxygen content, ferrous iron concentration, dissolved sulfide concentration, water alkalinity, and the depth to the water table in each monitoring well. The depth to the water table that was recorded each month is outlined in Table 4. The water table at the industrial site is shallow, and before the injection, it was less than four feet deep in all of the wells. Changes to the water table depth were consistently parallel in all wells, meaning that changes in depth between sampling events were of similar magnitudes for all the wells on site. The water table depth reached its deepest points for most of the wells in the October and November, due to low rainfall amounts received during dry months. The monthly rainfall changes at the site is shown in Table 5. Rainfall amounts were at its highest during the summer months from June through September 2016, followed by a decline in precipitation in late fall. Table 6 displays ORP values for the injection and monitoring wells through time. Background levels for ORP at the industrial site showed mildly reducing conditions prior to the injection. The average ORP was placed at 53.2 mV, and values varied from a low of -69 mV in LH-10 to a high of 125 mV in both injection wells I-1 and I-2. One week after the injection the ORP values drop significantly, and data showed a change to highly reducing conditions in the groundwater environment for the injection wells and the affected monitoring wells M-1 and M-2. Within one

week after injection average ORP was down to -45.5 mV across the ten monitoring wells. The largest decrease was observed in both injection wells. I-1, which received the "weak" injection solution, had an ORP of -142.1 mV, a decrease of -267.8 mV. I-2, receptor of the "strong" injection solution, boasted a very low ORP of -236.2 mV, an even larger decrease of -361.7 mV. The presence of the highly reducing environment relative to pre-injection conditions persisted for the next several months and into the summer, as evidenced by ORP values remaining negative in affected wells. Overall, the reducing conditions persist for the remainder of the year. However, a series of heavy precipitation events in July and August served to cause a slight uptick in trend back toward 0 mV.

Pre-injection pH conditions reflected a slightly acidic groundwater environment, and average pH across the ten monitoring wells was 6.04. After the injection operation, we observed some drastic fluctuation in measurements in the weeks following the injection as the environment adjusted to the new inputs and biogeochemical conditions (Table 7). The injection wells and monitoring wells M-1 and M-2 exhibited the most extreme changes in pH measures immediately following injection. One week after injection I-1 and I-2 now had pH readings of 8.00 and 8.32, respectively, compared to 6.24 and 6.21 just days before. While M-1 and M-2 had background pH of 5.59 and 5.69, their readings showed 7.82 and 8.22 the following week. These changes preceded the next set of fluctuations that we observed the following week on March 2nd (Table 7). Two weeks after injection, pH values for injection and monitoring wells incurred a steep drop. I-1, M-1, and M-2 each had a pH reading below 5.00, and average pH across the ten monitoring wells was 5.6. Lower pH conditions were observed for approximately three months

after the initial injection, and pH values across the affected wells did not push above pre-injection level until the heavy rain events occurred over the summer months. Through the fall and into the end of 2016, pH conditions in the affected wells dropped to either at, or slightly below, the pre-injection levels. Injection well I-1 underwent a sharp change in pH in the two months of sampling in 2017. In January, I-1 groundwater pH was highly acidic, registering at 3.16. In February, I-1 pH was 3.46. While significant in the magnitude of decrease, these changes only occurred in the I-1 well, and the other affected wells that were sampled did not show such a noticeable difference.

Trends in dissolved oxygen (DO) values show a steep decline in dissolved oxygen in the injection wells after the injection was carried out. While the overall site characteristics show an anaerobic environment, pre-injection DO levels in the injection wells were the highest on the industrial site (Table 8). I-1 had a DO concentration of 1.47 mg/L and I-2 had a DO concentration of 1.01. These levels take a swift drop after the injection, and an even more anaerobic environment took hold at the site. The pre-injection average DO at the site was 0.425 mg/L, and in the weeks and months following injection an general declining DO throughout the ten affected wells were observed. The dominant anaerobic environment at the site continued for the next eight months, where we did not record any shift closer to aerobic redox conditions until the month of October, where we DO values of I-2 and RA-9 push above 1.0 mg/L. By the conclusion of the sampling period in February we observed aerobic conditions (>1.0 mg/L DO) in wells I-1, I-2, RA-9, RA-10, and RA-12.

Electrical conductivity of the groundwater measures the ability of groundwater to carry electrical currents (Table 9), which reflects the level of dissolved ions and metals in solution. After the injection, significant conductivity spikes in the two injection wells and the new monitoring wells M-1 and M-2. Conductivity characterize the activity and presence of ions in the water and thus the degree of sequestration of metals in solids. The data show that the wells experienced the greatest increases in conductivity were the five wells closest to the injection wells, including I-1, I-2, M-1, M-2, and LH-10 (Table 9). Conductivity values reached as high as 2,296 μS/cm the first week after injection in I-1, and M-1 followed with an increase in conductivity as high as 1,075 μS/cm the week after the injection. These were the wells that received the weak injection solution but also a greater volume of injection solution at 2000 gallons. I-2, recipient of the strong solution, and M-2, also displayed a significant rise in conductivity in the weeks after injection as well. However, the value was not as high for these wells as observed in I-1 and M-1. High conductivity values in those affected wells dropped close to background levels (i.e., a couple hundreds of μS/cm) two months after the injection. The remaining monitoring wells on site recorded consistent conductivity values over the year worth of sampling. The only well out of this group that showed a delayed upward shift in conductivity was the downgradient well LH-10, where injected plume reached there in one month after the injection. In 2017 the only well that registered a sharp jump in conductivity was I-1 in January with 616 μS/cm.

There are a set of parameters that were measured in the field that required the use of a variety of portable instruments. These parameters are alkalinity, dissolved sulfide concentration,

and concentration of ferrous iron. The methods by which we measured these have been previously described. The amount of alkalinity as $CaCO_3$ over the course of sampling is laid out in Table 10. Pre-injection groundwater alkalinity at the site ranged as low as 16 mg/L in LH-2, to 200 mg/L in LH-10. The month after the injection increased alkalinity concentration was observed, in four affected wells. In particular, I-1 and LH-10 showed significant spikes in alkalinity for the two weeks after injection. I-2 and M-2 had more moderate but noticeable gains in alkalinity. It should be noted that alkalinity cannot be measured directly in the field by the titration method as the pH values drop significantly below 5 when carbonate species in solution is dominated by H_2CO_3. However, in the following months alkalinity did not develop any sweeping changes or a broad variation over one year period.

Ferrous iron concentration was measured in the field immediately after collection of groundwater (Table 11). Pre-injection levels for ferrous iron ranged as low as 0.02 mg/L to a 1.58 mg/L high. Average ferrous iron of the ten wells on site prior to the injection was 0.77 mg/L. Considerable changes in ferrous iron concentration were observed in the first few weeks following the injection. The ferrous sulfate from the injection solution provided a boost in ferrous iron content in both the injection wells and monitoring wells. I-1, which received 2,000 gallons of the weak injection solution, reached ferrous iron concentrations of 54 mg/L one week after injection and a high of 138 mg/L two weeks after the injection. The monitoring well M-1 mirrored this response, where we recorded ferrous iron concentration at 99 mg/L just one week after injection and 92 mg/L two weeks after injection. The second injection well, I-2, had a less intense response to the injection compared to its counterpart. I-2 was given 1,000 gallons of the

strong injection solution, and peak ferrous iron concentration was at 51.6 mg/L one week after injection. Ferrous iron in M-2 was recorded at a peak concentration of 77 mg/L two weeks after the injection. Once the sulfate-reducing conditions were established on site, ferrous iron concentration in these four wells decreased after a span of several months. By the mid-summer ferrous iron concentration had reduced back to near the original pre-injection levels. The six remaining monitoring wells did not demonstrate sharp changes in the same way as the previously described wells. These wells, located farther away from the injection wells, had concentrations that were not heavily influenced over the year. Most ferrous iron concentrations in these wells were within the range of <1 mg/L of the pre-injection, background concentration.

The evolution of dissolved sulfide concentration in the site's ten wells is summarized in Table 12. Prior to the injection, levels of dissolved sulfide were quite low, with only M-1 and M-2 wells having a sulfide concentration greater than 0.1 mg/L. The input of the injection solution had an immediate impact on dissolved sulfide concentrations. In the injection well I-1, concentration of dissolved sulfide peaked at 6.02 mg/L, and the concentration for I-2 reached 0.48 mg/L one week after injection. Ferrous iron shows a similar trend, where I-1 received a higher volume of injection solution, and subsequently registered higher concentrations of both ferrous iron and dissolved sulfide compared to those of I-2. In fact sulfide concentration for I-2 did not peak until a month after the injection, recording a sulfide concentration of 1.4 mg/L in mid-March. The sharp increase of dissolved sulfide in the downgradient monitoring wells M-1, M-2, and LH-10 did not occur until one month after the injection, where we observed concentrations reaching 3.95, 4.45, and 2.25 mg/L respectively. Over the next several months,

sulfide concentrations gradually decreased to background level in the two injection wells and three monitoring wells in closest proximity downgradient. We observed another spike in sulfide concentration in all the wells expect for I-2 in the month of July (Table 12). This spike coincided with heavy rainfall events that occurred in June and early July. Sampling events in the fall showed a decrease in dissolved sulfide until November, where another spike in sulfide concentration occurred, this time only in the three monitoring wells M-1, M-2, and LH-10. December measurements also had high dissolved sulfide concentration in multiple wells, but data collected from the two sampling events in 2017 showed the concentration trending downward once again. The other five monitoring wells had limited responses to the injection in terms of sulfide concentration. LH-2, which is up gradient from the injection wells, appeared to register a change due to the injection in the few weeks following the injection, but these increases were not on a dramatic scale in the same fashion as the injection wells and downgradient monitoring wells. Sulfide concentration in RA-12, which is not a downgradient well, showed consistent measurements throughout the sampling period. RA-9, RA-10, and LH-5, located further downgradient, showed a substantial increase in the sulfide concentration one week after the injection.

Laboratory Analysis of Groundwater

Laboratory work focused on accurately and precisely evaluating parameters that could not be done while in the field. Our analysis of the groundwater that was collected from the industrial site was carried out using two main methods. The ICP-MS housed at Auburn

University was used to measure major cations (in parts per million) and trace elements (in parts per billion) in groundwater samples. The reported data in this paper has concentrations converted to mg/L. The lab at Test America was utilized to test for anion concentration, as well as measure the amount of dissolved organic carbon (DOC) in samples.

The DOC concentration in unaffected monitoring wells is consistent in magnitude. We did not observe significant shifts in concentration that contrasted from pre-injection levels. For much of the test period, DOC levels in these wells registered below 20 mg/L. In comparison, the injection wells (I-1 and I-2) and two closest downgradient monitoring wells (M-1 and M-2) experienced an increase in DOC up to hundreds of mg/L one week after the injection (Table 13). These elevated concentrations fall back down to background levels by April through the biodegradation of sulfate-reducing bacteria. There was a delayed increase in DOC in the affected downgradient monitoring well LH-10 up to 65 mg/L in May 2016, but by the end of the year the DOC concentration had again fallen near background levels.

The data for sulfate concentration are presented in Table 14. Background sulfate concentrations at the industrial site were low, the new injection wells recorded pre-injection sulfate concentration of 16 mg/L for I-1 and 25 mg/L for I-2. The injection of ferrous sulfate had a substantial impact on sulfate concentration in the four new wells at the industrial site. The greatest increase in sulfate concentration occurred in I-1 with 800 mg/L after one week and 330 mg/L the following week. This observation closely follows the trend that I-1 typically records higher peaks in concentrations for measured field and lab parameters. The four new wells drilled on site are the only wells to register sharp increases in sulfate concentration following the

injection. Sulfate concentration rapidly decreases over the course of the second month following the injection. Sulfate concentration falls to near background levels by late April and remain consistently in the low range for the remainder of the pilot test period.

Phosphate concentrations in ten wells are outlined in Table 15. A similar trend that was observed for sulfate concentration is reflected in the phosphate concentrations over the course of the experiment. For this parameter the largest concentration increases for wells I-1, I-2, LH-2, and M-1. M-2 has little to no response to the injection solution in terms of measured phosphate. As seen for sulfate concentration, phosphate concentration dropped back to pre-injection levels within two months after the injection.

Nitrate (Table 16) and chloride (Table 17) also exhibit a similar behavior to DOC and phosphate of quick increase in concentration one week after injection, and then rapidly shift back to pre-injection levels over the first two months of the experiment.

The parameters measured in the ICP-MS laboratory at Auburn University helped further examine the evolution of the hydrogeochemical environment. The ICP-MS was used to measure the concentrations of major cations and trace elements in groundwater samples. Total iron concentrations in the injection and affected monitoring wells reflect significant increases in concentration soon after the injection (Table 18). I-1, I-2, and M-1 each recorded total Fe concentration higher than 100 mg/L one week after the injection, compared to less than 1 mg/L prior to the injection. I-1 again registered the highest concentration at the industrial site with a peak iron concentration of 483 mg/L. The new injection wells, and affected monitoring wells hydrologically downgradient, again showed the largest increases in iron concentration two weeks

after the injection. Iron levels in these wells then decreased to near pre-injection levels (a few mg/L) by the end of spring 2016, the other monitoring wells farther downgradient did not respond with significant jumps in iron concentration and instead remained close to background levels throughout the sampling period.

Calcium, magnesium, sodium, potassium, and aluminum (Tables 19-23) all follow the same pattern of concentration change as was described for iron. There was a sharp rise in concentration for each of these parameters as a result of the contents of the injection solutions, which contained elevated levels of select cations (Tables 2 and 3). This spike in concentration lasted one to two weeks after the injection in the four new wells, followed by a return to pre-injection levels within the next two months. Unaffected monitoring wells farther away from the injection site do not register major shifts in concentration from original pre-injection measurements.

Sequestration of Arsenic

Unfiltered arsenic (As) concentration prior to the injection ranged from 0.19-1.2 mg/L in the ten wells sampled (Table 24). These values range well above the established regulatory standard of 0.05 mg/L of arsenic that applies to this industrial site. After injection a spike in arsenic concentrations was observed in I-1 and I-2. The nearest downgradient monitoring wells M-1, M-2, and LH-10 recorded gradual decreases in unfiltered arsenic concentrations beginning two weeks after the injection. For the next eight months arsenic levels were recorded below their pre-injection values for these three treated wells. Both M-1 and LH-10 had at least one sampling

event with concentrations below or near the regulatory clean-up goal of 0.05 mg/L. The lowest arsenic concentration for LH-10 was 0.01 mg/L, and the arsenic concentrations in M-1 fell to 0.03 mg/L in the month of August. It is also interesting to note that starting in late spring and into the summer we recorded a significant drop in arsenic in the downgradient well RA-9, a well outside the fenced perimeter at the industrial site. The RA-9 well had pre-injection arsenic level of 0.84 mg/L, and it then recorded decreased arsenic levels beginning in April and had a minimum arsenic level of 0.11 mg/L in September 2016. The remaining monitoring wells on site did not showcase any drastic increases or decreases in arsenic concentration at their respective locations.

The filtered arsenic concentration data showcase a similar story to that of the unfiltered arsenic data. Prior to the injection experiment arsenic concentration ranged from 0.12-1.09 mg/L in the wells monitored (Table 25). The injection created the expected spike in As concentration for the injection wells, followed by a subsequent fall in As concentration to near background levels in the third week post-injection. Within three weeks after the injection, significant decreases in arsenic concentrations were observed for the three affected downgradient wells (M-1, M-2, and LH-10). Within two months after the injection, these three wells all had arsenic levels drop below 0.05 mg/L, achieving this site's established clean-up goal. LH-10 had a concentration of 0.04 mg/L, M-1 and M-2 both had concentrations of 0.02 mg/L. Arsenic levels in these downgradient wells remained below the 0.05 mg/L threshold for another six months through the month of October. It was not until the November arsenic levels rise above 0.05 mg/L for M-1 and M-2 wells. The arsenic level in LH-10 remains below the regulation limit of 0.05

mg/L over the entire one year period after the injection. Much like the unfiltered arsenic data the remaining monitoring wells did not show significant increase or decrease in their arsenic levels over the course of the pilot test. Also similar to the unfiltered data was the shifts in RA-9 arsenic concentration. In our filtered samples a decrease in arsenic concentration was observed in RA-9 about two months after the initial injection. The As concentration for RA-9 remained low relative to its background levels for about six months until the November sampling event.

As(III) and As(V) concentrations in filtered samples were measured over the course of the experiment to examine the speciation of arsenic in groundwater (Tables 26 and 27). The As(III) concentration was measured in the water samples that was passed through an arsenic speciation cartridge (see Method section). As(III) concentration follows a similar pattern to that of total arsenic concentration. Results show the fall of As(III) concentration in the three downgradient wells that closely mirrors both filtered and unfiltered total As concentration trends. Tables 26 and 27 show that As(III) is the dominant dissolved arsenic species in the groundwater under reducing conditions, with consistently higher concentration of As(III) than that of As(V). These analytical results are consistent with the geochemical models and field pH-Eh data where dominant arsenic aqueous species are found in the form of $As(OH)_3$ or As(III) under reducing conditions.

Date	I-1	I-2	LH-2	LH-5	LH-10	M-1	M-2	RA-9	RA-10	RA-12
2/15/2016	3.6	2.7	2.8	3.0	2.9	1.8	1.5	3.2	2.8	3.1
2/24/2016	3.2	2.8	2.7	4.3	4.0	3.1	2.0	1.5	1.2	2.7
3/2/2016	3.5	3.5	3.4	4.8	4.6	3.3	3.4	2.0	1.6	2.3
3/9/2016	3.6	3.8	3.6	4.9	4.6	3.4	3.5	2.1	1.8	3.4
3/17/2016	3.7	3.6	3.9	4.7	7.5	3.5	3.4	2.0	1.9	2.6
4/21/2016	3.0	3.0	3.3	4.3	6.9	3.0	3.2	1.5	1.7	1.9
5/19/2016	4.5	4.2	4.2	4.6	6.0	4.5	4.3	3.0	2.8	3.4
6/15/2016	3.7	3.7	3.6	5.0	4.8	3.5	3.3	2.2	1.8	3.6
7/20/2016	4.3	4.5	4.4	5.0	5.5	4.2	4.0	4.3	4.0	4.3
8/17/2016	3	2.7	2.8	3.2	3.5	2.6	2.5	3.0	2.5	2.6
9/21/2016	3.1	3.5	3.7	4.0	4.4	3.3	3.3	3.3	3.1	3.6
10/26/2016	5.3	5.5	5.3	5.3	6.9	5.2	5.2	5.1	4.9	5.5
11/15/2016	5.6	5.9	5.8	5.5	7.1	5.6	5.8	4.6	3.8	5.9
12/13/2016	4.8	5.0	4.8	4.7	5.7	4.6	4.7	4.6	4.4	5.0
1/25/2017	2.6	2.5	2.6	2.3	3.8	2.6	2.6	2.8	2.4	2.7
2/15/2017	3.2	3.4	3.3	2.4	4.4	3.5	3.1	3.0	2.4	3.5

Table 4. Time series of water table depth (feet) in groundwater wells.

Month	Precipitation Total (in)
Jan-16	18.08
Feb-16	2.32
Mar-16	6.91
Apr-16	6.32
May-16	2.59
Jun-16	8.84
Jul-16	3.82
Aug-16	15.59
Sep-16	8.05
Oct-16	0.2
Nov-16	0.21
Dec-16	5.17
Jan-17	4.78
Feb-17	5.28

Table 5. Monthly precipitation totals (in) near the industrial site (data sourced from noaa.gov)

Date	I-1	I-2	LH-2	LH-5	LH-10	M-1	M-2	RA-9	RA-10	RA-12
2/15/2016	125.7	125.5	15.5	114.7	-69.0	8.3	55.0	1.5	105.3	49.5
2/24/2016	-142.1	-236.2	-25.5	52.0	-87.0	-203.5	-159.8	27.0	314.0	5.9
3/2/2016	-37.0	-20.0	21.3	49.0	-21.8	20.6	-15.4	31.0	51.0	73.4
3/9/2016	-22.1	-69.0	69.0	59.0	-79.6	-62.3	-66.2	57.0	50.0	137.4
3/17/2016	1.0	-34.0	46.0	51.0	-97.0	-7.0	-22.0	51.0	35.0	49.0
4/21/2016	-26.0	-23.0	3.0	51.0	-140.0	-11.0	-34.0	32.0	28.0	32.0
5/19/2016	-29.1	-40.1	-1.2	-31.0	-104.5	-16.8	-50.0	45.0	16.0	20.0
6/15/2016	-104.7	-23.2	-28.4	-62.0	-120.0	-92.7	-99.7	-2.0	-6.0	-30.0
7/20/2016	-145.4	320.8	-5.4	-56.6	-117.8	-100.0	-114.1	30.1	-2.3	52.1
8/17/2016	-8.8	68.1	-0.3	-38.7	-102.1	-85.4	-97.2	-11.0	14.4	-25.5
9/21/2016	-57.7	17.0	11.0	-12.2	2.0	-14.4	-1.6	-43.7	-35.5	13.8
10/26/2016	-38	44.2	13.7	-53.2	-56.2	-163.4	-32.0	16.5	-34.5	78.7
11/15/2016	-40.9	79.7	-75.8	-45.8	-93.7	-141.0	-69.0	-4.5	-6.7	80.2
12/13/2016	22.7	204.4	-10.6	-95.2	-135.9	-194.1	-132.5	42.8	33.1	63.2
1/25/2017	455.7	87.9	6.1	21.8	14.6	-7.5	25.0	183.4	26.1	92.2
2/15/2017	342.2	-18.1	10.0	24.9	-62.2	-86.4	-36.6	144.0	33.7	67.7

Table 6. Time series of field measured ORP (mV) for groundwater in monitoring wells.

Date	I-1	I-2	LH-2	LH-5	LH-10	M-1	M-2	RA-9	RA-10	RA-12
2/15/2016	6.24	6.21	5.45	6.14	7.00	5.59	5.69	5.91	6.64	5.53
2/24/2016	8.00	8.32	5.66	6.00	7.09	7.82	8.22	5.70	6.50	5.27
3/2/2016	4.78	5.81	5.67	5.96	5.99	4.33	4.75	5.73	6.51	6.40
3/9/2016	4.73	5.85	5.34	5.92	6.72	4.46	5.04	5.62	6.53	5.46
3/17/2016	5.48	6.04	5.30	5.95	6.66	4.57	4.97	5.54	6.56	5.40
4/21/2016	6.07	6.02	5.41	5.71	6.59	4.96	5.30	5.26	6.63	5.26
5/19/2016	6.13	6.33	5.33	6.02	6.12	4.99	5.47	5.58	6.67	5.48
6/15/2016	6.29	6.42	5.77	6.11	5.88	5.53	5.80	5.79	6.99	6.36
7/20/2016	6.26	5.43	5.70	6.26	6.64	5.46	5.60	5.72	6.93	6.13
8/17/2016	5.29	6.61	5.59	6.14	6.00	5.47	6.01	5.46	6.75	6.80
9/21/2016	6.07	6.25	5.22	6.06	5.83	5.38	5.58	5.37	6.68	5.56
10/26/2016	6.37	6.09	5.12	6.16	5.71	5.53	5.40	5.92	6.78	5.69
11/15/2016	6.30	5.74	5.10	6.22	5.68	5.65	5.48	6.08	6.88	5.74
12/13/2016	5.58	4.25	5.17	6.38	5.76	5.79	5.53	6.06	6.60	5.71
1/25/2017	3.16	5.97	5.18	6.42	5.90	5.57	5.48	5.80	6.63	6.01
2/15/2017	3.46	6.42	5.23	6.32	5.85	5.51	5.52	5.62	6.52	5.91

Table 7. Time series of field measured pH for groundwater wells.

Date	I-1	I-2	LH-2	LH-5	LH-10	M-1	M-2	RA-9	RA-10	RA-12
2/15/2016	1.47	1.01	0.17	0.38	0.23	0.13	0.15	0.24	0.34	0.13
2/24/2016	0.07	0.11	0.12	0.17	0.06	0.06	0.12	0.21	0.45	0.11
3/2/2016	0.16	0.20	0.11	0.06	0.09	0.07	0.12	0.06	0.27	0.26
3/9/2016	0.08	0.09	0.10	0.05	0.17	0.72	0.16	0.09	0.04	0.27
3/17/2016	0.08	0.03	0.06	0.10	0.06	0.14	0.10	0.09	0.04	0.07
4/21/2016	0.05	0.12	0.19	0.14	0.03	0.14	0.12	0.21	0.15	0.08
5/19/2016	0.06	0.25	0.11	0.16	0.07	0.12	0.09	0.23	0.05	0.18
6/15/2016	0.07	0.54	0.08	0.09	0.08	0.11	0.08	0.10	0.12	0.40
7/20/2016	0.20	0.42	0.26	0.18	0.22	0.14	0.17	0.15	0.13	0.20
8/17/2016	0.10	0.91	0.06	0.08	0.07	0.08	0.08	0.10	0.05	0.09
9/21/2016	0.04	0.26	0.06	0.06	0.06	0.08	0.07	0.05	0.04	0.10
10/26/2016	0.08	1.78	0.05	0.06	0.05	0.06	0.08	4.83	0.05	0.19
11/15/2016	0.02	0.25	0.03	0.05	0.03	0.05	0.05	3.20	1.22	1.53
12/13/2016	1.47	0.15	0.11	0.18	0.08	0.12	0.13	3.78	4.88	0.20
1/24/2017	1.80	5.81	0.07	0.29	0.05	0.08	0.10	2.37	1.03	2.04
2/15/2017	0.35	4.81	0.06	0.12	0.05	0.07	0.06	0.91	0.76	0.12

Table 8: Time series of dissolved oxygen concentration (mg/L) in groundwater wells.

Date	I-1	I-2	LH-2	LH-5	LH-10	M-1	M-2	RA-9	RA-10	RA-12
2/15/2016	1.47	1.01	0.17	0.38	0.23	0.13	0.15	0.24	0.34	0.13
2/24/2016	0.07	0.11	0.12	0.17	0.06	0.06	0.12	0.21	0.45	0.11
3/2/2016	0.16	0.20	0.11	0.06	0.09	0.07	0.12	0.06	0.27	0.26
3/9/2016	0.08	0.09	0.10	0.05	0.17	0.72	0.16	0.09	0.04	0.27
3/17/2016	0.08	0.03	0.06	0.10	0.06	0.14	0.10	0.09	0.04	0.07
4/21/2016	0.05	0.12	0.19	0.14	0.03	0.14	0.12	0.21	0.15	0.08
5/19/2016	0.06	0.25	0.11	0.16	0.07	0.12	0.09	0.23	0.05	0.18
6/15/2016	0.07	0.54	0.08	0.09	0.08	0.11	0.08	0.10	0.12	0.40
7/20/2016	0.20	0.42	0.26	0.18	0.22	0.14	0.17	0.15	0.13	0.20
8/17/2016	0.10	0.91	0.06	0.08	0.07	0.08	0.08	0.10	0.05	0.09
9/21/2016	0.04	0.26	0.06	0.06	0.06	0.08	0.07	0.05	0.04	0.10
10/26/2016	0.08	1.78	0.05	0.06	0.05	0.06	0.08	4.83	0.05	0.19
11/15/2016	0.02	0.25	0.03	0.05	0.03	0.05	0.05	3.20	1.22	1.53
12/13/2016	1.47	0.15	0.11	0.18	0.08	0.12	0.13	3.78	4.88	0.20
1/25/2017	1.80	5.81	0.07	0.29	0.05	0.08	0.10	2.37	1.03	2.04
2/15/2017	0.35	4.81	0.06	0.12	0.05	0.07	0.06	0.91	0.76	0.12

Table 9. Time series of electrical conductivity (µS/cm) in groundwater wells.

Date	I-1	I-2	LH-2	LH-5	LH-10	M-1	M-2	RA-9	RA-10	RA-12
2/15/2016	53	45	10	48	161	20	22	22	110	13
2/24/2016	N/A	43	10	70	169	N/A	120	34	160	21
3/2/2016	110	74	16	56	166	N/A	56	N/A	150	28
3/9/2016	65	78	200	25	162	21	61	17	98	264
3/17/2016	67	79	15	22	56	56	40	20	94	12
4/21/2016	48	78	15	33	156	62	53	18	94	22
5/19/2016	71	79	16	30	56	50	65	24	82	29
6/15/2016	31	32	50	21	60	40	120	18	70	160
7/20/2016	62	N/A	25	18	76	44	41	12	55	60
8/17/2016	N/A	53	21	20	114	44	39	14	55	65
9/21/2016	33	76	33	20	124	53	43	11	110	65
10/26/2016	116	65	17	20	77	68	48	35	150	47
11/15/2016	128	31	12	16	69	68	47	43	150	48
12/13/2016	27	10	22	20	62	92	33	47	110	26
1/25/2017	N/A	25	20	19	69	48	38	29	69	71
2/15/2017	N/A	70	21	22	82	37	25	34	92	76

Table 10. Time series of field measured alkalinity (mg/L) for groundwater wells.

Date	I-1	I-2	LH-2	LH-5	LH-10	M-1	M-2	RA-9	RA-10	RA-12
2/15/2016	0.47	0.23	0.49	0.40	1.58	0.78	0.76	1.56	0.02	1.37
2/24/2016	53.80	51.60	0.46	0.02	1.71	99.00	41.40	0.03	0.02	1.32
3/2/2016	138.50	29.50	0.65	0.02	1.70	92.00	77.00	0.02	0.02	1.14
3/9/2016	40.50	10.50	0.68	0.09	1.65	51.50	42.00	1.10	0.06	0.81
3/17/2016	2.96	2.76	0.85	0.26	0.92	5.00	4.50	1.17	0.18	1.33
4/21/2016	4.80	1.31	0.82	0.49	1.39	4.50	6.20	2.40	0.09	1.49
5/19/2016	3.20	1.24	0.29	0.33	1.56	3.40	5.30	2.80	0.12	1.34
6/15/2016	2.70	1.12	0.37	0.17	1.27	2.70	0.33	2.00	0.10	0.71
7/20/2016	1.90	1.24	0.20	0.11	1.11	0.24	0.41	1.70	0.15	0.32
8/17/2016	2.50	1.27	0.21	0.11	1.11	2.50	0.40	1.40	0.11	0.97
9/21/2016	2.00	0.88	0.27	0.10	1.42	1.80	0.24	1.50	0.10	1
10/26/2016	1.80	1.07	0.35	0.10	1.25	1.80	0.34	1.50	0.09	0.13
11/15/2016	2.30	0.99	0.22	0.08	1.07	1.80	0.24	1.40	0.02	0.14
12/13/2016	1.30	0.88	0.22	0.09	1.11	1.40	0.27	1.70	0.08	0.32
1/25/2017	1.72	0.17	0.61	0.11	0.67	7.95	2.12	1.66	0.07	0.01
2/15/2017	1.08	0.16	0.39	0.08	0.89	5.52	0.40	1.50	0.04	0.00

Table 11. Time series of field measured ferrous iron concentration (mg/L) in groundwater wells.

Date	I-1	I-2	LH-2	LH-5	LH-10	M-1	M-2	RA-9	RA-10	RA-12
2/15/2016	0.044	0.018	0.036	0.006	0.057	0.128	0.128	0.079	0.001	0.023
2/24/2016	6.020	0.480	0.032	2.800	0.050	1.500	0.080	6.300	1.100	0.039
3/2/2016	0.350	0.200	0.240	1.100	0.095	2.600	0.900	2.000	1.100	0.024
3/9/2016	0.550	0.450	0.284	0.010	0.720	3.950	4.450	0.010	0.010	0.012
3/17/2016	0.270	1.400	0.250	0.010	2.250	1.750	1.600	0.010	0.010	0.010
4/21/2016	0.250	0.800	0.250	0.010	0.010	0.400	0.250	0.010	0.200	0.030
5/19/2016	0.022	0.100	0.319	0.010	3.240	0.128	0.067	0.010	0.300	0.052
6/15/2016	0.687	0.088	0.219	0.010	0.518	0.532	0.407	0.010	0.010	0.068
7/20/2016	1.750	0.017	0.207	0.010	3.250	6.500	6.100	0.010	0.010	0.011
8/17/2016	0.440	0.064	0.240	0.010	1.690	1.400	3.110	0.010	0.010	0.024
9/21/2016	0.250	0.080	0.200	0.010	1.550	0.800	1.070	0.010	0.010	0.100
10/26/2016	0.070	0.140	0.200	0.010	3.750	2.200	2.650	0.010	0.010	0.030
11/15/2016	0.110	0.210	0.160	0.010	4.240	7.600	5.520	0.010	0.010	0.040
12/13/2016	0.030	0.060	0.160	0.010	4.100	8.260	6.500	0.010	0.010	0.050
1/25/2017	0.010	0.100	0.100	0.010	2.240	7.900	3.850	0.010	0.010	0.030
2/15/2017	0.050	0.060	0.090	0.010	2.320	5.600	2.160	0.010	0.010	0.020

Table 12. Time series of field measured dissolved sulfide concentration (mg/L) in groundwater wells.

Date	I-1	I-2	LH-2	LH-5	LH-10	M-1	M-2	RA-9	RA-10	RA-12
2/15/2016	10.0	15.0	4.9	26.0	3.9	8.0	17.0	46.0	6.7	22.0
2/24/2016	1600.0	340.0	5.4	17.0	4.2	660.0	200.0	34.0	5.3	20.0
3/2/2016	820.0	52.0	5.1	17.0	3.8	570.0	370.0	26.0	5.7	18.0
3/9/2016	310.0	29.0	5.7	15.0	4.4	460.0	250.0	24.0	5.8	17.0
3/17/2016	120.0	23.0	5.0	16.0	14.0	410.0	170.0	25.0	5.0	17.0
4/21/2016	21.0	12.0	6.7	15.0	21.0	95.0	56.0	30.0	4.5	24.0
5/19/2016	20.0	10.0	7.3	17.0	65.0	94.0	51.0	26.0	5.8	19.0
6/15/2016	13.0	9.7	6.9	15.0	58.0	83.0	38.0	17.0	5.3	19.0
7/20/2016	16.0	1.3	8.7	21.0	53.0	57.0	30.0	16.0	39.0	29.0
8/17/2016	3.3	13.0	5.7	11.0	39.0	36.0	17.0	34.0	4.5	19.0
9/21/2016	7.9	8.3	4.4	7.5	9.2	19.0	13.0	18.0	4.3	18.0
10/26/2016	5.9	9.4	5.5	6.5	16.0	28.0	17.0	10.0	4.1	11.0
11/15/2016	5.4	8.5	5.6	5.9	13.0	28.0	17.0	9.1	4.3	11.0
12/13/2016	2.6	2.8	4.3	5.1	14.0	17.0	14.0	7.3	5.7	11.0
1/24/2017	2.5	13.0	4.2	5.4	10.0	12.0	11.0	13.0	6.4	15.0
2/15/2017	2.3	8.3	3.9	5.3	9.3	8.1	12.0	11.0	4.8	15.0

Table 13. Time series of dissolved organic carbon concentration (mg/L) in groundwater wells.

Date	I-1	I-2	LH-2	LH-5	LH-10	M-1	M-2	RA-9	RA-10	RA-12
2/15/2016	16.0	25.0	17.0	16.0	20.0	21.0	27.0	1.4	14.0	27.0
2/24/2016	800.0	180.0	18.0	25.0	21.0	340.0	150.0	1.4	12.0	30.0
3/2/2016	330.0	21.0	15.0	20.0	19.0	210.0	310.0	1.4	11.0	25.0
3/9/2016	34.0	13.0	14.0	34.0	16.0	130.0	150.0	1.4	8.6	26.0
3/17/2016	13.0	12.0	15.0	24.0	5.4	140.0	56.0	1.4	4.6	30.0
4/21/2016	1.4	1.4	14.0	9.8	4.0	5.8	1.4	1.4	27.0	35.0
5/19/2016	1.4	21.0	15.0	76.0	1.4	4.6	1.4	1.4	4.7	13.0
6/15/2016	32.0	28.0	14.0	12.0	5.6	9.7	15	61.0	10.0	26.0
7/20/2016	67.0	74.0	16.0	18.0	14.0	1.4	1.6	31.0	13.0	8.9
8/17/2016	53.0	14.0	14.0	23.0	12.0	18.0	44.0	26.0	1.4	46.0
9/21/2016	14.0	5.8	13.0	47.0	8.0	15.0	20.0	6.2	6.5	14.0
10/26/2016	29.0	28.0	18.0	20.0	12.0	25.0	14.0	38.0	6.9	4.7
11/15/2016	56.0	49.0	19.0	28.0	14.0	1.4	14.0	22.0	11.0	10.0
12/13/2016	86.0	93.0	18.0	26.0	14.0	32.0	20.0	33.0	8.0	11.0
1/25/2017	140.0	23.0	18.0	19.0	15.0	99.0	23.0	26.0	9.5	24.0
2/15/2017	49.0	9.6	15.0	13.0	12.0	74.0	18.0	25.0	18.0	17.0

Table 14. Time series of sulfate concentration (mg/L) in groundwater wells.

Date	I-1	I-2	LH-2	LH-5	LH-10	M-1	M-2	RA-9	RA-10	RA-12
2/15/2016	0.10	0.10	0.10	0.10	0.10	0.10	0.21	0.10	0.10	0.10
2/24/2016	22.00	4.00	5.00	0.10	0.10	1.00	0.10	0.10	0.10	0.10
3/2/2016	1.80	0.10	0.10	0.10	0.10	0.81	0.10	0.10	0.10	0.10
3/9/2016	1.70	0.17	0.10	0.10	0.10	0.69	0.10	0.10	0.10	0.10
3/17/2016	2.30	1.50	0.06	0.05	0.22	1.50	0.13	0.03	0.24	0.04
4/21/2016	0.76	0.17	0.04	0.04	0.24	1.10	0.15	0.01	0.15	0.06
5/19/2016	0.36	0.13	0.08	0.03	0.20	0.49	0.17	0.02	0.20	0.07
6/15/2016	0.22	0.20	0.09	0.09	0.19	0.28	0.16	0.02	0.12	0.04
7/20/2016	0.21	0.01	0.18	0.06	0.13	0.12	0.26	0.01	0.14	0.04
8/17/2016	0.31	0.08	0.06	0.07	0.15	0.37	0.14	0.01	0.06	0.02
9/21/2016	0.32	0.09	0.06	0.05	0.21	0.43	0.36	0.01	0.28	0.05
10/26/2016	0.16	0.42	0.12	0.11	0.19	0.12	0.27	0.10	0.35	0.12
11/15/2016	0.34	0.51	0.21	0.06	0.19	0.09	0.15	0.37	0.22	0.22
12/13/2016	0.16	0.25	0.17	0.03	0.18	0.31	0.25	0.15	0.16	0.16
1/25/2017	0.01	0.05	0.13	0.05	0.18	0.20	0.22	0.04	0.14	0.05
2/15/2017	0.01	0.04	0.09	0.23	0.17	0.22	0.29	0.02	0.24	0.05

Table 15. Time series of ortho-phosphate concentration (mg/L) in groundwater wells.

Date	I-1	I-2	LH-2	LH-5	LH-10	M-1	M-2	RA-9	RA-10	RA-12
2/15/2016	0.022	0.028	0.024	0.014	0.014	0.014	0.012	0.018	0.022	0.013
2/24/2016	0.120	0.016	0.820	0.020	0.016	0.230	0.017	0.014	0.024	0.014
3/2/2016	0.150	0.025	0.024	0.024	0.026	0.130	0.012	0.023	0.036	0.024
3/9/2016	0.012	0.012	0.022	0.022	0.012	0.012	0.012	0.012	0.023	0.012
3/17/2016	0.018	0.018	0.018	0.018	0.018	0.018	0.018	0.018	0.018	0.018
4/21/2016	0.018	0.018	0.018	0.018	0.018	0.018	0.018	0.018	0.018	0.018
5/19/2016	0.018	0.018	0.018	0.018	0.018	0.018	0.018	0.018	0.018	0.018
6/15/2016	0.018	0.021	0.018	0.018	0.018	0.029	0.018	0.018	0.018	0.018
7/20/2016	0.018	0.018	0.018	0.018	0.018	0.018	0.018	0.018	0.028	0.018
8/17/2016	0.018	0.037	0.018	0.018	0.018	0.018	0.025	0.018	0.065	0.018
9/21/2016	0.018	0.027	0.018	0.018	0.018	0.018	0.018	0.018	0.018	0.018
10/26/2016	0.018	0.028	0.018	0.018	0.018	0.018	0.018	0.018	0.018	0.018
11/15/2016	0.018	0.018	0.018	0.018	0.018	0.018	0.018	0.140	0.018	0.018
12/13/2016	0.036	0.018	0.018	0.018	0.018	0.018	0.018	0.160	0.018	0.018
1/25/2017	0.120	0.086	0.018	0.049	0.018	0.018	0.018	0.032	0.049	0.018
2/15/2017	0.030	0.018	0.018	0.042	0.018	0.018	0.018	0.018	0.041	0.018

Table 16. Time series of nitrate concentration (mg/L) in groundwater wells.

Date	I-1	I-2	LH-2	LH-5	LH-10	M-1	M-2	RA-9	RA-10	RA-12
2/15/2016	8.0	20.0	13.0	26.0	17.0	10.0	22.0	11.0	5.3	40.0
2/24/2016	180.0	51.0	13.0	28.0	17.0	93.0	43.0	11.0	2.8	31.0
3/2/2016	110.0	20	14.0	24.0	18.0	79.0	64.0	11.0	3.6	30.0
3/9/2016	39.0	15	12.0	35.0	17.0	63.0	47.0	12.0	3.7	29.0
3/17/2016	21.0	15	13.0	23.0	19.0	70.0	42.0	14.0	3.1	31.0
4/21/2016	11.0	11	14.0	20.0	19.0	31.0	31.0	12.0	3.1	24.0
5/19/2016	8.5	7.9	10.0	16.0	23.0	34.0	30.0	11.0	2.7	15.0
6/15/2016	5.1	6.0	8.6	8.3	24.0	26.0	22.0	10.0	2.2	16.0
7/20/2016	3.5	2.8	7.8	4.8	22.0	26.0	23.0	7.6	2.8	15.0
8/17/2016	2.8	7.7	9.9	11.0	22.0	17.0	9.9	22	1.8	35.0
9/21/2016	3.8	3.6	11.0	6.3	19.0	12.0	11.0	6.7	1.5	18.0
10/26/2016	3.3	5.1	7.9	2.7	17.0	15.0	10.0	6.6	1.7	9.1
11/15/2016	4.6	7.8	8.9	3.7	17.0	15.0	12.0	4.9	2.7	9.2
12/13/2016	3.9	7.9	9.9	3.6	16.0	12.0	13.0	4.4	5.6	11.0
1/24/2017	4.0	9.9	9.8	4.0	18.0	8.3	11.0	7.6	8.0	12.0
2/21/2017	3.9	7.9	11.0	3.9	19.0	7.5	9.9	7.7	32.0	19.0

Table 17. Time series of chloride concentration (mg/L) in groundwater wells.

Date	I-1	I-2	LH-2	LH-5	LH-10	M-1	M-2	RA-9	RA-10	RA-12
2/15/2016	0.310	0.412	0.417	0.495	1.506	0.685	0.589	1.609	0.017	1.385
2/24/2016	483.417	120.942	0.446	0.694	0.870	106.473	10.712	1.569	0.010	1.320
3/2/2016	195.185	21.634	0.622	0.416	1.755	91.313	86.459	1.306	0.090	1.278
3/9/2016	68.266	12.435	0.586	0.521	1.699	70.739	52.333	1.187	0.171	1.276
3/17/2016	28.120	8.970	0.658	0.252	1.269	57.505	29.789	0.945	0.028	1.320
4/21/2016	4.191	1.299	0.629	0.528	1.162	9.392	7.826	2.101	0.161	1.351
5/19/2016	2.591	2.959	0.668	2.160	1.339	10.385	6.548	1.103	0.119	1.350
6/15/2016	6.890	7.923	0.548	2.005	1.172	11.078	7.185	1.782	0.103	0.718
7/20/2016	8.319	3.544	0.576	3.678	1.114	7.502	4.343	0.375	0.093	0.329
8/17/2016	21.113	1.627	0.496	3.716	1.038	5.177	6.041	1.589	0.085	1.003
9/21/2016	3.004	0.192	0.522	3.225	1.055	4.133	3.445	1.192	0.820	1.065
10/26/2016	0.668	0.456	0.499	2.473	0.925	4.288	3.055	0.131	0.478	0.241
11/15/2016	0.457	0.740	0.499	3.174	0.878	4.199	3.427	0.076	0.035	0.197
12/13/2016	0.498	18.192	0.550	4.932	0.806	3.214	4.095	0.110	0.028	0.506
1/25/2017	6.962	0.307	0.483	1.678	0.694	8.164	3.89	0.083	0.024	0.052
2/15/2017	5.091	0.293	0.443	1.821	0.681	7.276	3.22	0.162	0.06	0.224

Table 18. Time series of total iron concentration (mg/L) in filtered groundwater.

Date	I-1	I-2	LH-2	LH-5	LH-10	M-1	M-2	RA-9	RA-10	RA-12
2/15/2016	25.160	33.253	9.966	33.091	72.756	14.445	19.354	15.248	56.331	18.668
2/24/2016	78.223	31.595	9.902	33.913	33.495	77.490	83.182	14.257	59.616	18.141
3/2/2016	68.240	28.442	10.179	28.870	76.082	70.652	109.075	14.075	58.280	18.061
3/9/2016	34.987	29.734	9.531	39.436	58.052	77.574	62.003	14.189	52.640	19.193
3/17/2016	29.213	31.136	9.762	32.241	73.630	62.194	42.903	12.569	45.418	18.320
4/21/2016	19.015	30.289	9.575	19.975	84.690	14.565	14.201	8.398	70.543	21.746
5/19/2016	27.744	35.220	7.935	43.749	98.872	15.467	14.427	9.719	45.152	13.667
6/15/2016	24.499	24.895	7.923	24.560	93.465	19.682	17.590	25.460	49.626	24.637
7/20/2016	48.687	28.123	8.191	28.641	57.119	19.018	15.142	15.889	59.797	27.808
8/17/2016	13.023	26.890	8.048	28.089	74.458	18.651	18.016	17.275	23.906	36.532
9/21/2016	17.789	29.746	8.506	42.485	84.792	11.988	10.905	6.359	45.944	31.937
10/26/2016	51.901	31.354	8.162	23.537	47.649	18.311	9.137	25.247	57.626	18.055
11/15/2016	54.308	24.486	8.591	25.628	47.517	23.128	11.164	20.417	54.969	15.313
12/13/2016	42.184	24.120	9.036	45.086	39.856	20.586	11.739	25.865	39.041	14.789
1/25/2017	25.235	15.102	8.287	36.712	35.699	34.493	10.973	14.235	36.348	28.203
2/15/2017	14.962	24.631	7.880	35.673	53.574	23.304	8.647	15.604	35.940	27.378

Table 19. Time series of calcium concentration (mg/L) in filtered groundwater.

Date	I-1	I-2	LH-2	LH-5	LH-10	M-1	M-2	RA-9	RA-10	RA-12
2/15/2016	1.904	3.586	1.542	3.613	3.800	1.834	3.018	1.941	3.864	6.668
2/24/2016	28.556	8.090	1.633	3.438	3.340	16.971	11.637	1.876	4.398	5.095
3/2/2016	18.569	3.814	1.650	3.080	3.947	15.943	17.066	1.947	4.380	5.080
3/9/2016	7.535	3.560	1.579	4.399	4.180	14.943	10.696	1.967	4.259	5.196
3/17/2016	3.978	3.570	1.533	3.168	4.252	12.256	6.827	2.003	3.536	5.207
4/21/2016	1.507	3.355	1.643	2.318	4.992	2.421	2.818	1.979	3.894	4.025
5/19/2016	2.351	3.178	1.149	5.438	7.498	2.553	2.541	2.104	3.197	3.255
6/15/2016	1.905	1.955	1.223	2.773	6.617	3.008	2.992	4.276	2.674	3.975
7/20/2016	3.218	2.015	1.151	3.143	5.540	2.409	2.275	3.461	3.004	3.585
8/17/2016	1.275	2.293	1.298	2.882	5.764	1.891	2.506	3.959	1.260	5.990
9/21/2016	1.423	2.200	1.376	3.581	5.549	1.453	1.421	1.533	2.476	3.101
10/26/2016	3.302	2.138	1.068	2.297	4.133	1.892	1.214	3.277	2.830	2.621
11/15/2016	3.236	1.672	1.177	2.358	3.795	2.182	1.431	2.275	2.715	2.417
12/13/2016	2.338	1.735	1.367	3.970	3.461	1.897	1.432	2.542	2.644	2.286
1/25/2017	1.788	1.302	1.249	1.973	3.014	2.852	1.382	2.255	2.397	3.483
2/15/2017	0.875	1.874	1.160	2.237	3.172	2.265	1.022	2.179	2.727	3.192

Table 20. Time series of magnesium concentration (mg/L) in filtered groundwater.

Date	I-1	I-2	LH-2	LH-5	LH-10	M-1	M-2	RA-9	RA-10	RA-12
2/15/2016	3.939	8.483	8.987	18.986	18.577	7.227	11.671	6.989	4.041	20.965
2/24/2016	15.395	9.774	9.276	15.667	12.604	12.775	15.350	6.366	2.040	15.508
3/2/2016	11.388	7.623	9.223	14.492	18.497	12.523	15.057	7.081	1.928	15.225
3/9/2016	6.378	6.632	9.017	20.188	14.154	11.130	13.745	7.072	1.731	14.969
3/17/2016	3.134	6.027	8.939	12.453	15.300	9.730	11.609	7.474	1.707	14.423
4/21/2016	2.293	5.001	9.271	8.715	14.314	7.753	9.606	5.361	2.359	12.135
5/19/2016	2.644	4.059	10.054	9.737	13.008	4.984	8.732	6.400	1.760	8.749
6/15/2016	2.718	3.628	8.644	4.901	12.139	4.456	8.358	7.803	1.363	8.569
7/20/2016	1.927	2.957	8.873	3.410	12.882	6.354	7.328	6.607	2.055	6.391
8/17/2016	2.080	5.001	8.135	5.491	13.964	6.618	5.329	10.717	0.998	14.231
9/21/2016	1.847	3.705	8.784	4.200	11.516	4.873	5.578	5.236	1.287	8.747
10/26/2016	1.612	2.602	9.211	3.077	10.052	5.221	5.467	4.879	1.484	5.640
11/15/2016	1.817	2.009	8.407	2.701	9.497	5.092	5.864	3.722	1.204	5.289
12/13/2016	1.897	3.381	8.506	2.046	9.625	5.208	7.428	3.205	2.269	6.497
1/25/2017	1.410	3.236	7.382	1.376	8.943	3.064	5.400	3.596	3.160	5.336
2/15/2017	1.249	2.521	6.835	1.643	11.194	3.001	3.840	3.772	10.597	6.971

Table 21. Time series of sodium concentration (mg/L) in filtered groundwater.

Date	I-1	I-2	LH-2	LH-5	LH-10	M-1	M-2	RA-9	RA-10	RA-12
2/15/2016	0.262	1.033	0.882	0.314	0.986	0.864	0.670	0.201	0.486	0.144
2/24/2016	318.372	64.372	0.871	0.676	0.988	110.027	10.650	0.188	0.433	0.125
3/2/2016	183.368	5.641	0.878	0.260	1.010	103.223	61.788	0.273	0.477	0.156
3/9/2016	68.847	2.850	0.853	0.328	1.035	100.275	51.842	0.243	0.454	0.179
3/17/2016	20.440	2.613	0.819	0.298	1.010	80.701	34.476	0.159	0.418	0.162
4/21/2016	1.565	0.270	0.926	0.206	1.043	20.841	9.739	0.184	0.403	0.234
5/19/2016	0.967	0.222	0.697	2.414	1.642	17.621	6.282	0.168	0.406	0.106
6/15/2016	0.634	0.124	0.726	2.018	1.74	14.25	5.760	0.184	0.328	0.130
7/20/2016	0.480	0.126	0.735	2.442	2.229	11.793	4.514	0.619	0.446	0.075
8/17/2016	0.421	0.194	0.792	1.450	2.184	8.792	3.995	0.291	0.754	0.214
9/21/2016	0.254	0.131	0.847	1.682	2.733	8.601	3.082	0.160	0.508	0.152
10/26/2016	0.296	0.250	0.705	0.830	3.021	6.358	2.786	0.619	0.560	0.068
11/15/2016	0.528	0.326	0.734	0.838	3.061	5.216	2.910	0.638	0.437	0.097
12/13/2016	0.395	0.982	0.856	0.721	3.330	5.664	3.155	0.767	0.426	0.252
1/25/2017	0.178	0.079	0.772	0.538	2.999	5.681	2.658	0.281	0.520	0.134
2/15/2017	0.149	0.113	0.732	0.715	2.756	6.689	2.018	0.266	0.627	0.090

Table 22. Time series of potassium concentration (mg/L) in filtered groundwater.

Date	I-1	I-2	LH-2	LH-5	LH-10	M-1	M-2	RA-9	RA-10	RA-12
2/15/2016	0.08	0.19	0.07	0.55	0.02	0.08	0.15	1.73	0.02	1.00
2/24/2016	12.51	1.51	0.06	0.43	0.04	3.34	0.66	1.49	0.02	0.86
3/2/2016	2.52	0.36	0.06	0.46	0.01	1.54	1.88	1.25	0.06	0.85
3/9/2016	0.69	0.14	0.07	0.28	0.03	1.26	0.92	1.11	0.06	0.77
3/17/2016	0.28	0.13	0.53	0.26	0.02	0.96	0.56	1.03	0.03	0.76
4/21/2016	0.19	0.13	0.08	0.47	0.02	0.36	0.24	1.45	0.02	0.89
5/19/2016	0.09	0.11	0.12	0.19	0.02	0.39	0.15	1.01	0.02	0.62
6/15/2016	0.21	0.16	0.12	0.17	0.03	0.28	0.13	0.69	0.04	0.51
7/20/2016	0.05	0.39	0.10	0.08	0.03	0.35	0.18	0.39	0.03	0.29
8/17/2016	0.39	0.16	0.07	0.12	0.02	0.14	0.09	1.12	0.03	0.53
9/21/2016	0.40	0.05	0.08	0.08	0.03	0.18	0.22	1.01	0.03	0.64
10/26/2016	0.03	0.08	0.09	0.08	0.05	0.14	0.15	0.19	0.01	0.26
11/15/2016	0.03	0.07	0.08	0.09	0.05	0.12	0.15	0.19	0.02	0.28
12/13/2016	0.06	0.99	0.06	0.03	0.06	0.11	0.13	0.14	0.04	0.32
1/24/2017	3.68	0.18	0.06	0.02	0.07	0.07	0.13	0.46	0.03	0.25
2/15/2017	1.86	0.17	0.23	0.03	0.13	0.08	0.52	0.38	0.03	0.32

Table 23. Time series of aluminum concentration (mg/L) in filtered groundwater.

Date	I-1	I-2	LH-2	LH-5	LH-10	M-1	M-2	RA-9	RA-10	RA-12
2/15/2016	0.19	0.28	0.32	1.20	0.28	0.39	0.43	0.84	0.45	0.25
2/24/2016	3.80	5.80	0.27	1.10	0.29	0.55	0.10	0.88	0.40	0.20
3/2/2016	13.00	3.50	0.19	0.65	0.25	0.19	0.18	0.74	0.38	0.15
3/9/2016	6.50	2.20	0.17	0.89	0.19	0.35	0.22	0.62	0.38	0.17
3/17/2016	4.00	1.30	0.16	0.68	0.11	0.06	0.14	0.69	0.42	0.16
4/21/2016	1.40	0.24	0.11	0.94	0.04	0.05	0.14	0.21	0.37	0.16
5/19/2016	0.66	0.31	0.24	1.10	0.02	0.11	0.06	0.20	0.37	0.17
6/15/2016	0.30	0.26	0.30	1.40	0.02	0.07	0.08	0.22	0.40	0.13
7/20/2016	0.28	0.14	0.54	1.30	0.01	0.07	0.06	0.12	0.48	0.16
8/17/2016	0.48	0.15	0.26	1.70	0.03	0.03	0.11	0.19	0.31	0.20
9/21/2016	0.61	0.27	0.31	3.70	0.02	0.06	0.20	0.11	0.67	0.17
10/26/2016	0.40	1.00	0.71	1.70	0.01	0.09	0.29	0.28	0.64	0.22
11/15/2016	1.10	1.50	0.78	1.50	0.01	0.24	0.56	1.10	0.34	0.28
12/13/2016	0.33	2.20	0.49	1.00	0.01	0.50	0.23	1.50	0.30	0.41
1/25/2017	0.01	0.03	0.31	1.07	0.02	0.39	0.36	0.38	0.19	0.07
2/15/2017	0.09	0.15	0.28	2.99	0.03	0.21	0.31	0.23	0.18	0.11

Table 24. Time series of total arsenic concentration (mg/L) in unfiltered groundwater.

Date	I-1	I-2	LH-2	LH-5	LH-10	M-1	M-2	RA-9	RA-10	RA-12
2/15/2016	0.12	0.12	0.24	1.09	0.25	0.32	0.34	0.66	0.16	0.13
2/24/2016	4.83	6.15	0.18	0.90	0.20	0.24	0.05	0.76	0.34	0.12
3/2/2016	9.13	3.42	0.16	0.59	0.23	0.15	0.08	0.66	0.34	0.12
3/9/2016	5.37	1.70	0.15	0.81	0.09	0.18	0.06	0.55	0.34	0.12
3/17/2016	2.64	0.79	0.14	0.51	0.11	0.02	0.05	0.29	0.29	0.14
4/21/2016	0.54	0.14	0.09	0.89	0.04	0.02	0.02	0.17	0.26	0.12
5/19/2016	0.31	0.12	0.22	0.72	0.01	0.02	0.01	0.17	0.33	0.17
6/15/2016	0.15	0.13	0.26	1.36	0.02	0.03	0.03	0.21	0.34	0.12
7/20/2016	0.13	0.02	0.43	1.05	0.01	0.02	0.03	0.07	0.46	0.14
8/17/2016	0.34	0.09	0.21	1.47	0.01	0.02	0.03	0.16	0.30	0.21
9/21/2016	0.37	0.19	0.27	2.97	0.02	0.02	0.03	0.099	0.58	0.16
10/26/2016	0.20	0.65	0.59	1.49	0.01	0.05	0.04	0.25	0.52	0.18
11/15/2016	0.33	0.33	0.64	1.31	0.01	0.07	0.22	0.87	0.29	0.22
12/13/2016	0.09	1.52	0.41	0.83	0.01	0.18	0.11	1.23	0.26	0.35
1/25/2017	0.01	0.03	0.31	1.07	0.01	0.16	0.17	0.38	0.19	0.07
2/15/2017	0.09	0.15	0.28	2.99	0.02	0.07	0.14	0.23	0.18	0.11

Table 25. Time series of total arsenic concentration (mg/L) in filtered groundwater.

Date	I-1	I-2	LH-2	LH-5	LH-10	M-1	M-2	RA-9	RA-10	RA-12
2/15/2016	0.055	0.085	0.229	0.874	0.248	0.276	0.291	0.632	0.137	0.125
2/24/2016	5.089	5.089	0.146	0.839	0.201	0.249	0.051	0.695	0.011	0.096
3/2/2016	8.368	3.252	0.142	0.483	0.211	0.123	0.088	0.614	0.256	0.084
3/9/2016	4.666	1.433	0.130	0.684	0.086	0.138	0.054	0.499	0.216	0.107
3/17/2016	2.442	0.482	0.136	0.412	0.091	0.017	0.035	0.325	0.040	0.132
4/21/2016	0.443	0.102	0.081	0.830	0.035	0.011	0.009	0.163	0.043	0.114
5/19/2016	0.187	0.118	0.205	0.676	0.007	0.016	0.008	0.109	0.027	0.141
6/15/2016	0.118	0.165	0.241	1.180	0.013	0.018	0.025	0.179	0.151	0.102
7/20/2016	0.098	0.013	0.408	0.531	0.007	0.019	0.017	0.017	0.052	0.078
8/17/2016	0.320	0.044	0.194	1.473	0.014	0.006	0.017	0.148	0.013	0.195
9/21/2016	0.313	0.019	0.242	2.663	0.010	0.017	0.028	0.092	0.529	0.131
10/26/2016	0.156	0.419	0.577	1.103	0.007	0.026	0.035	0.069	0.163	0.065
11/15/2016	0.203	0.305	0.615	1.178	0.007	0.044	0.080	0.164	0.032	0.042
12/13/2016	0.089	1.452	0.346	0.769	0.008	0.086	0.054	0.299	0.018	0.083
1/25/2017	0.011	0.009	0.276	1.076	0.013	0.044	0.071	0.135	0.023	0.015
2/15/2017	0.057	0.032	0.202	2.783	0.018	0.028	0.107	0.061	0.023	0.029

Table 26. Time series of As(III) concentration (mg/L) from filtered groundwater.

Date	I-1	I-2	LH-2	LH-5	LH-10	M-1	M-2	RA-9	RA-10	RA-12
2/15/2016	0.068	0.038	0.016	0.220	0.004	0.041	0.052	0.025	0.025	0.008
2/24/2016	0	1.066	0.032	0.062	0.007	0	0.001	0.068	0.329	0.027
3/2/2016	0.766	0.272	0.016	0.110	0.016	0.028	0	0.049	0.084	0.039
3/9/2016	0.661	0.313	0.017	0.130	0.011	0.046	0.010	0.050	0.122	0.015
3/17/2016	0.202	0.036	0.007	0.102	0.019	0.001	0.016	0	0.258	0.008
4/21/2016	0.095	0.035	0.009	0.057	0.008	0.008	0.009	0.004	0.213	0.008
5/19/2016	0.126	0.001	0.013	0.048	0.002	0.006	0.001	0.065	0.301	0.026
6/15/2016	0.037	0	0.021	0.183	0.004	0.008	0.010	0.031	0.192	0.015
7/20/2016	0.028	0.002	0.025	0.516	0	0.006	0.011	0.049	0.405	0.067
8/17/2016	0.018	0.048	0.015	0	0.002	0.005	0.013	0.017	0.288	0.012
9/21/2016	0.053	0.172	0.029	0.306	0.009	0.005	0.003	0.007	0.053	0.028
10/26/2016	0.047	0.231	0.021	0.395	0.002	0.022	0.007	0.183	0.358	0.122
11/15/2016	0.123	0.027	0.024	0.206	0.002	0.032	0.138	0.704	0.259	0.181
12/13/2016	0.009	0.065	0.063	0.064	0.002	0.091	0.053	0.931	0.245	0.266
1/25/2017	0.003	0.019	0.033	0.000	0.000	0.116	0.104	0.243	0.174	0.058
2/15/2017	0.040	0.122	0.079	0.213	0.006	0.041	0.032	0.167	0.162	0.078

Table 27. Time series of As(V) concentration (mg/L) in filtered groundwater.

Laboratory Analysis of Solids

Solid slurry that was recovered from well bottoms every other month was first analyzed by X-ray diffraction (XRD), Figure 10 displays a spectra from well I-2 that shows well defined peaks that closely match arsenian-pyrite that was reported in lignite from the Czech Republic (Reider et al., 2007). The arsenian pyrite diffraction peaks are apparent when compared with pure pyrite analyses. Observations show the strongest presence of pyrite to be in the months March, April, and June, where counts of peak intensity from the spectra exceed 5000 in some spaces (Figures 10 and 11). These are the months in which the formation of pyrite peaks is most intense, and represent the main biomineralization or arsenic sequestration stage. After these months of main sequestration stage, pyrite formation appears to drop off slightly, with decreased presence of pyrites and less intense pyrite peaks in sediments collected from August to October (Figure 12).

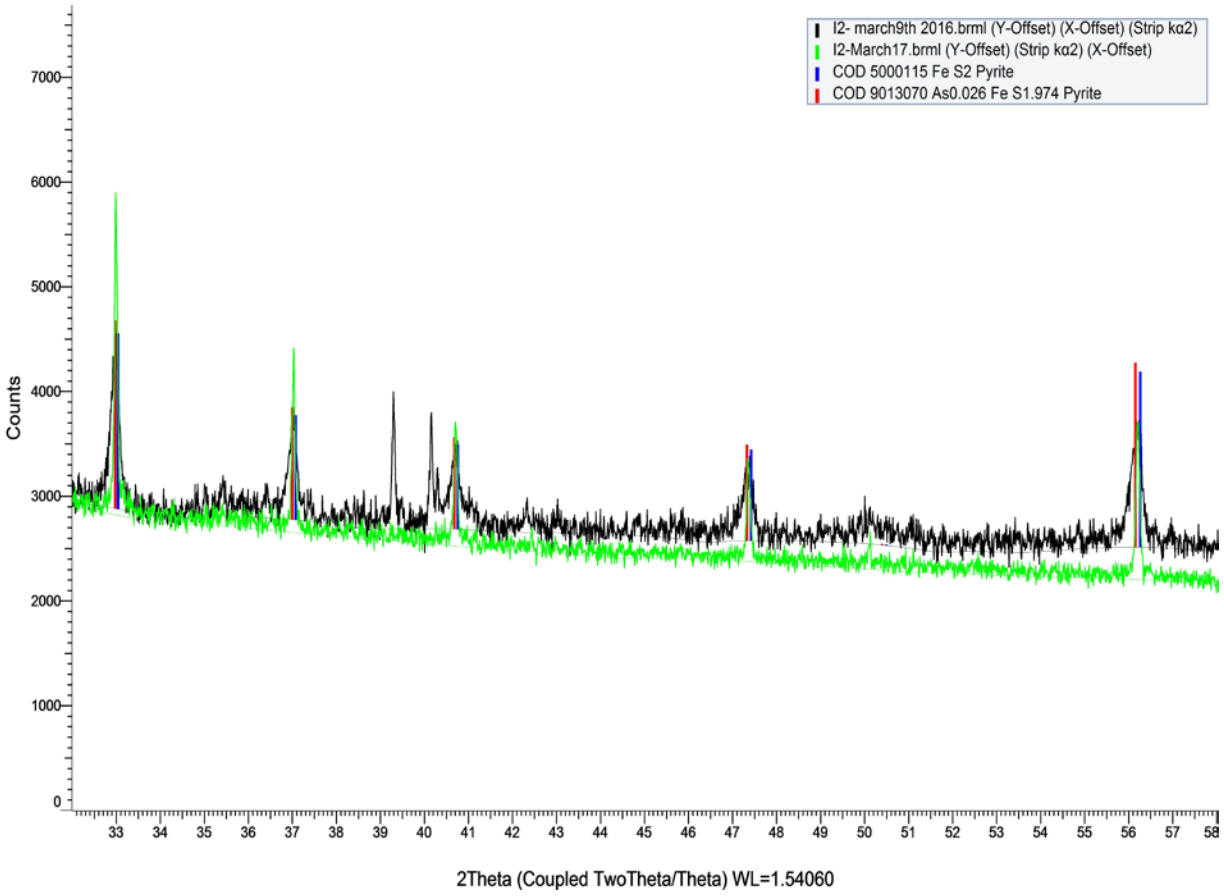

Figure 10. XRD spectra showing representative pyrite and arsenian-pyrite peaks in sediments from well I-2 in March 2016. The blue and red vertical lines serve as indicators for pure pyrite and arsenian-pyrite, respectively.

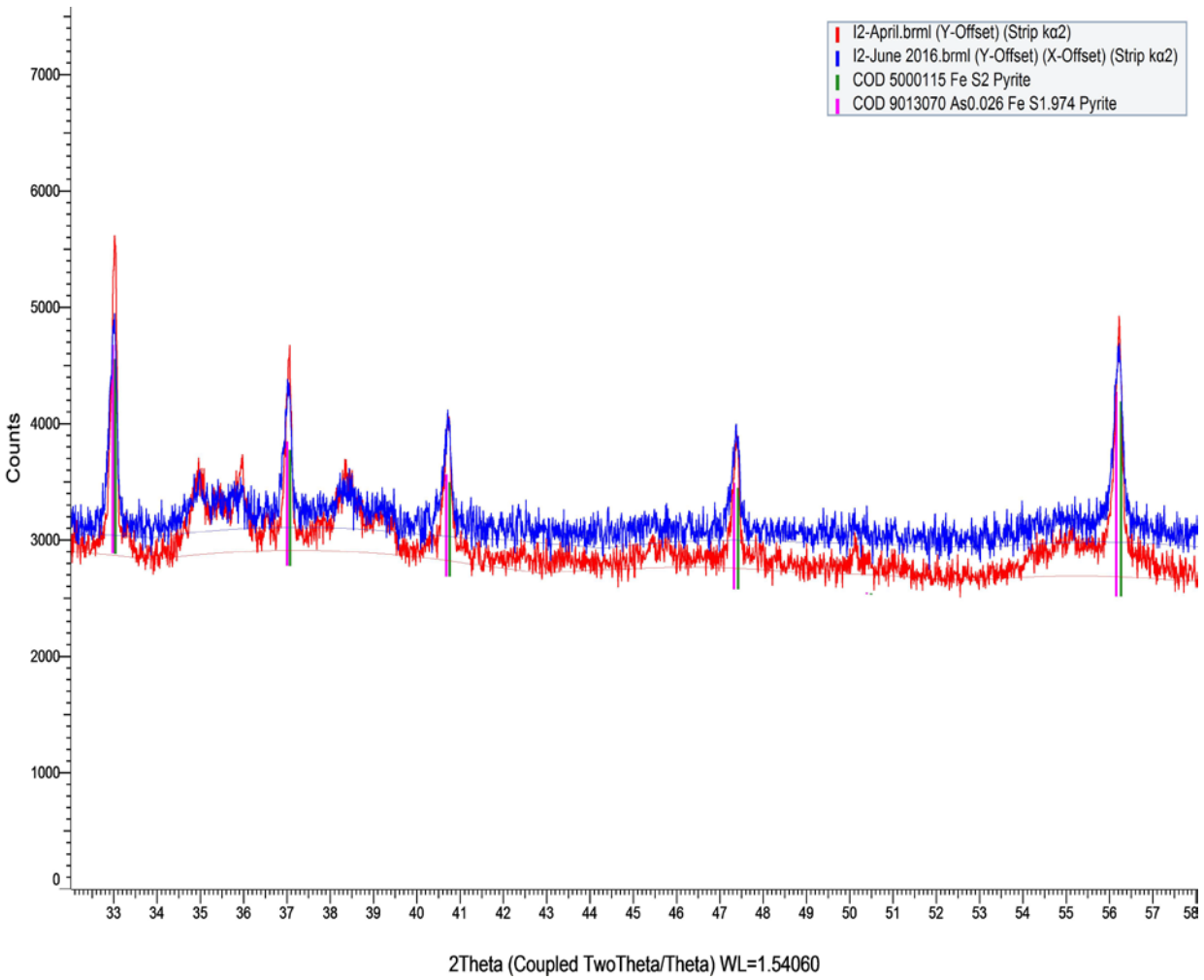

Figure 11. XRD spectra showing representative pyrite and arsenian-pyrite peaks in sediments from well I-2 in April and June 2016. The green and magenta vertical lines indicate pure pyrite and arsenian-pyrite, respectively.

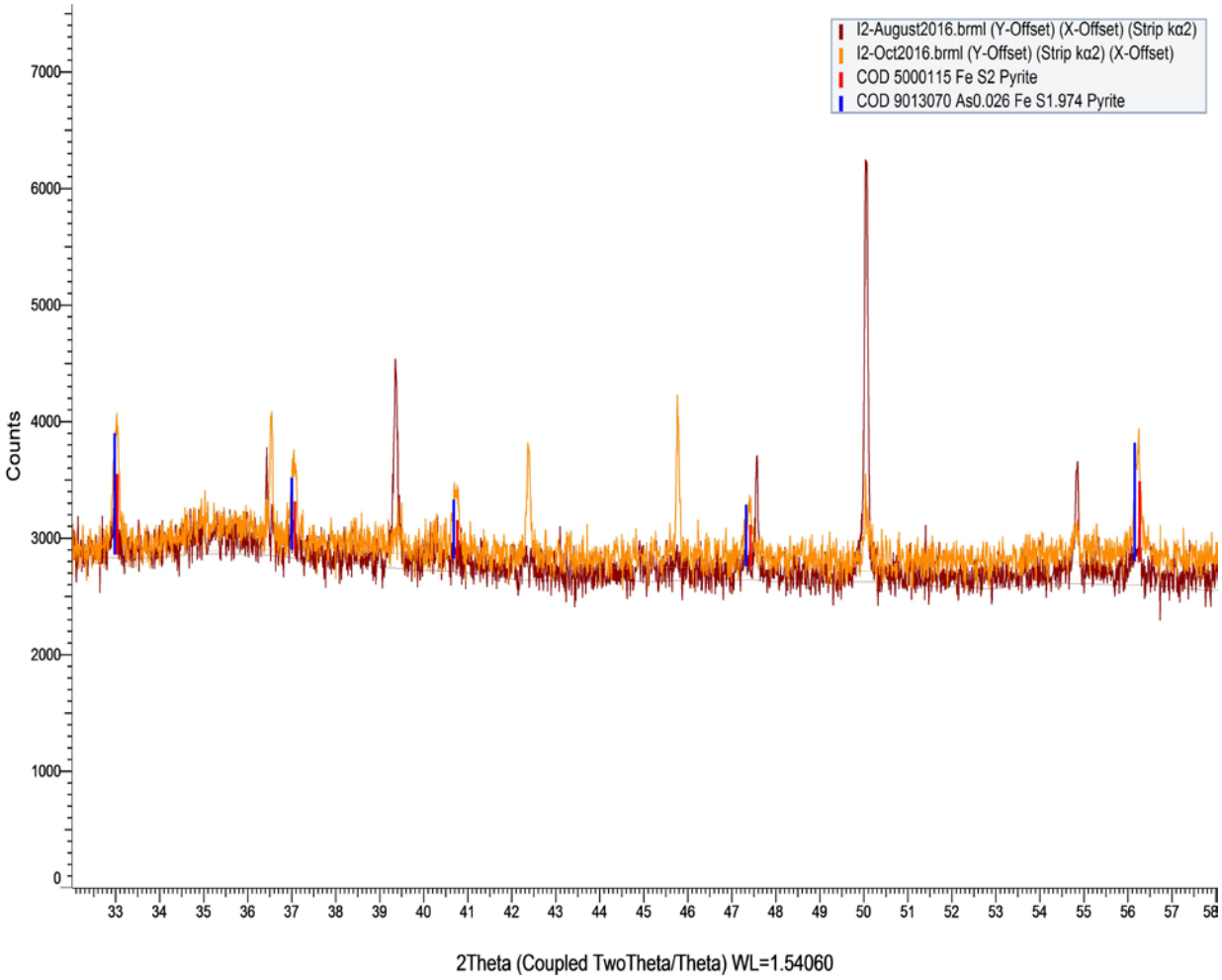

Figure 12. XRD spectra showing representative pyrite and arsenian-pyrite peaks in sediments from well I-2 in August and October 2016. The red and blue vertical lines are indicators for pure pyrite and arsenian-pyrite, respectively.

Solids that were imaged using polarizing microscope in reflected light revealed iron sulfides that were essentially all pyrite. The grains observed were isotropic and they occurred as crystals and framboids (spherical aggregates of pyrite nanoparticles) between 1 and 10 μm in diameter (Figure 13). The SEM images (Figures 14-16) further confirmed that the pyrite occurs in the recovered solids in the form of framboids. The images showed them commonly attached to the silicate phases in the aquifer as secondary growth. The pyrites were the only crystalline Fe-S or As-S phase that was detected through XRD and optic study. The X-ray fluorescence (XRF) analysis consistently resulted in peaks for iron, sulfide, and arsenic (Figure 17). This was consistent with the XRD spectrums and petrographic analysis. Arsenic content in the polished pyrite solids were quantified using the JEOL 8600 electron microprobe. The microprobe results further confirm that the solids formed were arsenian pyrites with 0.1 to 0.4 weight percentage of arsenic (Figure 18). This percentage range is much higher than the level of arsenic in fluvial sediments typically in the parts per million level (Horneman et al., 2004; Lee et al., 2007; Shamsudduha et al., 2008).

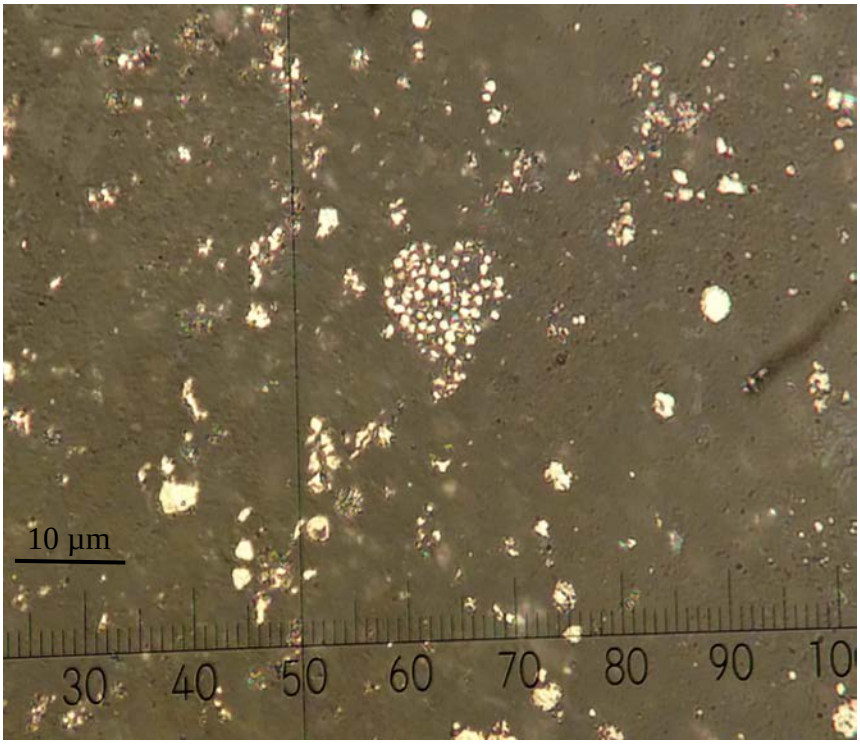

Figure 13. Photomicrograph in reflected light of arsenian pyrite aggregates in framboid form.

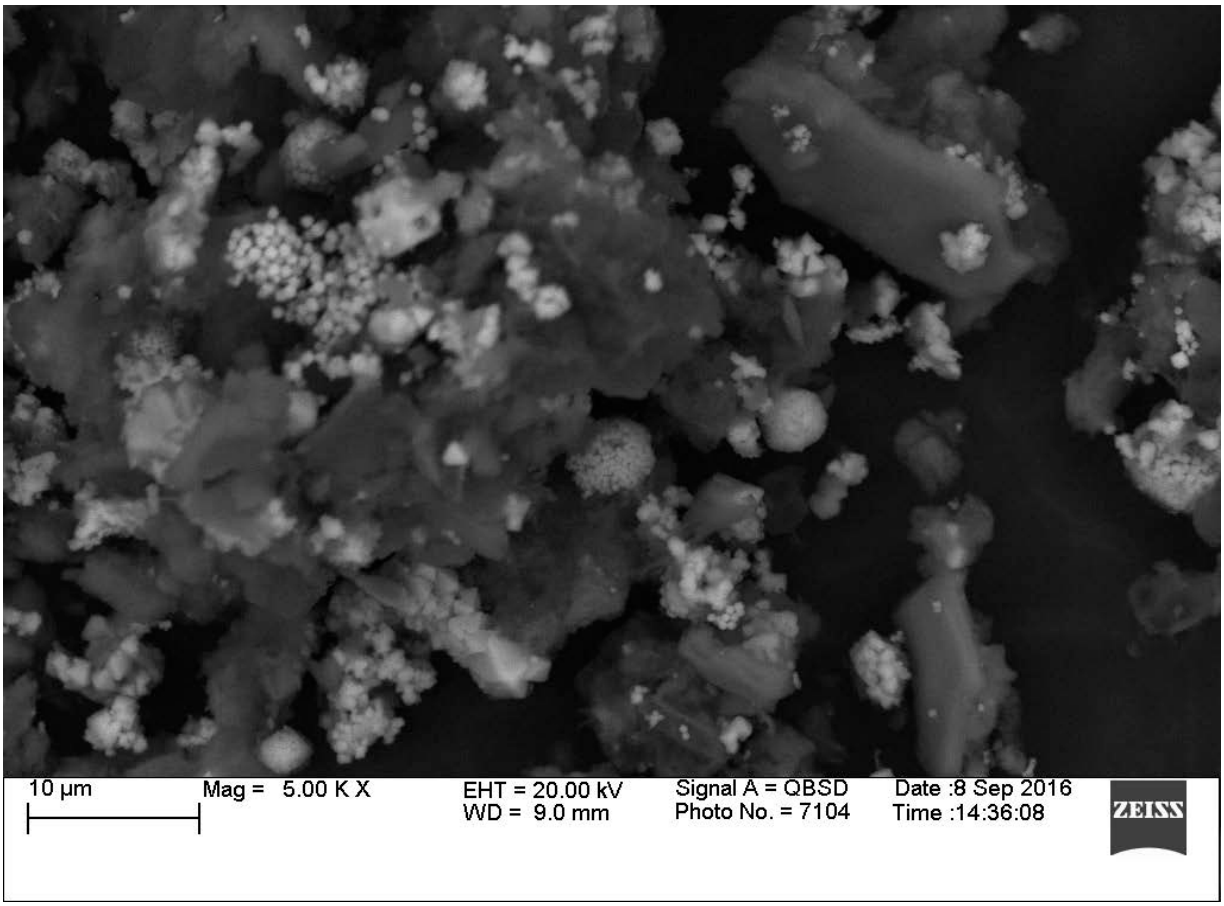

Figure 14. Scanning electron microscope image of framboidal and crystalline pyrite at 5.00 K X magnification.

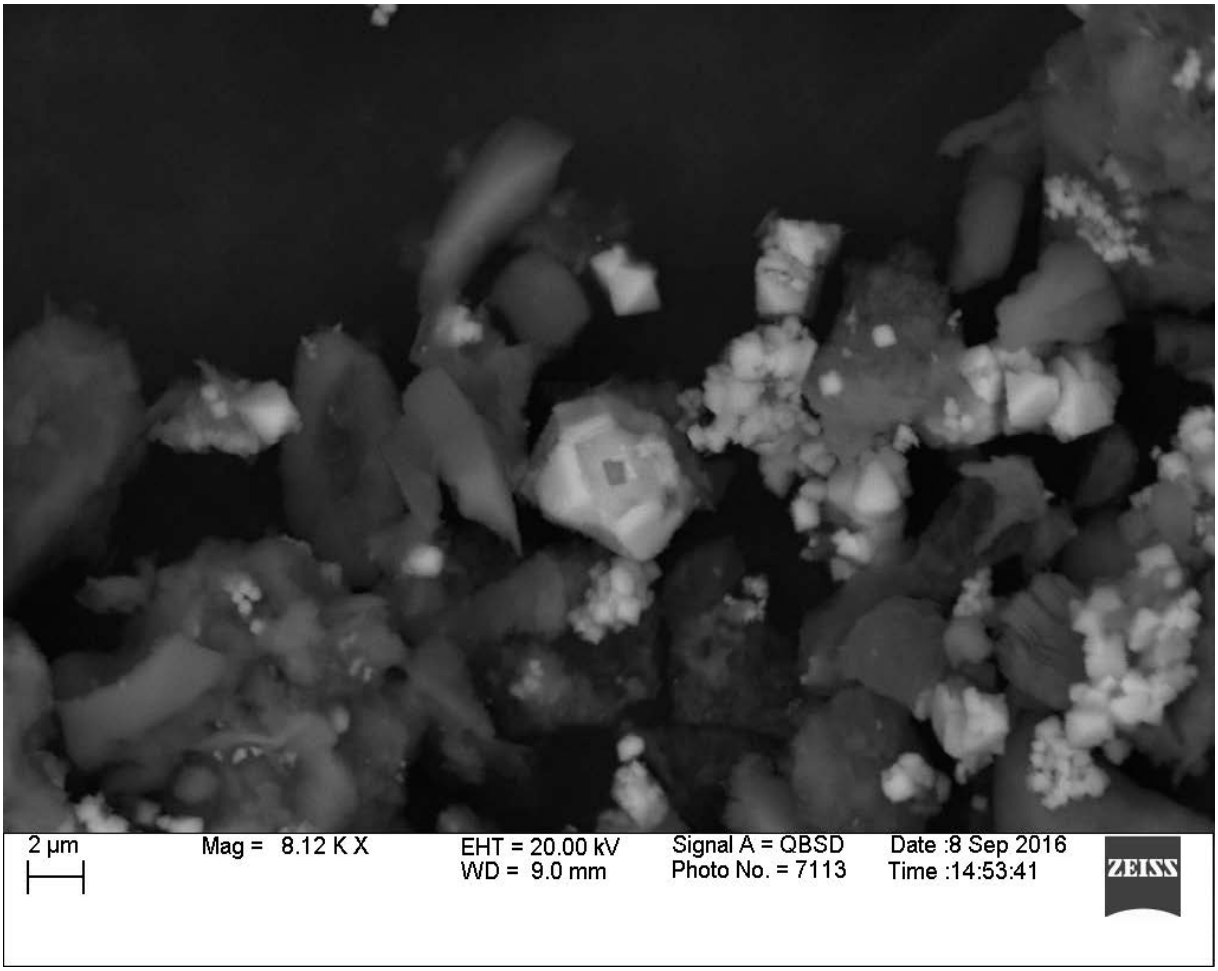

Figure 15. Scanning electron microscope image of framboidal and crystalline pyrite at 8.12 K X magnification.

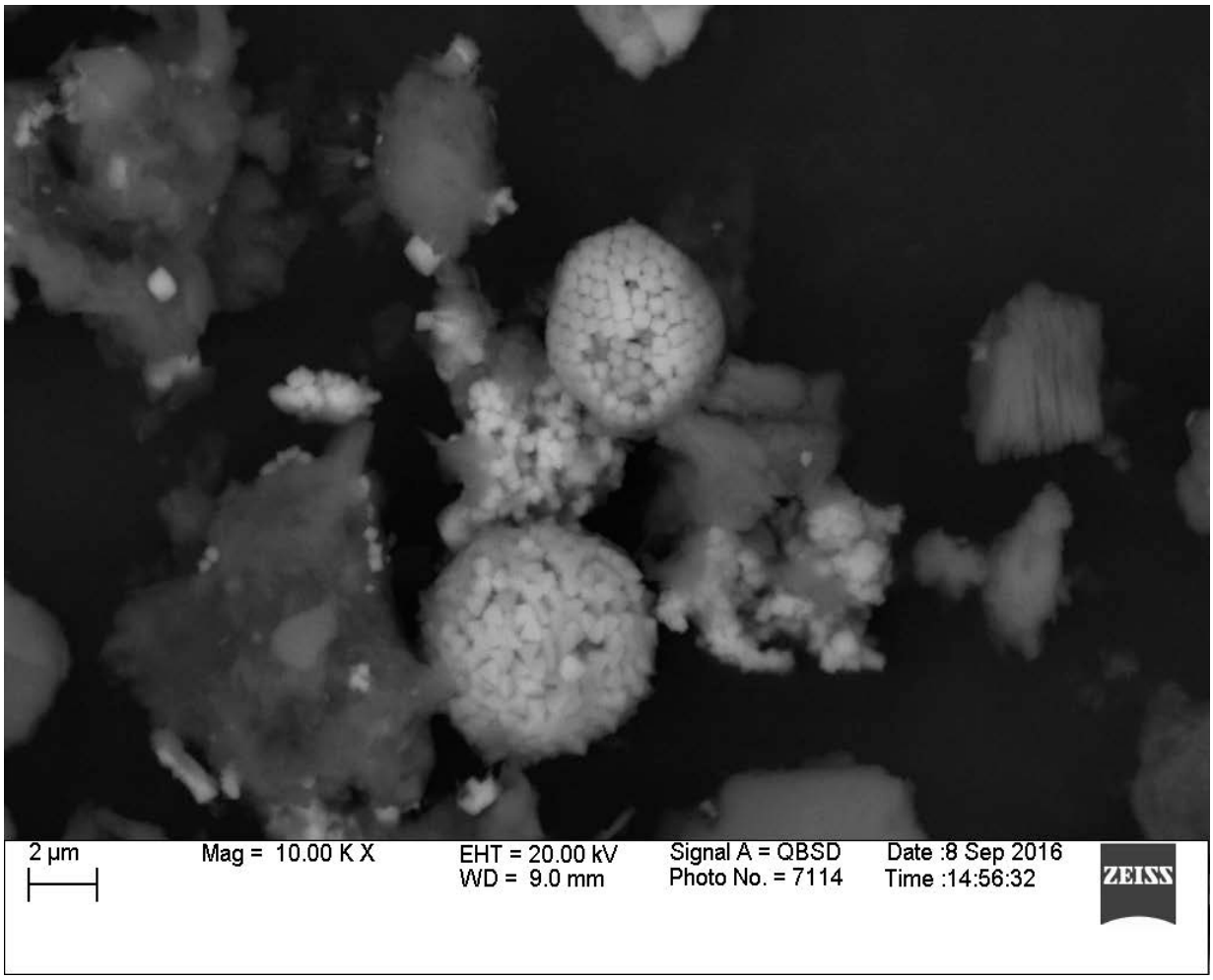

Figure 16. Scanning electron microscope image of pyrite framboids at 10.00 K X magnification.

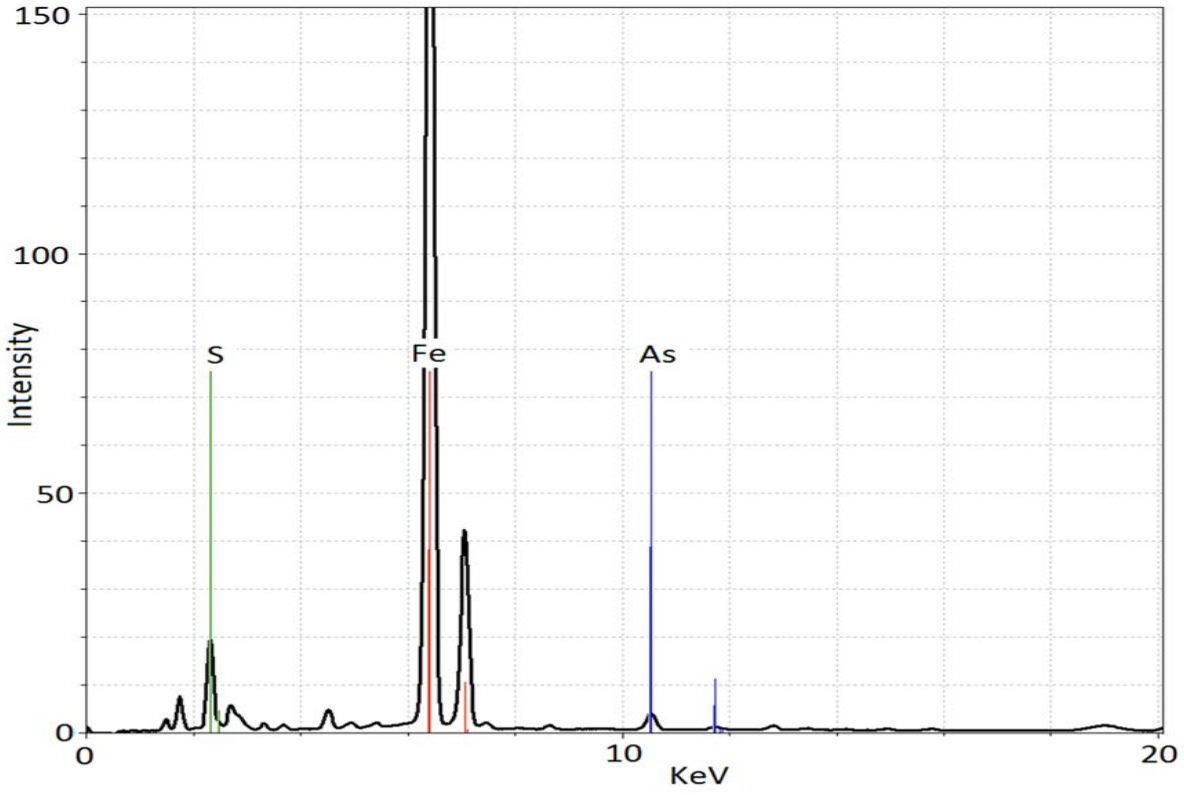

Figure 17. XRF spectra of elements present in sediment sample from well M-2.

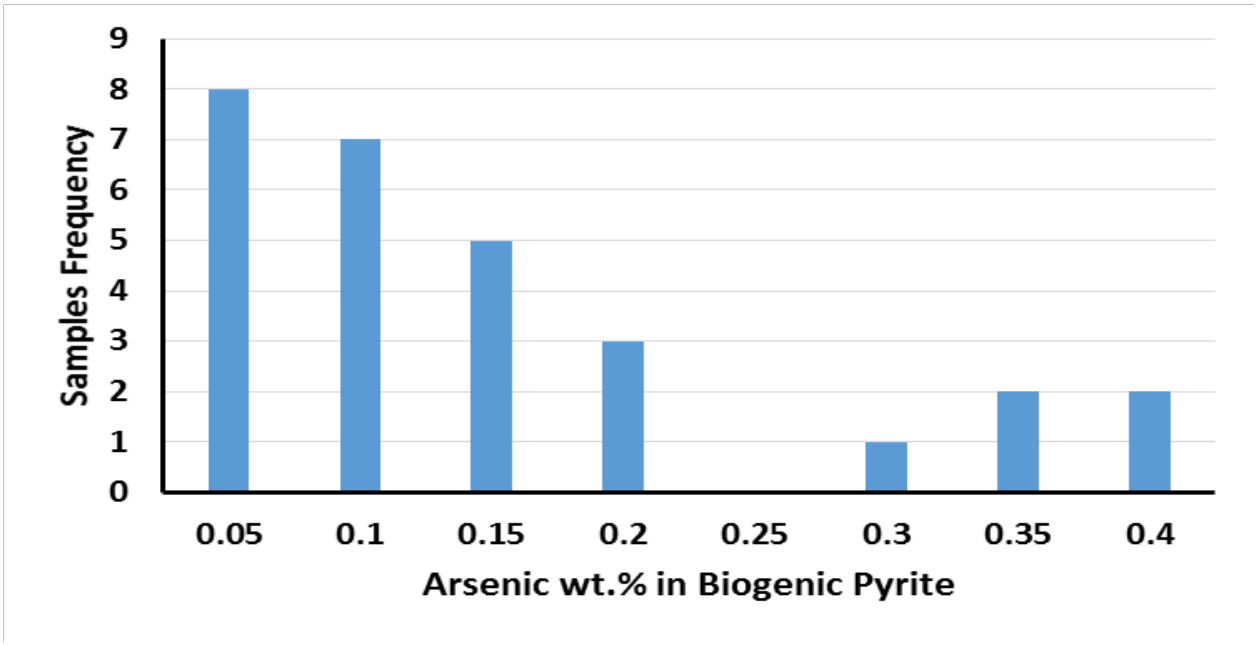

Figure 18. Histogram showing the JEOL 8600 electron microprobe results showing arsenic weight percentage in biogenic pyrite.

Microbial Changes

The changes in the total sulfate-reducing bacteria (SRB) aqueous slurry samples were determined through real-time PCR targeting the *dsr*A gene. The gathered results show concentration of sulfate-reducing bacteria prior to the injection were below the limit of detection (1.01 Log_{10} copies/µl). While SRB concentration was low pre-injection, our results for samples from both injection wells and monitoring wells (I-1, I-2, M-1, M-2) contained significantly higher amount of SRB for two months after the injection process (Figures 19-20). Concentration of SRB DNA found in those samples were approximately 3 Log_{10} copies/µl. The quantitative PCR helped confirm SRB activities at the industrial site. This method detects the adenosine-5'-phosphosulfate, and the results show *Desulfovibrio spp*., *Desulfotomaculum spp*., as the main functional SRB in the samples on site.

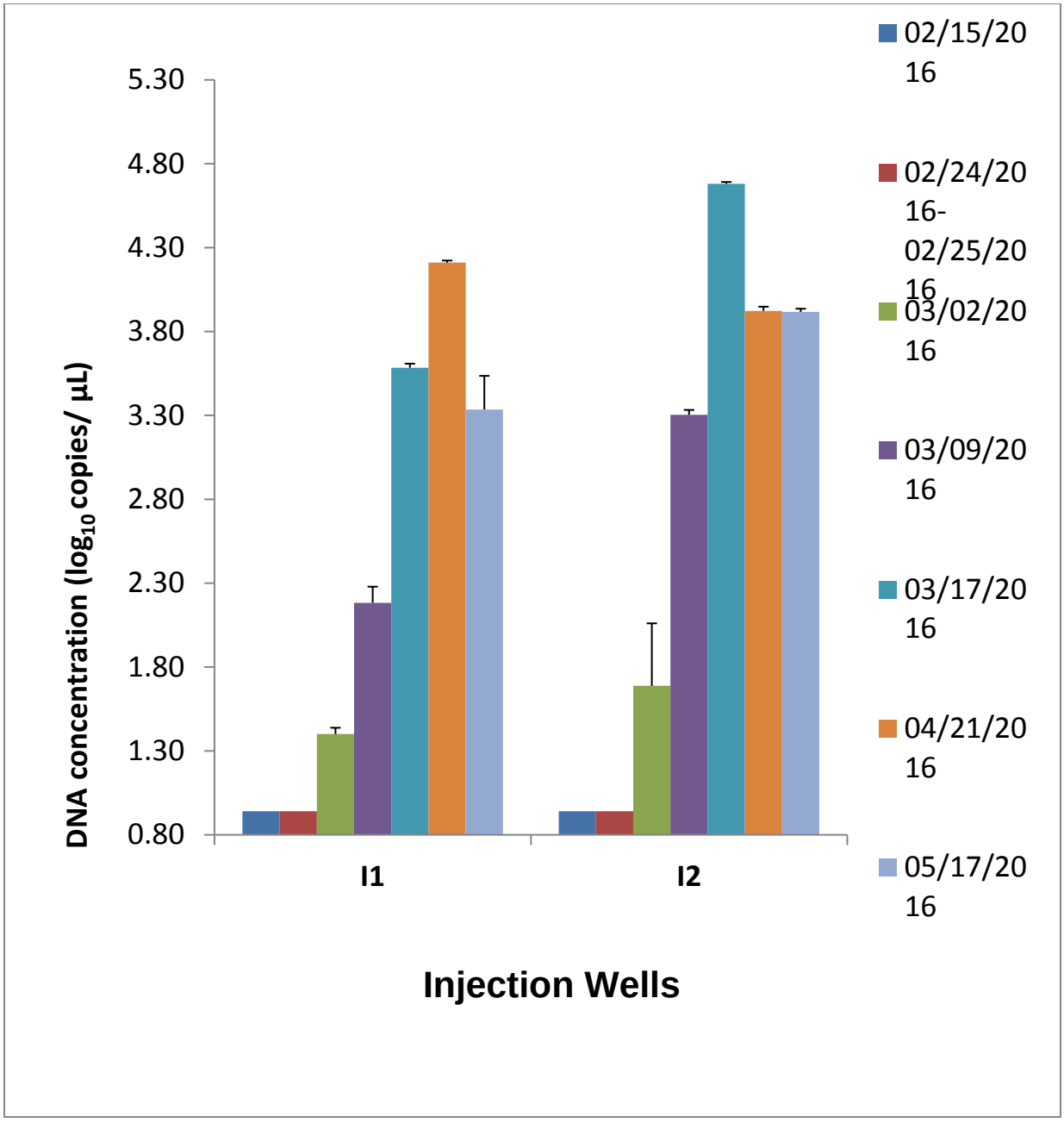

Figure 19. Histograms showing the real-time PCR results for sulfate reducing bacteria concentrations in injection wells I-1 and I-2.

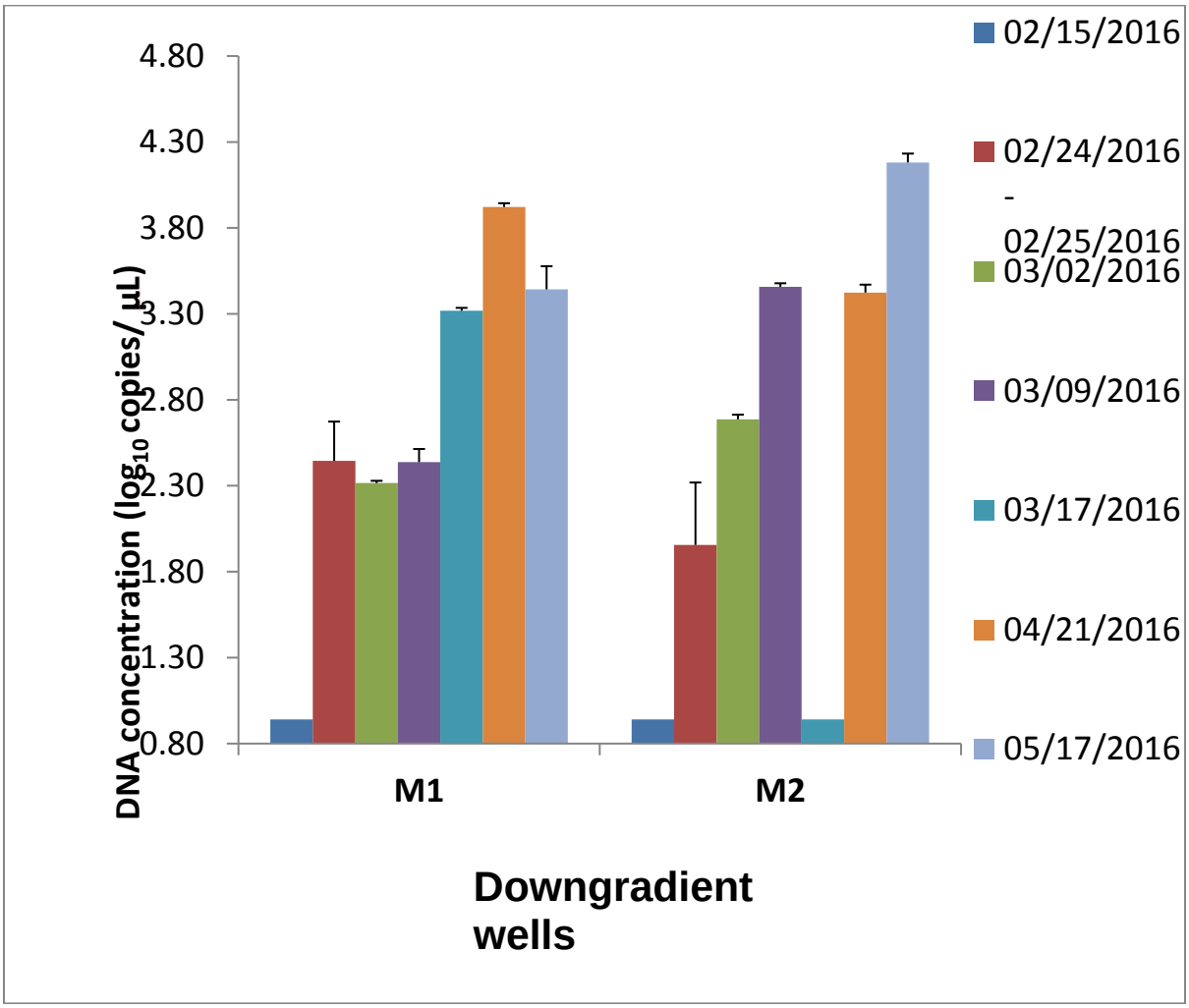

Figure 20. Histograms showing the real-time PCR results for sulfate reducing bacteria concentrations in monitoring wells M-1 and M-2.

Geochemical Modeling of Arsenic Speciation and Pyrite Biomineralization

The goal of geochemical modeling was to track whether the injection procedure was successful in creating the reducing environment necessary to stimulate bacterial sulfate reduction and biomineralization at the industrial site. This was done by modeling calculating arsenic speciation under measured field Eh-pH conditions in an activity diagram using Geochemist's Workbench (Bethke et al., 2008). Field measured Eh-pH values are plotted to evaluate their stability within the activity fields of various phases of arsenic-bearing aqueous species and solid compounds. In the models, only seven wells that are inside the fencing near the injection points with significant Eh-pH changes are included in the calculations. The model shows and compares the Eh-pH conditions and dominant arsenic species at the site before and after the input of the injection solution (Figures 21-23). The pre-injection conditions reflect a slightly reducing environment with Eh just above 0 volts for most wells (only LH-10 has negative Eh). The pH values range from 5.45-7.00. Arsenic is mobile under such slightly reducing conditions and the dominant arsenic species is $As(OH)_3$ or arsenite, It is clear from the model that the potential arsenian-pyrite solid phase is not a thermodynamically stable phase under the pre-injection condition. One week and four weeks after the injection, the field data and model shows the dramatic shift to more reducing conditions in the two injection wells I-1 and I-2, and monitoring wells M-1, M-2, and LH-10 (Figures 22 and 23). Most importantly, the model four weeks after the injection reflects conditions where the solid arsenian-pyrite phase is the most stable phase under highly reducing conditions in which aqueous arsenic species are sequestered in solid sulfides.

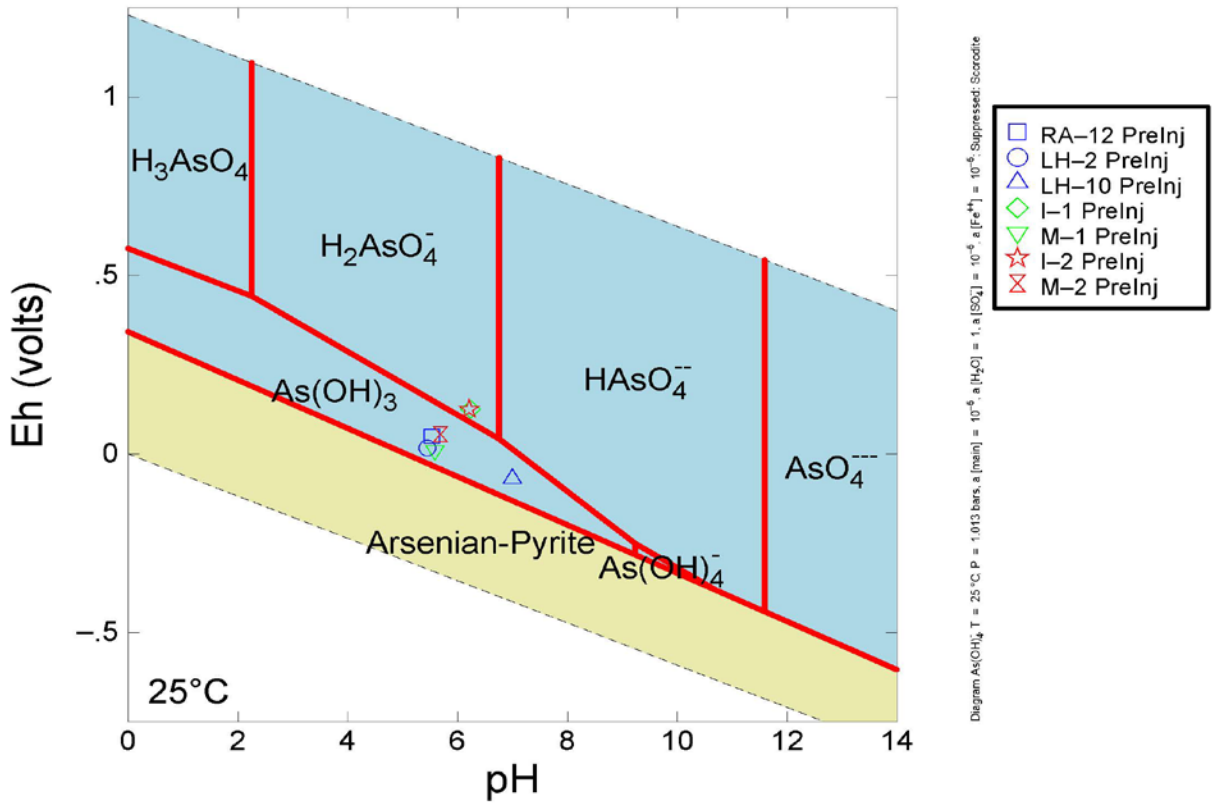

Figure 21. Eh-pH diagram showing stable As species under various redox conditions with plotted well conditions prior to the injection.

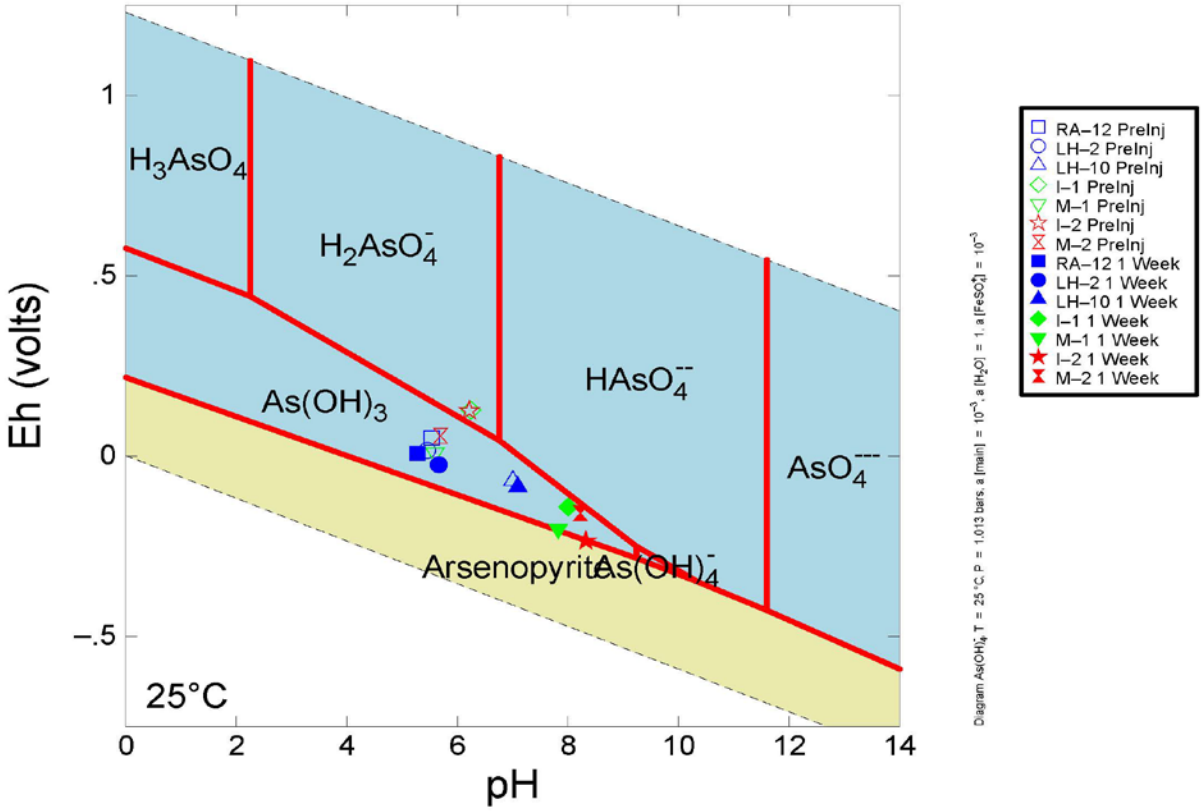

Figure 22. Eh-pH diagram showing stable As species under various redox conditions with plotted well conditions 1 week after the injection.

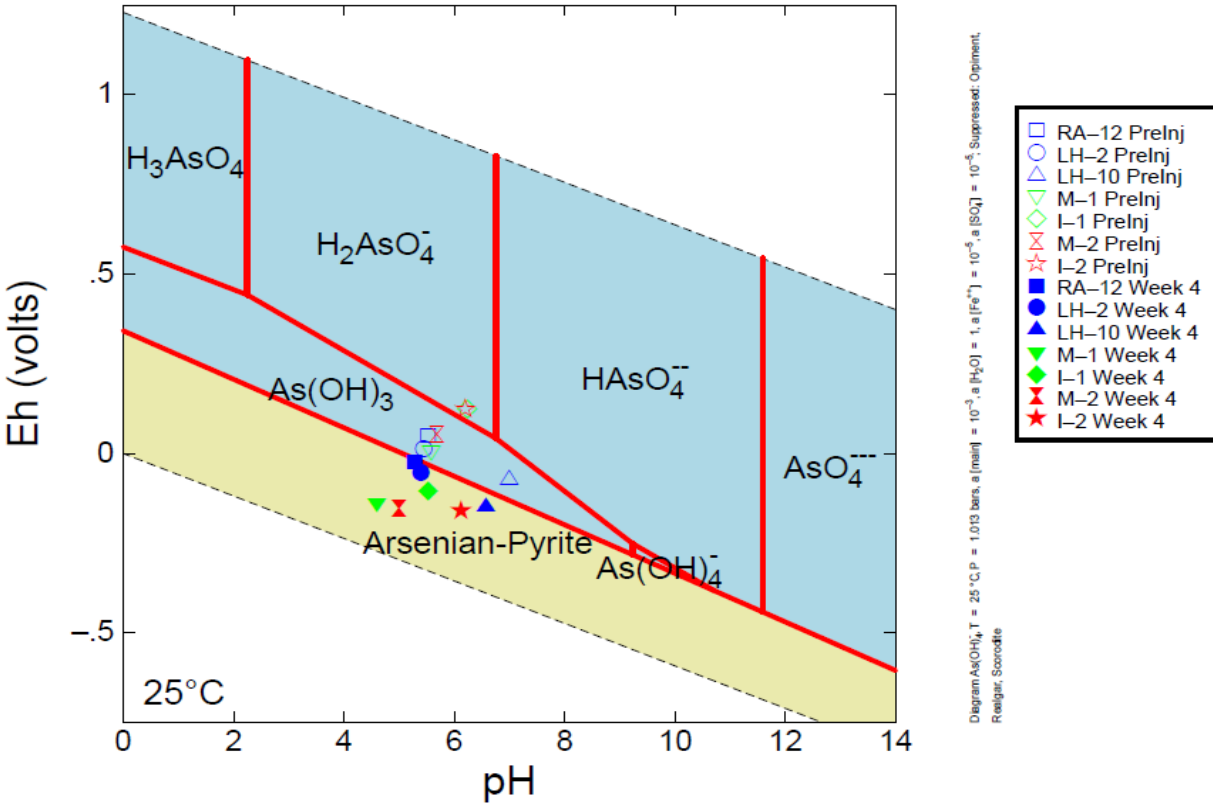

Figure 23. Eh-pH diagram showing stable As species under various redox conditions. It is shown that 4 weeks after the injection, the groundwater Eh-pH conditions for multiple wells on site plot in the stable arsenian-pyrite solid phase.

A reaction path model in the React tool of Geochemist's Workbench was used to predict the mineralogical reactions in response to $FeSO_4$ amendments and sliding Eh conditions (Figure 24). The program first calculated the equilibrium state of the initial condition using the pre-injection groundwater geochemistry data from well I-1. Reactants of 0.01 mmol of $FeSO_4$ were then added to the initial system to simulate the effect of well amendments. The model predicted that pyrite precipitation at the industrial site would occur as the Eh values decrease from an initial condition of -0.09 mV to -0.15 mV. The geochemical modeling results support the hypothesis and the field data of pyrite biomineralization under sulfate reduction conditions.

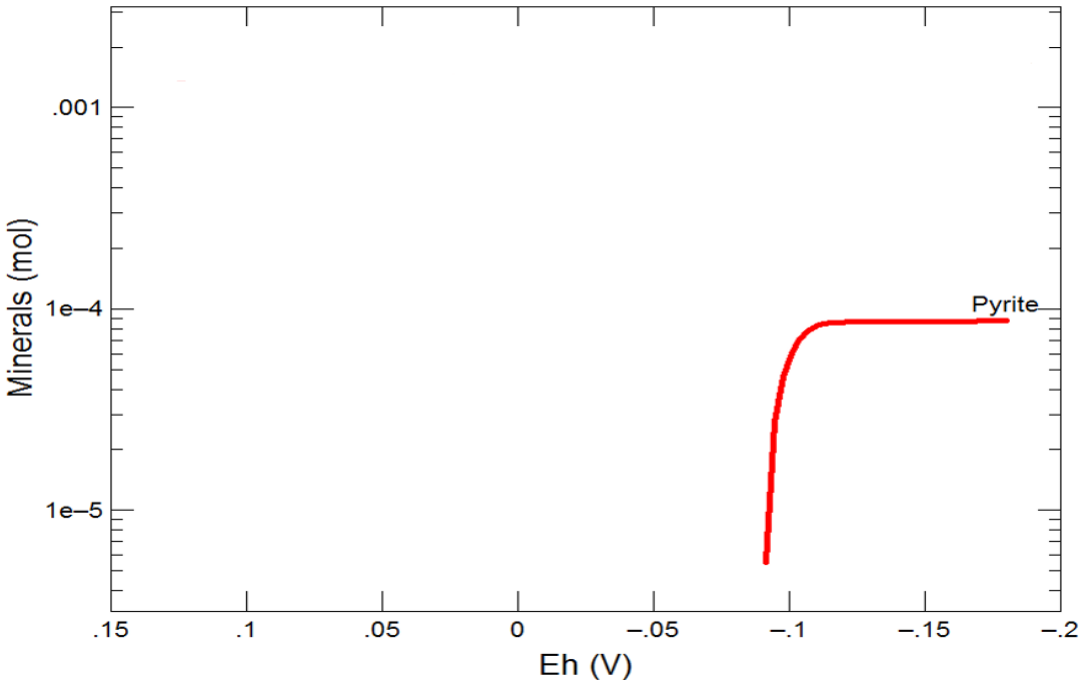

Figure 24. Plot showing results of a reaction path model for pyrite created with Geochemist's Workbench.

Discussion

Field Parameters

This field pilot test is meant to demonstrate that biomineralization of pyrite can effectively remove dissolved arsenic from contaminated groundwater at the industrial site. To accomplish this, natural sulfate-reducing bacteria in the groundwater were stimulated to precipitate pyrite nanoparticles capable of sorbing and co-precipitating arsenic. After the injection into two new wells installed on site, SRB metabolism and its biogeochemical effects began approximately one week later. This study explores the major patterns and trends observed in the laboratory and field over a total period of one year after biostimulation. The relationships and trends of multiple field parameters lead to a better understanding of biomineralization mechanisms and reveal a finite time interval during which the SRB process is effective and forming Fe-S biominerals for arsenic sequestration.

ORP values before the injection showed mildly reducing conditions at the industrial site (44.4±63.6 mV). One week after the injection the ORP values dropped significantly to more reducing values (below -120 mV) in the injection wells and monitoring wells M-1 and M-2. These lower ORP values indicate that sulfate-reducing conditions were quickly established in the aquifer just one week after the injection, which was also confirmed by the quantitative microbiology analysis (Figures 19, 20). The ORP values remained negative in the affected wells for months after the injection, and this implies that reducing conditions were effectively maintained at the site. Moreover, these reducing conditions persisted along with the decreasing

arsenic concentrations in the months following the injection. When examining ORP changes in response to long-term hydrologic and climatic changes, it appears that the ORP on site is influenced by variations in precipitation and water levels after the main arsenic sequestration stage when the amended carbon source is exhausted and the aquifer redox condition fluctuates. For example, in the affected monitoring wells (M-1, M-2, LH-10), lower ORP values reflect lower precipitation over time, which can be clearly seen in the dry months of October and November (Figure 25). In contrast ORP responds with an increase when the precipitation increases. These results imply that patterns of precipitation can bring more oxygen into the aquifer and create the variations observed in ORP measurements.

Ferrous iron concentration increases significantly in the weeks following the injection of $FeSO_4 \bullet 7H_2O$. However, it is possible that ferrous iron in addition to what was injected, was added to the groundwater through bacterial-iron reduction. Bacterial iron reduction occurs under more oxidizing conditions, and sulfate reducing bacterial activities take place under moderately reducing conditions (Chapelle et al., 1992; Nickson et al., 2000, Lowers et al., 2007). Concurrently, a sharp increase in dissolved sulfide concentration was observed in the wells following the injection due to the establishment of sulfate reducing conditions (Table 10). The ferrous-sulfate injection served to spur the increase in ferrous iron and sulfate concentration in the groundwater, which in turn facilitated the rapid establishment of sulfate-reducing conditions on site. This quickly leads to the precipitation of iron sulfides from the groundwater and the eventual decrease in overall ferrous iron and sulfide concentrations in the aquifer. Over time the ferrous iron and sulfide concentrations in the affected wells began to fall back to near

background levels, indicating that precipitation of iron sulfide solids from the groundwater was indeed the main factor in decreasing levels of ferrous iron and sulfide in the water.

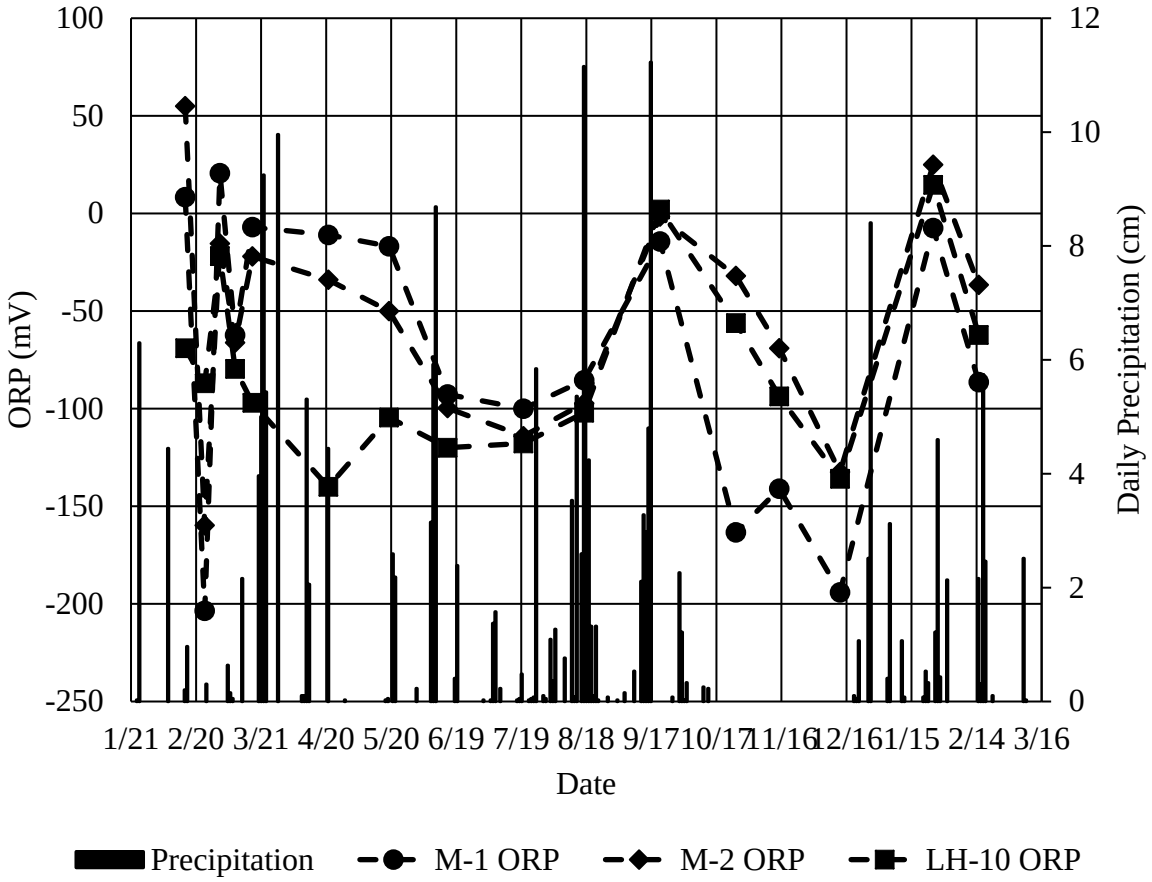

Figure 25. Plot of ORP (mV) for monitoring wells versus daily precipitation levels (cm).

Monitoring the water table elevation yielded important insight into how the aquifer responded to hydrologic and climate changes after the cessation of microbial activity. Fluctuations in water table elevation, particularly its decreases during extended dry periods, corresponded with the drops in ORP. This suggests that significant drops in water table allowed for some degree of re-oxidation of the iron sulfides at the site, which allowed for a short period where arsenic became remobilized in the system. Arsenic levels in M-1, M-2, and I-2 increased along with the drops in water table elevation during the dry October and November months (Figures 26-28). The LH-10 arsenic levels did not have a significant response to changes in the water table, this could be due to the fact that relative water table depth for LH-10 is markedly deeper than the surrounding wells on site (Table 2), which would not necessarily allow for as much re-oxidation of iron to take place. Changes in the water table elevation clearly correlate to the amount of local precipitation at the site. Naturally, dry periods with low precipitation are met with overall drops in the water table elevation (Figure 26), and instances of high precipitation between sampling events are met with noticeable increases in the water table elevation. After the dry period in October-November, precipitation values increased again in January and February, which led to relative water table levels rise. This corresponds to a drop in the arsenic levels for the three affected monitoring wells, as well as the two injection wells. This lends further evidence that the changes in local water table can have a noticeable but short-term impact on arsenic concentrations in the aquifer.

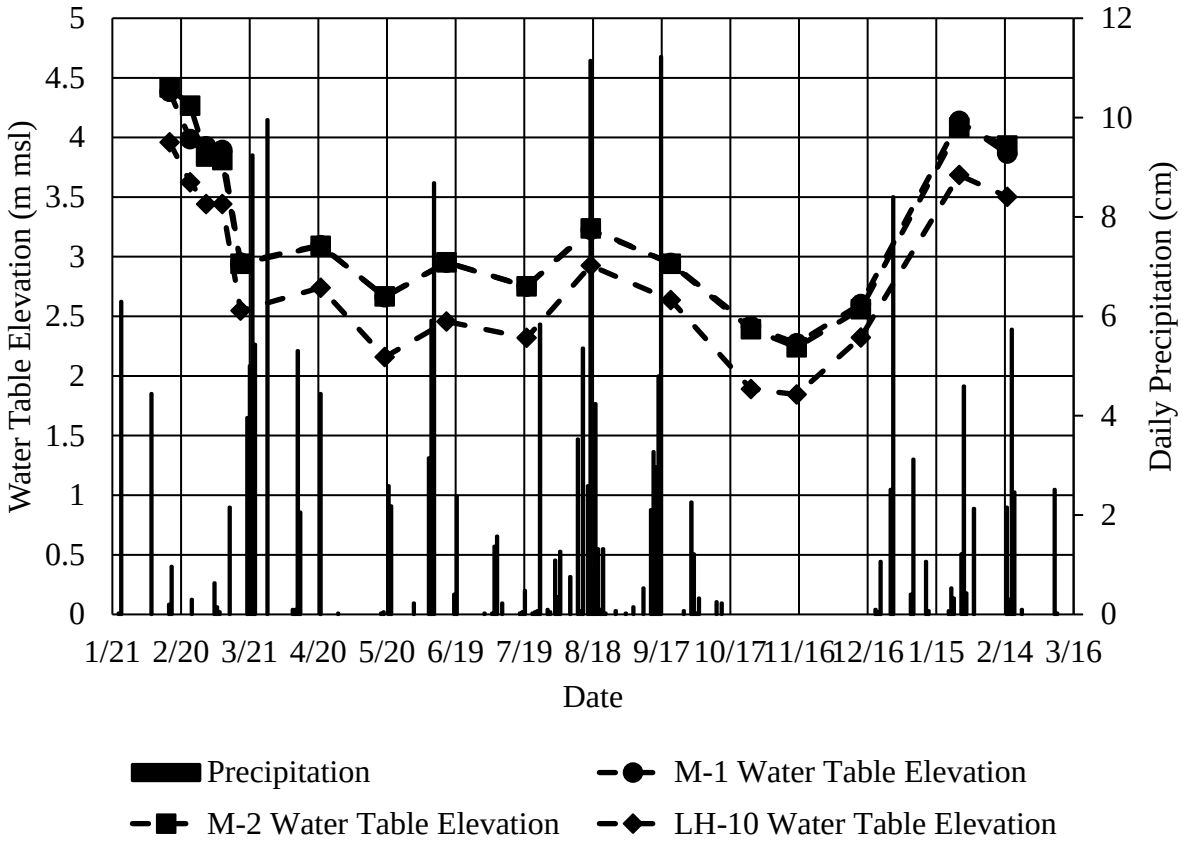

Figure 26. Plot of water table elevation (m msl) in monitoring wells versus daily precipitation levels (cm).

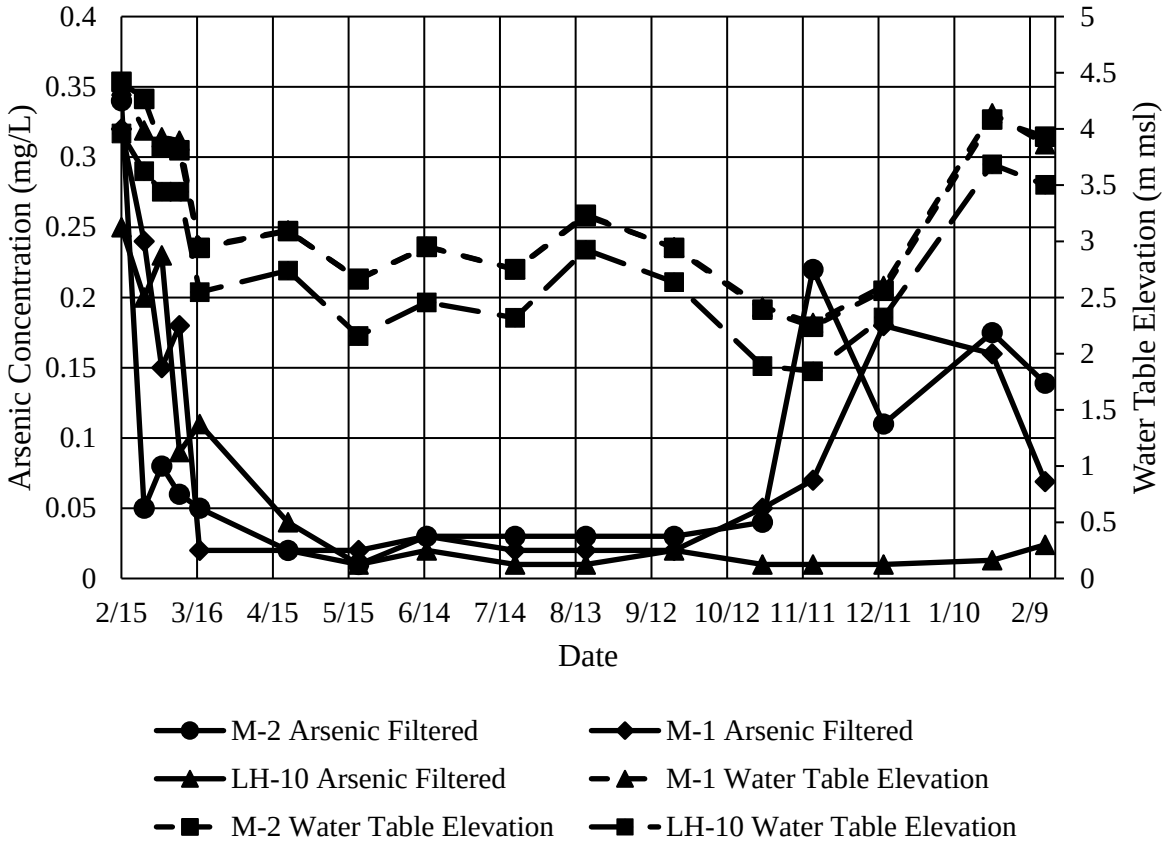

Figure 27. Plot of water table elevation (m msl) in monitoring wells versus arsenic concentration (mg/L).

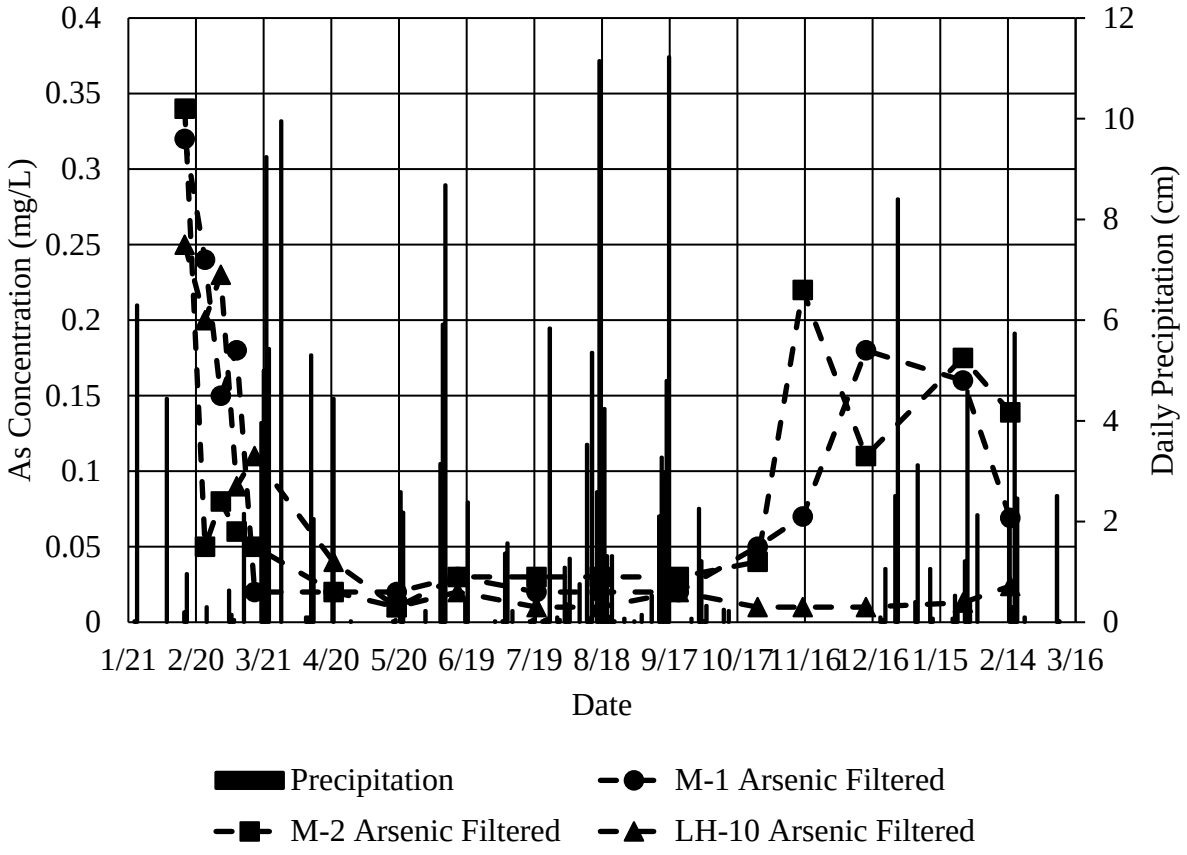

Figure 28. Plot of arsenic concentration (mg/L) in monitoring wells versus daily precipitation levels (cm).

The measured pH values in wells at the industrial site were used to evaluate if the amendments from the injection affected arsenic sorption onto the biogenic pyrite. Arsenic sorption on pyrite is uniquely dependent on pH (Bostick and Fendorf, 2003), and the pH dependence is distinctly different from other studies that investigated As sorption onto iron (oxy)hydroxides. Previous studies (Jingtai and Fyfe, 2000; Bulut et al. 2014; DeSisto et al. 2016; Farquhar et al. 2002; Bostick and Fendorf, 2003; Wolthers et al., 2005; Kim et al., 2009) indicated that arsenic sorption on pyrite increases with increasing pH, and markedly so between pH of 5 and 6. A common reason for this contrast is that As makes a strong inner-sphere complex with metal sulfide, unlike anion sorption onto iron (oxy)hydroxides which is essentially through ligand-exchange of the surface hydroxyl group (Bonnissel-Gissinger et al., 1998). Increase in As sorption can also be explained by formation of ≡Fe-OH surface sites that are the functional groups on the pyrite surface at higher pH levels (Chapelle and Lovley, 1992). The inner-sphere complexation, and metal surface site groups are likely to be involved in As sorption onto pyrite, which provides stable bonding for long term As-retention. In general bacterial sulfate reduction would consume H^+ in groundwater to raise the pH values, while re-oxidation of iron sulfide would lead to more acidic conditions. The field measurements showed a steep rise in pH (Table 5) due to bacterial sulfate reduction right after injection, followed by fluctuations in pH that corresponds to changing redox conditions. The pH values in monitoring wells M-1 and M-2 is found to be between 5 and 6 for a majority of the study period, suggesting that conditions were favorable to the previously discussed process of arsenic sorption onto pyrite. This shows

that the amendments were able to provide a favorable pH environment that would facilitate As sorption to pyrite and long term As-retention.

The conductivity over the one year period gave insights into potential behavior change of the solid sulfides under fluctuating redox conditions. The conductivity in the main monitoring wells M-1, M-2, and LH-10 showed a small range of fluctuation after the injection (Figure 29). The injection initially drove up conductivity in the monitoring wells and then quickly settled back down to background levels a month later due to biomineralization. There is a small amount of fluctuation in measured conductivity during and after the main arsenic sequestration stage, suggesting limited re-oxidation or dissolution of the biominerals formed at the site. These results imply that the solid sulfide biominerals precipitated from this experiment remain relatively stable under the changing redox conditions even when the amended carbon source is exhausted.

Despite the fluctuations in water table and ORP, filtered arsenic concentrations remain below the regulation level of 0.05 mg/L in three affected wells for at least six months (March to September) after the injection (Figure 27). After the main arsenic sequestration stage, periods of low rainfall induced some brief rises in arsenic concentration, this is likely due to drops in the water table that allowed for oxidation of some iron sulfide solids. Despite this, the arsenic concentrations remain below pre-injection levels in all three of the affected downgradient wells (M-1, M-2, and LH-10).

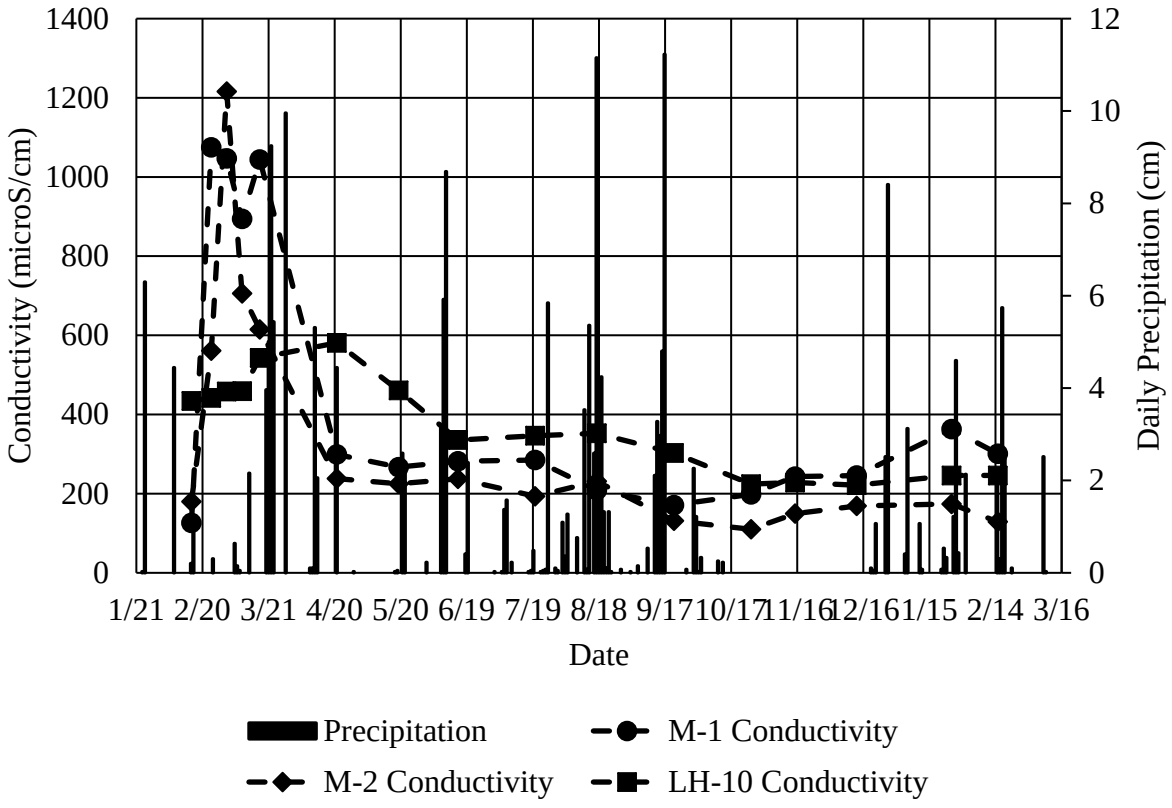

Figure 29. Plot of groundwater specific conductance (µS/cm) versus daily precipitation levels (cm) in monitoring wells.

Laboratory Data for Water Samples

Dissolved organic carbon contents in monitoring wells far from the injection site remained similar in magnitude to their pre-injection levels (Table 23). For the injection wells and affected monitoring wells (M-1, M-2, LH-10), DOC levels after the injection showed significant increases (Figure 30). These elevated DOC concentration eventually decreased to background levels when the organic carbon was biodegraded by the stimulated SRB in the aquifer. The LH-10 monitoring well recorded a delayed increase in DOC as the injected plume traveled downgradient from M-1 and M-2. These results indicate that DOC concentration in groundwater can be used to fingerprint changes in total organic loading in groundwater (compounds below 0.45 μm in size) and the resulting biodegradation following the injection. The measured phosphate and nitrate concentrations also increased significantly in the injection and affected monitoring wells one week after the injection (Figure 31). The high levels of nitrate and phosphate in the two injection and two monitoring wells were short lived. Nitrate and phosphate levels decreased sharply in the second week after the injection as a result of the stimulated bacterial activities, similar in pattern to DOC concentrations.

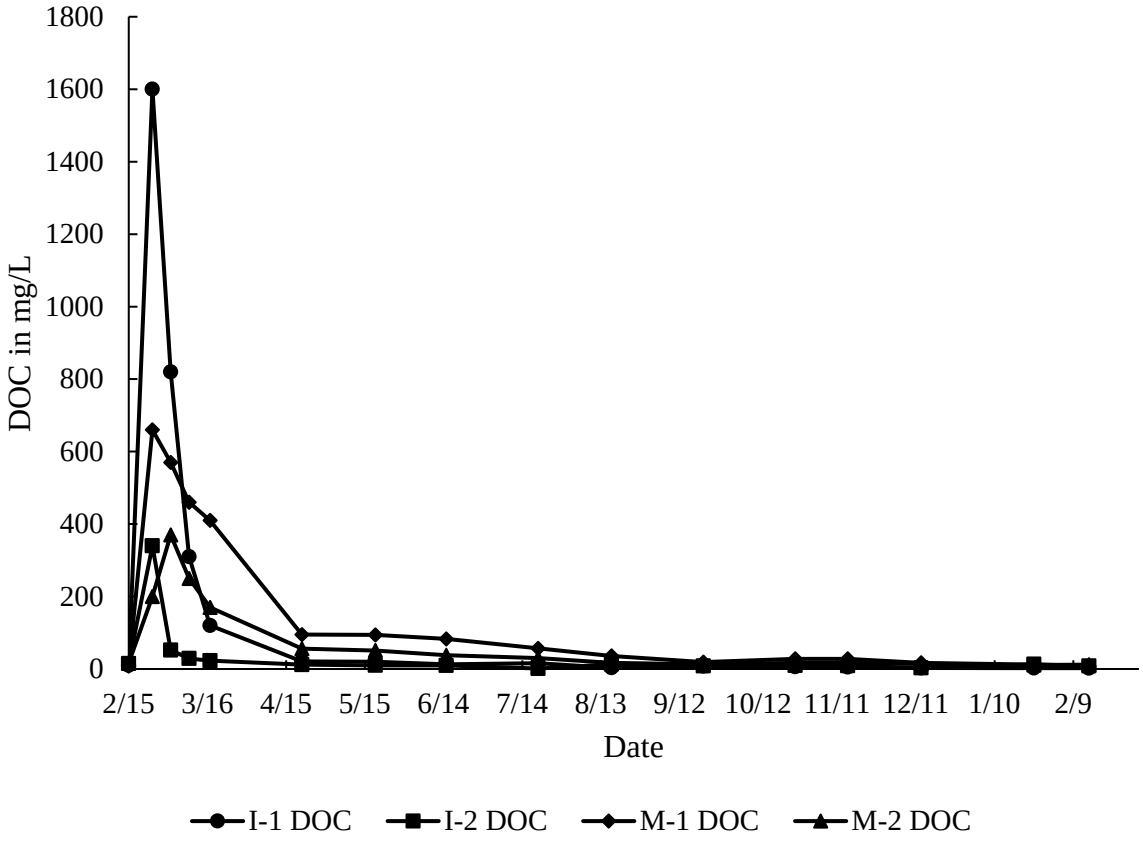

Figure 30. Plot showing changes in DOC (upper diagram), phosphate and nitrate (lower diagram) concentrations in injection wells (I-1 and I-2) and two closest downgradient wells (M-1, M-2) after injection.

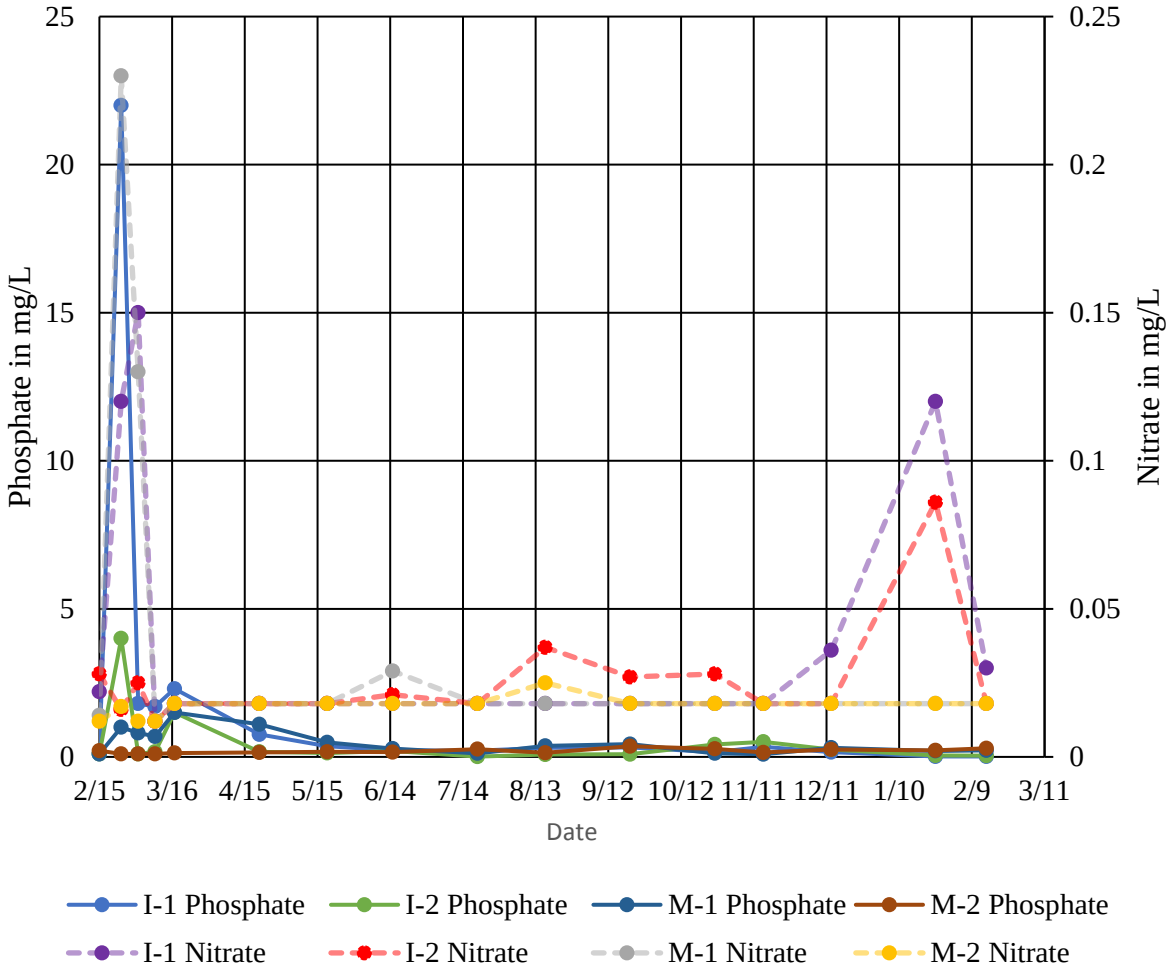

Figure 31. Plot showing nitrate and phosphate concentrations over time for injection and monitoring wells.

Total iron concentrations in the injection and affected monitoring wells increases significantly in the first week after injection. There was a concurrent rise in arsenic concentrations for two weeks after the injection but started to decrease in the third week post-injection. The concurrent rise in arsenic and iron levels is likely to be a result of bacterial iron reduction that took place prior to the onset of sulfate reducing conditions. This rise can occur when iron reducing bacteria out-compete sulfate reducing bacteria for organic carbon, causing As release from iron oxyhydroxides (Chapelle and Lovley, 1992). The input of nutrients from the injection solution may also cause the initial release of arsenic since phosphate and nitrate can be competitors for limited sorbing sites on the aquifer minerals. Phosphate can also cause arsenic release by either interfering with arsenic sorption or promoting desorption, serving as a sorption exchange for As on HFOs (Holm, 2002). In the few weeks and also months following the injection, arsenic levels in the three downgradient wells (M-1, M-2, and LH-10) undergo a significant decrease (Figures 32-35). Levels of arsenic remained below the site's regulatory clean-up goal of 0.05 mg/L in all three wells for at least six months after the date of injection.

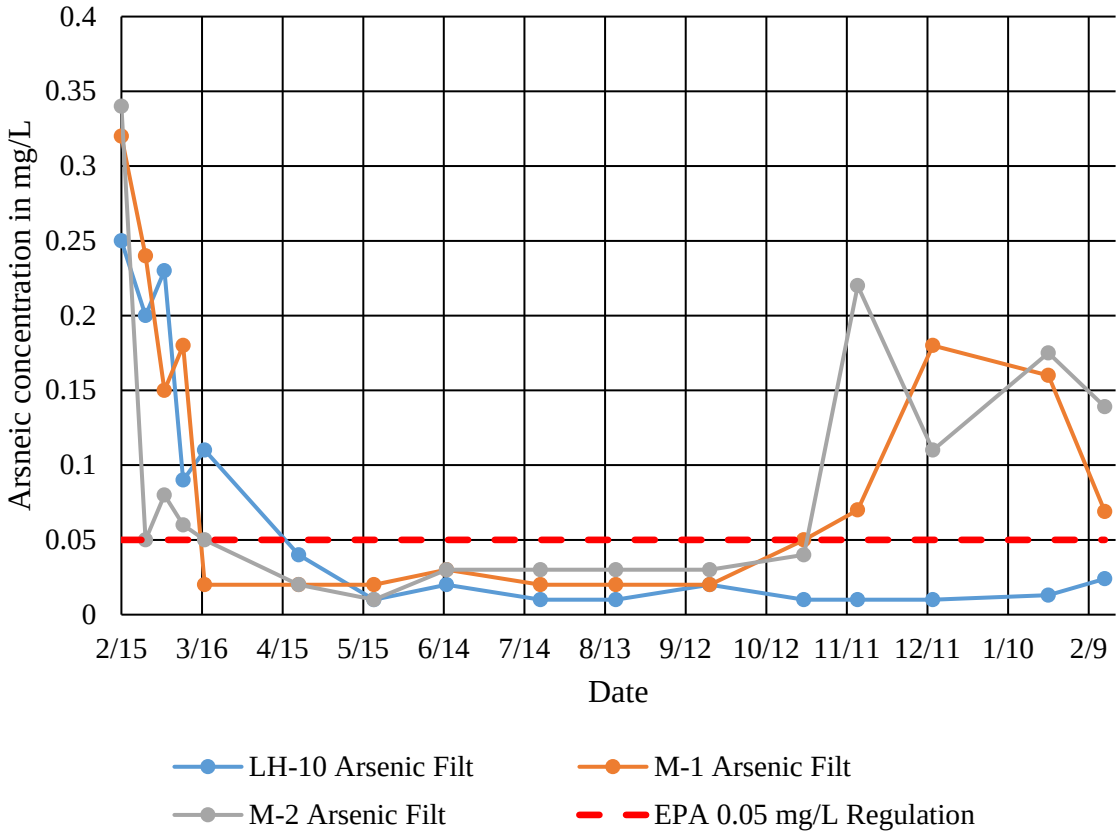

Figure 32. Plot of arsenic concentrations in filtered groundwater collected from affected monitoring wells over the year period. The red dashed line marks the 0.05 mg/L regulatory standard set for arsenic clean up goals at the industrial site.

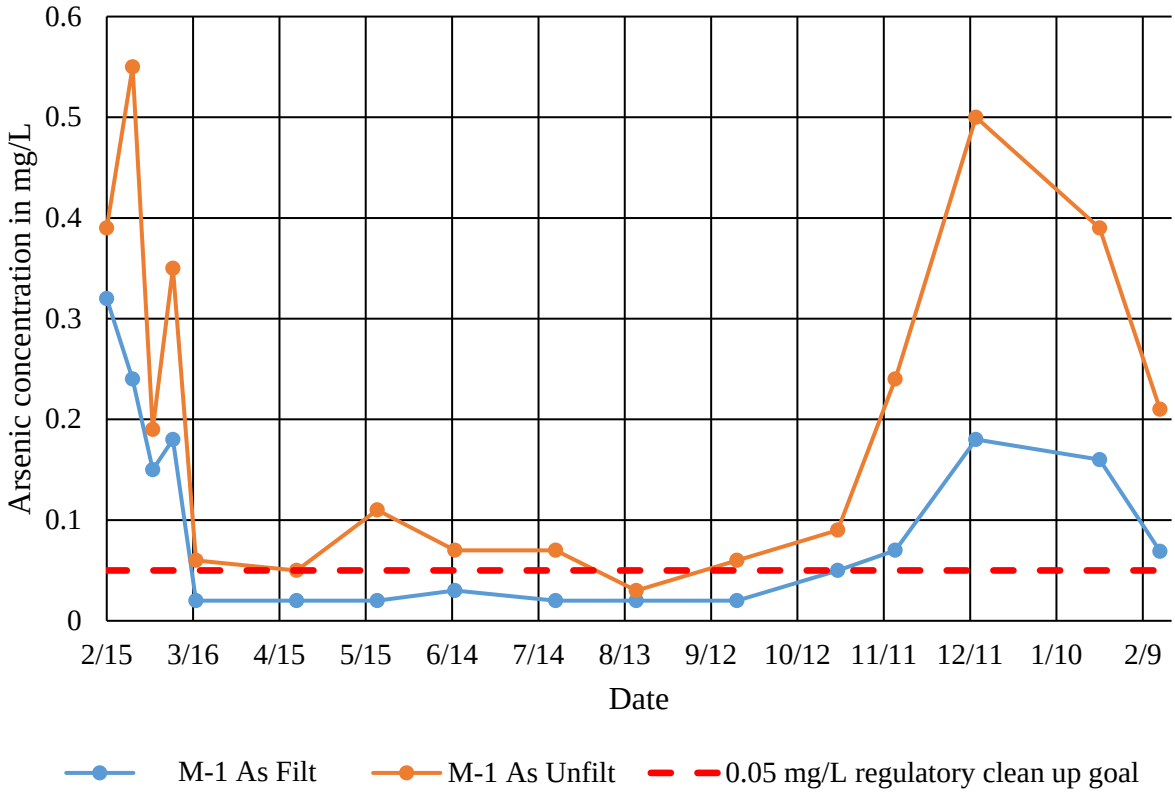

Figure 33. Plot of arsenic concentrations in filtered and unfiltered groundwater collected from well M-1 over the year period. The red dashed line marks the 0.05 mg/L regulatory standard set for arsenic clean up goals at the industrial site.

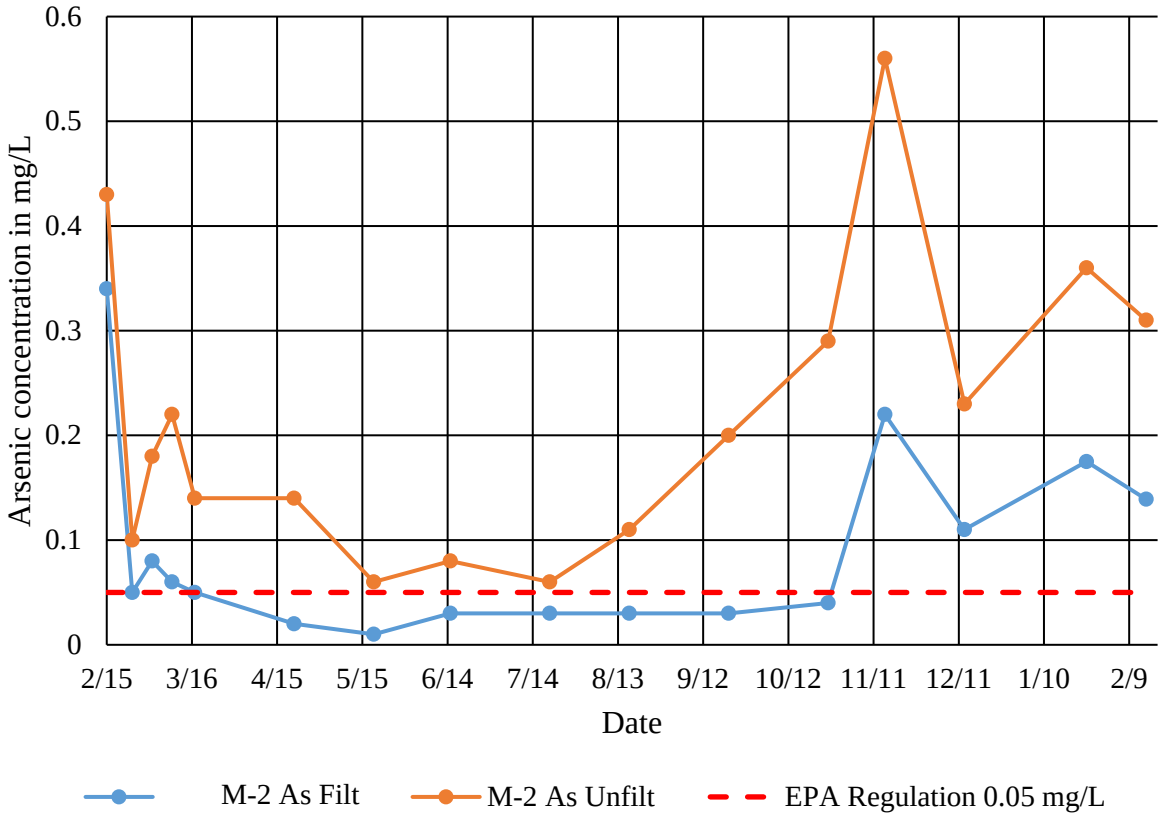

Figure 34. Plot of arsenic concentrations in filtered and unfiltered groundwater collected from well M-2 over the year period. The red dashed line marks the 0.05 mg/L regulatory standard set for arsenic clean up goals at the industrial site.

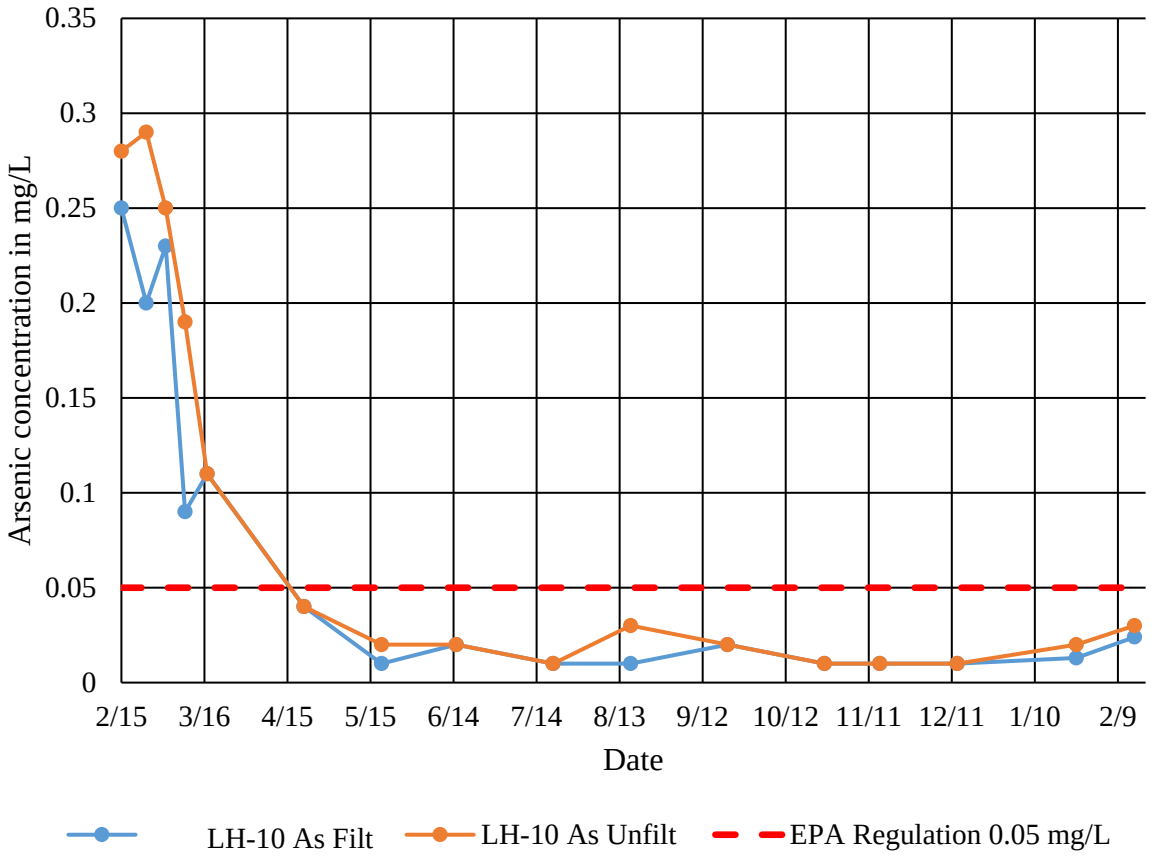

Figure 35. Plot of arsenic concentrations in filtered and unfiltered groundwater collected from well LH-10 over the year period. The red dashed line marks the 0.05 mg/L regulatory standard set for arsenic clean up goals at the industrial site.

Concurrent decreases are observed in Fe, SO_4, and As in the third week of sampling, followed by decreasing H_2S beginning in the fourth week. These results can be interpreted as a desired biogeochemical effect of bacterial sulfate reduction that caused the precipitation of pyrite and removal of arsenic from the groundwater (Figures 36-38). H_2S produced by SRB processes appears to be reacting with dissolved Fe (or Fe in solid phases) to make pyrite capable of removing arsenic from water by sorption and co-precipitation. These results also indicate that while the essential ingredients for SRB growth (DOC, Fe, and H_2S) return to background levels within the first few months, the iron sulfide minerals formed remain stable for arsenic sequestration in those solids. The levels of total arsenic and As(III) (Table 23 and 24) suggest that As(III) is the dominant aqueous species of arsenic in reducing environment. The activity diagram with measured Eh-pH values in Figure 21 confirmed that As(III) is the dominant aqueous arsenic species, which is expected under the moderately reducing conditions. The activity diagram and geochemical reaction-path model also show that solid arsenian pyrite will become the most stable phase for arsenic sequestration under highly reducing conditions induced by the injection. Comparisons of the results from filtered and unfiltered arsenic analyses reflect similar trends for all samples (Figures 32-35). The unfiltered arsenic concentrations were consistently higher than levels in the filtered samples, suggesting that a portion of arsenic does exist in particulate forms >0.45 μm in size. Calculations to find the relative percentages of particulate and dissolved arsenic were done for wells M-1, M-2, and LH-10. The average percent of arsenic dissolved across the three wells was 54%, and the average percent of arsenic in particulate forms was 46%. Gammons et al., (2000) found similar results and made the

suggestion that both the filtered and unfiltered samples are to be included in the context of environmental monitoring. Arsenic concentration increases for wells M-1 and M-2 occur in October and November, which correspond with drops in water table elevation, lack of precipitation, and a drop in ORP. The observed As increases in M-1 and M-2 is not accompanied by rises in Fe or SO_4, suggesting limited oxidation of iron sulfide solids (Figures 36 and 37). This also implies that the source of arsenic could be from the arrival of untreated groundwater that migrated from an area up-gradient from the wells. The arsenic concentration in LH-10 remains well below the regulatory limit at the site (Figure 38), and iron, sulfide, and sulfate measurements reached relative equilibrium at the end of the experiment. By contrast, a rise in arsenic in I-2 correlates with concurrent rises in Fe, SO_4, and ORP. This could be interpreted to be resulting from oxidation of the iron sulfides, which corresponds with a drop in the water table elevation during this dry period. The drops in water table in the well can drive up the O_2 levels, which could potentially be a factor in mobilizing arsenic and causing As levels to increase after the bacterial activities cease. Arsenic rise in the aquifer can also be tied to the eventual arrival of untreated groundwater plumes moving into the field site from areas upgradient from the injection wells that received treatment. Results from Starnes (2015) indicate that hydraulic conductivity at the site is 0.0014 cm/s, and groundwater travels west to northwest at an average rate of 13 m/year. The untreated plume eventually reaches the treated wells and has contributed to rises in arsenic concentrations in affected wells around six months after the initial injection.

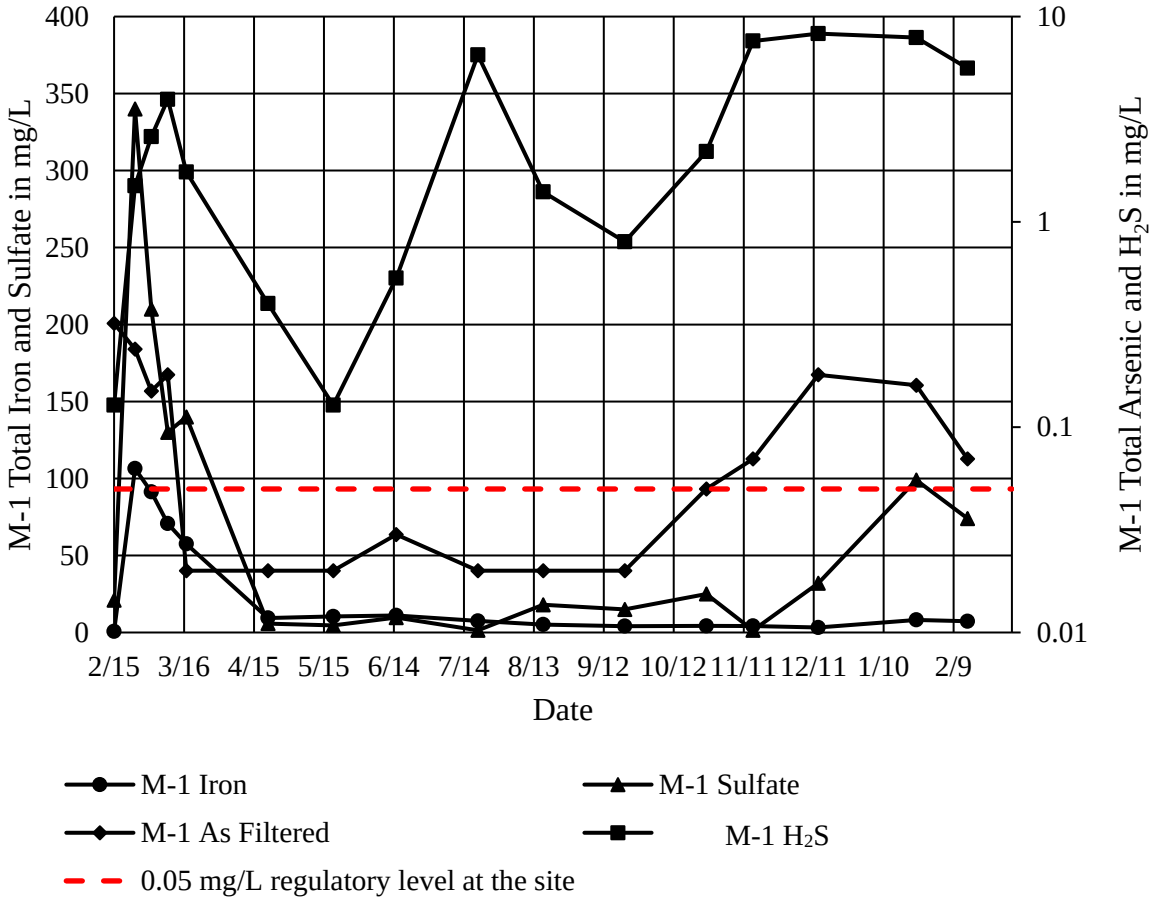

Figure 36. Plots of concentrations for iron, sulfate, sulfide, and arsenic in well M-1 .

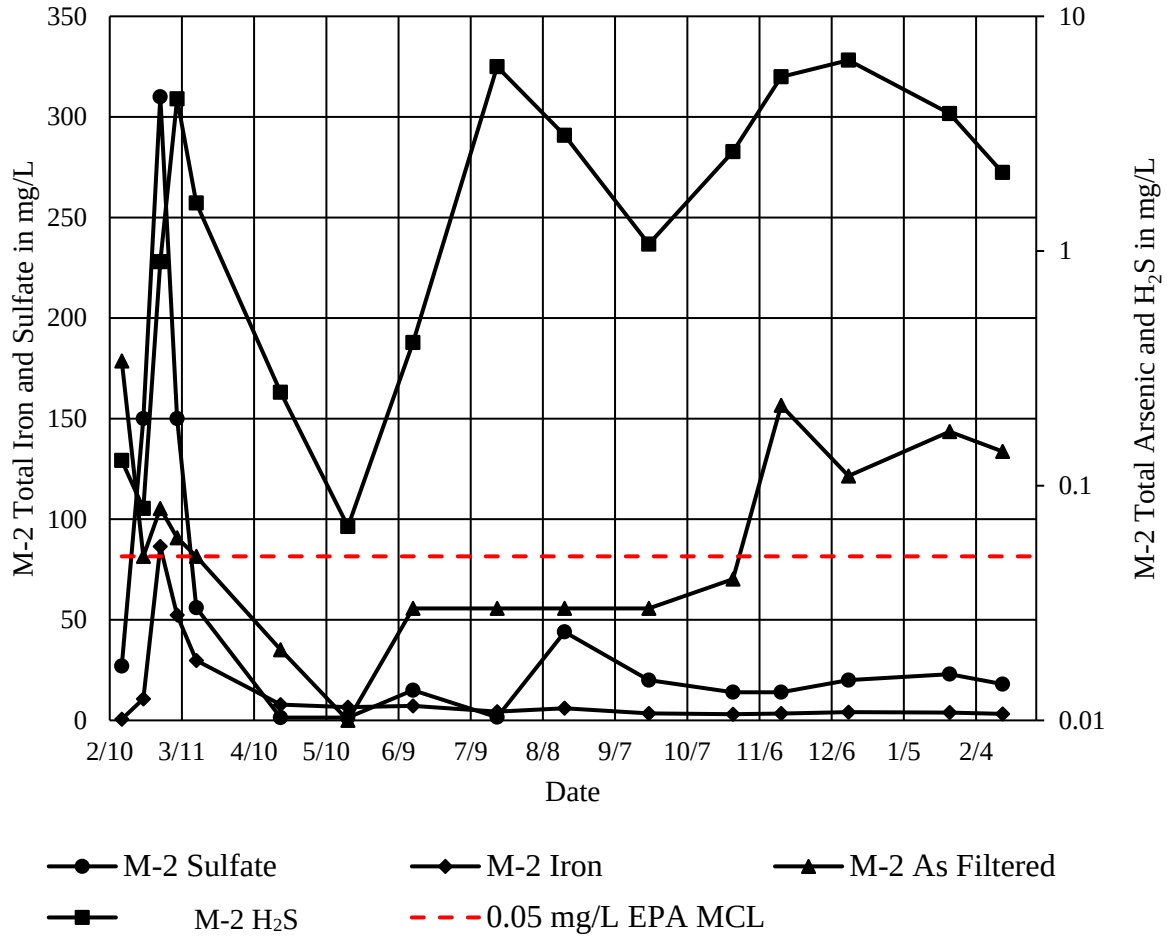

Figure 37. Plots of concentrations for iron, sulfate, sulfide, and arsenic in well M-2 over the year period.

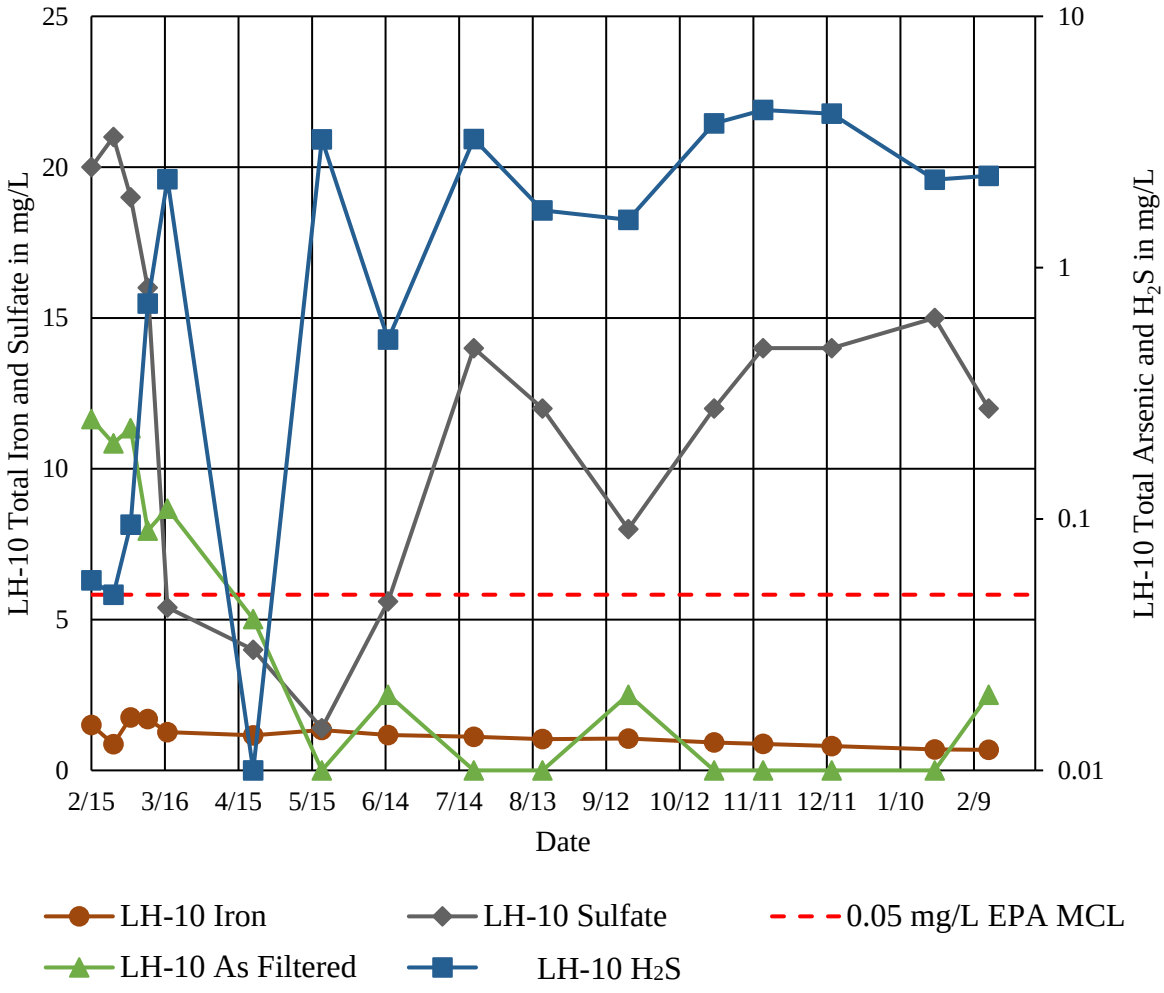

Figure 38. Plots of concentrations for iron, sulfate, sulfide, and arsenic in well LH-10 over the year period.

Biogenic Solids

The XRD analysis of dark slurry recovered from the bottom of affected wells show well-defined peaks (Figures 10-12) that closely matched arsenian-pyrites. The well-defined diffraction peaks indicate that at this field site biogenic sulfides formed quickly as stable bio-crystallines in the system. The optical microscopy and XRD studies show the solids to be crystalline arsenian pyrites. The SEM images (Figures 14-16) affirmed that the pyrite occurred as well-formed crystals and framboids that commonly attached to silicate phases in the aquifer. The images revealed that the pyrite grains typically range from 1-10 μm in diameter. X-ray fluorescence (XRF) analysis consistently results in peaks for Fe, S, and As (Figure 17), which is consistent with XRD spectrum and petrographic analysis that a single Fe-S-As solid phase was formed by the bacterial sulfate reduction. The results also indicate that the pure As-S phases such as realgar and orpiment are not likely to form in Fe- and S-rich, low-temperature and cirum-neutral pH environments at this industrial site after remediation.

The electron microprobe results confirmed that the biogenic pyrite formed at the site was an arsenian pyrite containing 0.1 to 0.4 wt % As (Figure 18). This percentage range is much higher than the level of arsenic (typically in the range of a few mg/kg) in fluvial sediments (Horneman et al., 2004; Shamsudduha et al., 2008), implying that biogenic pyrite produced in this study has excellent sequestration capacity.

Microbial Changes and Impact

The real-time PCR methods that analyzed the sulfate-reducing bacteria from the aqueous slurry samples yielded useful results. The results from this study show that while the pre-injection SRB concentrations were below the detection limit, measurements taken after the injection revealed significantly higher amounts of SRB in the injection and monitoring wells. Samples from the both the injection and monitoring wells (M-1, M-2, I-1, and I-2) have increased concentration of SRB for at least two months after the injection into the aquifer (Figures 19-20). Concentrations of the SRB DNA go from below detection limits to about 3 Log_{10} copies/µl. The results of the analysis support that the functional SRB species on site are the *Desulfovibrio spp*. and *Desulfotomaculum spp*. which are common soil-rich sulfate reducing bacteria species. The PCR analysis confirms that sulfate-reducing bacteria activities on site were enhanced by the amendments of organic carbon from the injection. These results demonstrate that SRB in an aquifer, if given the necessary supplies, are capable of utilizing anaerobic sulfate reduction to form insoluble metal sulfide solids that sequester dissolved arsenic from the groundwater under sulfate-reducing conditions.

Conclusions

This study represents the first long-term, field-scale study that investigates how biogeochemical reactions occur along groundwater flow paths during bioremediation of arsenic. The monitoring of changes in the aquifer, including changing redox conditions, stimulated biomineralization, and arsenic concentration, serves to document the geochemical effects of SRB metabolism in a contaminated groundwater environment. The field and laboratory data that were gathered demonstrated that, given ample supplies of organic carbon and nutrients, natural sulfate-reducing bacteria is capable of anaerobically executing sulfate reduction to form insoluble metal sulfide phases in an arsenic contaminated aquifer. This experiment provided the necessary supplies through the injection of electron donors in the form of biodegradable organic carbon, sulfate as electron acceptors, and ferrous iron. These amendments facilitated the precipitation of iron sulfides, which was confirmed through X-ray, optical, and electron microprobe analysis. The electron microprobe analysis verified the sequestration of arsenic by the precipitation of small crystalline pyrite containing 0.1 to 0.4 wt. % of arsenic. Dissolved arsenic is clearly sequestered under sulfate-reducing conditions via the adsorption on the surface of iron sulfides or through co-precipitation. It is shown that the stimulation of natural SRB can make biogenic pyrite in the field, and serves as an effective remediation agent in this low temperature environment.

Pure crystalline As-sulfide solids (e.g. realgar, orpiment) are not found in slurry samples recovered from this field site. It is plausible that their growth becomes kinetically hindered in

low-temperature environments (Lee and Saunders, 2003) or they are outcompeted by FeS amorphous precursors of pyrite. More work is needed to better address this research question. This study gave insight into the behavior of arsenic under changing redox conditions. It is possible that arsenic has the potential to react with the H_2S produced by SRB to form thioarsenite aqueous complexes. These complexes can then compete with arsenic for the growing pyrite surfaces (Lee and Saunders, 2003) and enhance arsenic solubility when dissolved iron is depleted in the aquifer. It is imperative for an effective bioremediation project to provide enough ferrous iron in the system so that high Fe/H_2S ratios favor the incorporation of arsenic into pyrite, rather than forming the aqueous complex. This experiment included the addition of nitrogen and phosphorous as nutrients into the aquifer to further help stimulate SRB growth. Phosphorous fertilizers may cause arsenic release due to ionic competition for limited mineral sorbing sites (Neumann et al., 2010; Aziz et al., 2016), so it is unclear if the application of additional nutrients actually adds in bioremediation effectiveness.

This field-scale project demonstrates that natural sulfate-reducing bacteria can be stimulated to make biogenic pyrite that acts to sequester dissolved arsenic in a contaminated aquifer. The data also imply that even when the injected organic carbon, sulfate, and iron is exhausted and consumed by microbial activity, the sequestration remains effective for at least six months under reducing conditions before the arrival of untreated groundwater from up-gradient. Depending on site conditions, long-term remediation of aquifers may need to be repeatedly amended with organic carbon to re-establish the reducing conditions that favor arsenic sequestration. The arsenic level in affected wells remain below their pre-injection level even as

redox conditions in the aquifer fluctuate, lending more credibility to the effectiveness of this technique as a remediation tool. The long-term sequestration effectiveness in the aquifer has several implications, one of these being that effective remediation can be applied at both natural and industrial sites where arsenic contaminates the water supply. For example, natural sources of arsenic contamination in fluvial aquifers in South Asia present a significant threat to human health in that region, and it is reasonable to suggest that this process can be modified and enhanced to treat aquifers adjacent to individual wells where arsenic contaminated groundwater is extracted for human use. For full-scale remediation operation, the biostimulation to sequester arsenic should start at positions hydrologically upgradient from the major plume (e.g., LH-4 and RA-14 at our field site, Figure 5) and proceed downgradient; such a scheme would prevent the re-contamination from untreated groundwater originated from up-gradient. This method of cost-effective remediation at the field scale perhaps could be adapted to provide safer, treated groundwater to individuals by sequestration of arsenic in stable iron sulfide minerals around well screens of the small hand-pumped wells common in South Asian countries like Bangladesh and India.

References

Aziz, Z., Bostick, B.C., Zheng, Y., Huq, M.R., Rahman, M.M., Ahmed, K.M., van Geen, A., 2016. Evidence of decoupling between arsenic and phosphate in shallow groundwater of Bangladesh and potential implications: Applied Geochemistry, 2016.

Ben-Dov, E., Brenner, A., & Kushmaro, A., 2007, Quantification of Sulfate-reducing Bacteria in Industrial Waste water, by Real-time Polymerase Chain Reaction (PCR) Using dsrA and apsA Genes: Microbial Ecology, 54, 439-451.

Bethke, C. M., 2008, Geochemical and biogeochemical reaction modeling, Cambridge University Press, 543 pp.

Bonnissel-Gissinger, P., Alnot, M., Ehrhardt , J-J, & Behra, P., 1998 Surface Oxidation of Pyrite as a Function of pH: Environmental Science and Technology, 32, 2839-2845.

Bostick, B.C., and Fendorf, S., 2003, Arsenic sorption on troilite (FeS) and pyrite (FeS_2): Geochimica et Cosmochimica Acta, 67, 909-921.

Bostick, B.C., Fendorf S., and Bruce A. Manning, B.A., 2003, Arsenite adsorption on galena (PbS) and sphalerite (ZnS): Geochimica et Cosmochimica Acta, 67, 895-907.

Bulut, G.; Yenial, U.; Emiroglu, E; Sirkesci, A.A., 2014, Arsenic removal from aqueous solution using pyrite: Journal of Cleaner Production, 84, 526-532.

Chapelle, F.H., Mcmahon, P.B., Dubrovsky, N.M., Fujii, R.F., Oaksford, E.T., and Vroblesky, D.A., 1995, Deducing the distribution of terminal electron accepting processes in hydrologically diverse groundwater systems: Water Resources Research, 31, 359-371.

Deflaun, M., J. Lanzon, M. Lodato, S. Henry, T.E. Onstott, E. Chan, and B. Otemuyiwa, 2009, Anaerobic Biostimulation for the In Situ Precipitation and Long-Term Sequestration of Metal Sulfides: Strategic Environmental Research and Development Program, Project ER-1373. April 2009.

DeSisto, S.L.; Jamieson, H.E.; Parsons, M. B.; 2016. Subsurface variations in arsenic mineralogy and geochemistry following long-term weathering of gold mine tailings: Applied Geochemistry, 73, 81-97.

Dhakal, P., 2010, Sorption of arsenic by iron sulfide made by sulfate-reducing bacteria: implications for bioremediation: Master Thesis, Auburn University, Auburn, Alabama.

Dowling, C.B., Poreda, R.J., Basu, A.R., Peters, S.L., 2002, Geochemical study of arsenic release mechanisms in the Bengal Basin groundwaters: Water Resources Research, 38, 1173-1190.

Farquhar, M.L., Charnock, J.M., Livens, F.R., Vaughan, D.J., 2002, Mechanisms of arsenic uptake from aqueous solution by interaction with goethite, lepidocrocite, mackinawite, and pyrite: An X-ray absorption spectroscopy study: Environmental Science and Technology, 36, 1757-1762.

Gammons, C.H.; Mulholland, T.P.; Frandsen A.K., 2000, A comparison of filtered and unfiltered metal concentrations in treated wetlands: Mine Water and the Environment, 19, 111-123.

Harvey, C. F., Swartz, C.H., Badruzzman, B., Keon, N.E., Yu. W., Ali, A., Jay, J., Beckie, R., Niedan, V., Brabander, D, Oates, P., Ashfaque, K., Islam, S., Hemond, H.F., Ahmed, F., 2002, Arsenic mobility and groundwater extraction in Bangladesh: Science, 298.

Holm, T., 2002, Effects of CO_3^{2-}/Bicarbonate, Si, and PO_4^{3-} on Arsenic Sorption to HFO: Journal (American Water Works Association), 94, 174-181.

Horneman, A., van Geen, A., Kent, D., Mathe, P.E., Zheng, Y., Dhar, R.K., O'Connell, S., Hoque, M., Aziz, Z., Shamsudduha, M., Seddique, A., Ahmed, K.M., 2004. Decoupling of As and Fe release to Bangladesh groundwater under reducing conditions. Part I: Evidence from sediment profiles: Geochimica et Cosmochimica Acta, 68, 3459–3473.

Jingtai, H. and Fyfe, W.S., 2000, Arsenic removal from water by iron-sulphide minerals: Chinese Science Bulletin, 45, 1430-1434.

Keimowitz, A.R, Simpson, H.J., Stute, M., Datta, S., Chillrud, S.N., Ross, J., Tsang, M, 2005, Naturally occurring arsenic: Mobilization at a landfill in Maine and implications for remediation: Applied Geochemistry, 20, 1985-2002.

Lee, M.-K. And Saunders, J.A., 2003, Effects of pH on metals precipitation and sorption: Field Bioremediation and geochemical modeling approaches: Vadose Zone Journal, 2, 177-185.

Lee, M.-K., Saunders, J.A., Wilkin, R.T. and Mohammad, S., 2005, Geochemical modeling of arsenic speciation and mobilization: Implications for bioremediation, in Advances in Arsenic Research: Integration of Experimental and Observational Studies and Implications for Mitigation, P. A. O'Day, D. Vlassopoulos, X. Meng, and L. G. Benning (eds.), American Chemical Society Symposium Series v. 915, 398-413.

Lee, M.-K., Griffin, J., Saunders, J.A., Wang, Y., Jean, J., 2007, Reactive transport of trace elements and isotopes in Alabama coastal plain aquifers: Journal of Geophysical Research, 112, G02026, doi:10.1029/2006JG000238.

Lee M.-K., Natter, M., Keevan, J., Querra, K., Saunders, J.A., Uddin, A., Humayun, M., Wang, Y., Alison R. Keimowitz, A.R., 2013, Assessing effects of climate change on biogeochemical cycling of trace metals in alluvial and coastal watersheds: British Journal of Environment and Climate Change, 3, 44-66.

Lowers, H.A., Breit, G.N., Foster, A.L., Whitney, J., Yount, J., Uddin, M.N, Muneem, A.A., 2007. Arsenic incorporation into authigenic pyrite, Bengal Basin sediment, Bangladesh: Geochimica et Cosmochimica Acta, 71, 2699-2717.

McArthur, J.M.; Banerjee, D.M.; Hudson-Edwards, K.A.; Mishra, R.; Purohit, R.; Raverscroft, P.; Cronin, A.; Howarth, R.J.; Chatterjee, A.; Talukder, 2004, T. Natural organic matter in sedimentary basins and its relation to arsenic in anoxic groundwater: the example of West Bengal and its worldwide implications: Applied Geochemistry, 19, 1255-1293.

Mintz, J., and Miller, J., 1993, Retired Substation Remedial Action Plan: Company Services, 196 p.

Mukherjee, P.K., Pal, T., Sengupta, S., Shomw, S., 2001, Arsenic rich phases from aquifer sediments from southern west Bengal: Journal of Geological Society of India, 58, 173-176.

Neumann, R.B.; Ashfaque, K.N.; Badruzzaman, A.B.M.; Ali, A.; Shoemaker, J.K.; Harvey, C.F., 2010. Anthropogenic influences on groundwater arsenic concentrations in Bangladesh: Nature Geoscience, 3, 46-52.

Nickson, R.T., McArthur, J.M., Ravenscroft, P., Burgess, W.G., and Ahmed, K.M., 2000, Mechanism of arsenic release to groundwater, Bangladesh and West Bengal: Applied Geochemistry, 15, 403-413.

Nordstrom, D.K., 2002, Worldwide occurrences of arsenic in ground water: Science, 296, 2143-2145.

O'Day, P.O., Vlassopoulos, D., Root, R., Rivera, N., 2004. The influence of sulfur and iron on dissolved arsenic concentrations in the shallow subsurface under changing redox conditions: Proceedings of the National Academy of Sciences, 101, 13703-13708.

O'Day, P.O., 2006. Chemistry and mineralogy of arsenic: Elements, 2, 77-83.

Onstott et al., 2011. Precipitation of arsenic under sulfate reducing conditions and subsequent leaching under aerobic conditions: Applied Geochemistry, v. 26 issue 3, p.269-285

Saunders, J.A., Pritchett, M.A., and Cook, R.B., 1997, Geochemistry of biogenic pyrite and ferromanganese stream coatings: A bacterial connection?: Geomicrobiology Journal, 14, 203-217.

Saunders, J.A., 1998, US Patent # 5,833,855, In Situ Bioremediation of Contaminated Groundwater.

Lee, M.-K. & Saunders, J.A., 2003, Effects of pH on metals precipitation and sorption: Field bioremediation and geochemical modeling approaches: Vadose Zone Journal, 2, 177–185.

Rieder et al., 2007, Arsenic in Iron Disulfides in a Brown Coal from the North Bohemian Basin, Czech Republic: International Journal of Coal Geology, 71, 115-121.

Saffari-Ghandehari, S., 2016, Bioremediation of an Arsenic-Contaminated Site, Using Sulfate-Reducing Bacteria, Bay County, Florida: Master Thesis, Auburn University, Auburn, Alabama.

Saunders, J.A., Mohammad, S. Korte, N.E., Lee, M.-K., Castle, D., Barnett, M.O., Fayek, M., and Riciputi, L., 2005a, Groundwater geochemistry, microbiology and mineralogy in two arsenic-bearing Holocene alluvial aquifers from the USA, in Advances in Arsenic Research: Integration of Experimental and Observational Studies and Implications for Mitigation, P. A. O'Day, D. Vlassopoulos, X. Meng, and L. G. Benning (eds.), American Chemical Society Symposium Series, 915, 191-205.

Saunders, J. A., Lee, M.-K., Uddin, A., S., Mohammad, S., Wilkin, R., Fayek, M., and Korte, N., 2005b, Natural arsenic contamination of Holocene alluvial aquifers by linked glaciation, weathering, and microbial processes: Geochemistry, Geophysics, Geosystems, 6, Q04006, doi:10.1029/2004GC000803.

Saunders, J. A., Lee, M.-K., Wolf, L.W., Morton, C., Feng, Y., Thomson, I., Park, S., 2005c, Geochemical, microbiological, and geophysical assessment of anaerobic bioremediation of metals-contaminated groundwater: A field experiment: Bioremediation Journal, 9, 33-48.

Saunders, J.A., Lee, M.-K., Shamsudduha, M., Dhakal, P., Uddin, A., Chowdury, M.T., and K.M. Ahmed, 2008, Geochemistry and mineralogy of arsenic in (Natural) anaerobic groundwaters: Applied Geochemistry, 23, 3205-3214.

Schmidt, W.; Clark, M.W., 1980, Geology of Bay County, Florida: Florida Geological Survey Bulletin, 57, 96 p.

Shamsudduha, M., Uddin, A., Saunders, J.A., Lee, M.-K., 2008, Quaternary stratigraphy, sediment characteristics and geochemistry of arsenic-contaminated alluvial aquifers in the Ganges-Brahmaputra floodplain in central Bangladesh: Journal of Contaminant Hydrology, 99, 112-136.

Smedley, P.L., and Kinniburgh, D.G., 2002, A review of the source, behavior and distribution of arsenic in natural waters: Applied Geochemistry, 17, 517-568.

Starnes, P., 2015, Hydrogeology and Geochemistry of Arsenic Contaminated Shallow Alluvial Aquifers in Florida and Alabama, Master Thesis: Auburn University, Auburn, Alabama, 143 Pages.

USEPA, 1995, Contaminants and Remedial Options at Selected Metal-Contaminated Sites: Washington DC, Office of Research and Development, U.S. Environmental Protection Agency, EPA/540/R-95/512, 268 p.

USEPA, 1997, Technology Alternatives for the Remediation of Soils Contaminated with As, Cd, Cr, Hg, and Pb: Washington DC, Office of Emergency and Remedial Response, U.S. Environmental Protection Agency, EPA/540/S-97/500, 21 p.

van Geen, A., Zheng, Y., Versteeg, R., Stute, M., Horneman, A., Dhar, R., Steckler, M., Gelman, A., Small, C., Ahsan, H., Graziano, J., Hussain, I., and Ahmed, K.M., 2003, Spatial variability of arsenic in 6000 contiguous tubewells of Araihazar, Bangladesh: Water Resources Research, 39, 1140.

Veach, O., and Stephenson, L.W., 1911, Preliminary Report on the Geology of the Coastal Plain of Georgia: Georgia Geological Survey Bulletin 26, 1-466.

Welch, A.H., Westjohn, D.B., Helsel, D.R., and Wanty, R.B., 2000, Arsenic in ground water of the United States; occurrence and geochemistry: Ground Water, 38, 589-604.

Wolthers, M., Charlet, L., Van Der C. H., Van Der Linde P. R., and Richard, D., 2005, Arsenic mobility in the ambient sulfidic environment: Sorption of arsenic(V) and arsenic(III) onto disordered mackinawite: Geochimica et Cosmochimica Acta, 69, 3483-3492.

Zouboulis , A.I.; Kydros K.A.; Matis, 1993. K.A. Arsenic(III) and Arsenic(V) removal from solutions by pyrite fines. Separation Science and Technology, 28, 2449-2463.